Spring 2015

THE SAUDI ARAMCO JOURNAL OF TECHNOLOGY
A quarterly publication of the Saudi Arabian Oil Company

Saudi Aramco Journal of Technology

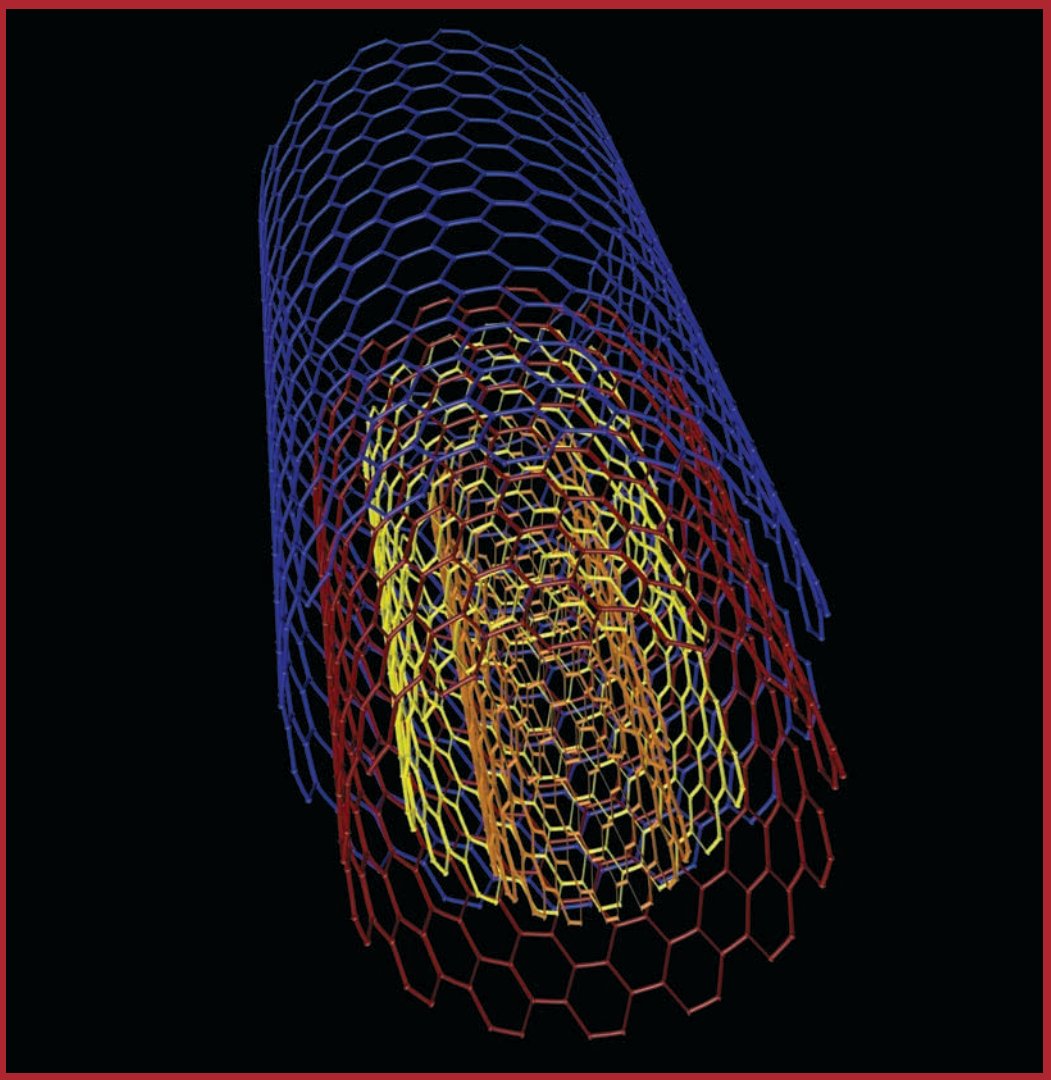

On the Cover

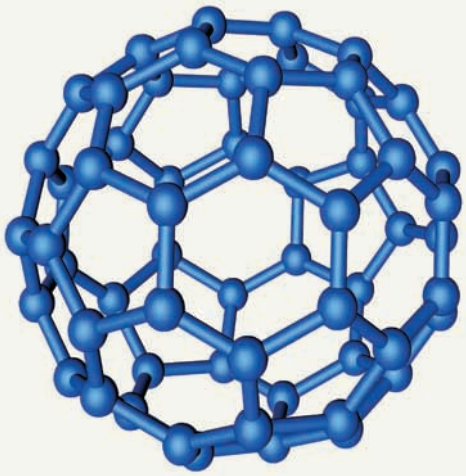

A concentric tubular structure of a multi-walled carbon nanotube (MWCNT), which can help overcome current and future extreme drilling and production challenges.

Buckyballs: With the development of nanomaterial, a series of interlocking hexagons and pentagons with hollow spheroids can revolutionize the fluid and tool design due to unique mechanical and chemical properties not seen in conventional materials.

MORE SAUDI ARAMCO JOURNAL OF TECHNOLOGY ARTICLES AVAILABLE ON THE INTERNET.

Additional articles that were submitted for publication in the *Saudi Aramco Journal of Technology* are being made available online. You can read them at this link on the Saudi Aramco Internet Website: www.saudiaramco.com/jot

The *Saudi Aramco Journal of Technology* is published quarterly by the Saudi Arabian Oil Company, Dhahran, Saudi Arabia, to provide the company's scientific and engineering communities a forum for the exchange of ideas through the presentation of technical information aimed at advancing knowledge in the hydrocarbon industry.

Complete issues of the Journal in PDF format are available on the Internet at: http://www.saudiaramco.com (click on "publications").

SUBSCRIPTIONS

Send individual subscription orders, address changes (see page 77) and related questions to:

Saudi Aramco Public Relations Department
JOT Distribution
Box 5000
Dhahran 31311, Saudi Arabia
Website: www.saudiaramco.com

CONTRIBUTIONS

Relevant articles are welcome. Submission guidelines are printed on the last page. Please address all manuscript and editorial correspondence to:

EDITOR

William E. Bradshaw
The *Saudi Aramco Journal of Technology*
C-86, Wing D, Building 9156
Dhahran 31311, Saudi Arabia
Tel: +966-013-876-0498
E-mail: william.bradshaw.1@aramco.com.sa

Unsolicited articles will be returned only when accompanied by a self-addressed envelope.

PRODUCTION COORDINATION

Richard E. Doughty

DESIGN

Pixel Creative Group, Houston, Texas, U.S.A.

ISSN 1319-2388.

The *Saudi Aramco Journal of Technology* gratefully acknowledges the assistance, contribution and cooperation of numerous operating organizations throughout the company.

أرامكو السعودية
Saudi Aramco

Spring 2015

THE SAUDI ARAMCO JOURNAL OF TECHNOLOGY
A quarterly publication of the Saudi Arabian Oil Company

Saudi Aramco Journal of Technology

Contents

Nanotechnology Can Overcome the Critical Issues of Extremely Challenging Drilling and Production Environments

Authors: Dr. Md. Amanullah and Dr. Jothibasu Ramasamy

ABSTRACT

Due to a progressively decreasing trend in finding easy oil and gas, the industry is shifting to high risk and extremely challenging drilling environments to meet global energy demands. This is reflected by increasingly higher drilling activities in complex geological areas, deepwater environments, extreme high-pressure/high temperature (HPHT) conditions, etc. The increasing shift from vertical to deviated, horizontal or extended reach drilling; from single lateral to multilateral drilling; from conventional completions to coiled tubing (CT) or casing while drilling; and from rotary drilling to downhole motor drilling, etc., also dictates the development of highly reliable tools and equipment for a trouble-free drilling operation. Moreover, critical issues such as HPHT, complex geology, greater water depth, and high rig rental and operating costs make oil and gas exploration and exploitation today highly risky and extremely costly. Therefore, drilling operations in these extreme environments need reliable, chemically resistive and mechanically stable surface and subsurface tools and equipment with short- and long-term fail-safe capability to overcome the technical limitations of conventional tools.

Nanotechnology has demonstrated that nanostructured materials with special mechanical, chemical, thermal, electrical and tribological properties exhibit significantly higher strength, hardness, material toughness, corrosion resistance, ductility, elastic properties, thermal stability and heat conductivity, etc., compared to conventional materials, in spite of having the same chemical and material compositions. As these materials have a very low density and high mechanical strength, and show superior chemical resistance and excellent thermal stability, tailor-made nanomaterials or nanocomposites — either alone or in combination with other macrostructural, microstructural and nanostructural materials — can provide much lighter equipment with significantly higher mechanical, thermal, chemical and tribological performance for challenging drilling environments. This article describes the application of nanomaterials and nanotechnology in the development of superior nano-enhanced tools and equipment that can overcome critical operational issues found in extreme drilling and production environments.

INTRODUCTION

In spite of the availability of several alternative sources of energy, hydrocarbons are still the main source of energy for the global community and will continue to be so over the coming years. As the numbers of readily accessible hydrocarbon basins are diminishing quickly, and the easily recoverable oil and gas reserves are declining rapidly, the oil and gas industry is looking for new reserves of oil and gas in every corner of the earth. Due to the reduced chance of finding high volumes of oil and gas resources in shallow and simple geological structures either onshore or near offshore, there has been a progressive shift in drilling operations from simple drilling environments to complex and challenging drilling environments. This is reflected by increased drilling operations in deepwater and ultra-deepwater environments, high-pressure/high temperature (HPHT) conditions, complex geological areas, etc.

Analyses of past and present oil and gas field discoveries show that it is rarely possible today to find giant oil and gas reserves in traditional onshore and offshore exploration areas. According to Shihab-Eldin (2002)[1], the average field size of new discoveries in traditional onshore and offshore areas has declined from 220 million barrels of oil equivalent (MMBoe) per discovery in the 1960s to less than 50 MMBoe in the 1990s. As a result, the industry is now navigating new areas having complex geology, difficult subsurface conditions, greater water depth, etc. Because the ocean, which occupies three quarters of the earth, shows a high prospect of hydrocarbon resources in addition to other valuable marine resources[2], exploration activities are increasing in deepwater and ultra-deepwater offshore areas to meet the global energy demand. Today, the potential of discovering future giant oil and gas fields in deepwater environments is much higher than in onshore and shallow water environments[3]. Liesman (2000)[4] points out that the reserves at depths approaching a mile or more now represent the biggest single new oil resources for world communities. Published information indicates that currently more than 20% of the world's proven reserves are in complex, troublesome and technically challenging offshore geological structures. According to the production forecast of hydrocarbon resources, about 40% to 50% of hydrocarbon production will be from offshore fields[5] with challenging

drilling and production environments. This is why the industry needs a new generation of tools and equipment with superior mechanical, physical, thermal and chemical stability for safe, economic and risk-free operation in complex and challenging drilling environments both onshore and offshore.

Due to the limited hydrocarbon production possible from conventional vertical boreholes, operators are shifting from vertical drilling to horizontal, extended reach and multilateral drilling, which significantly increases the complexity of drilling operations. The industry is also applying new drilling technologies, such as casing while drilling, expandable liner drilling, coiled tubing (CT) drilling, etc., for safer and more economic, efficient and trouble-free drilling operations. In addition, pioneering research on cutting-edge drilling technologies, such as laser drilling, cavitation jet drilling, resonance drilling, plasma drilling, thermal drilling, etc., is working to overcome the drilling challenges in current and future drilling operations. Technical challenges associated with development of this cutting-edge technology needed for future drilling and production in extreme environments have created a demand for new materials with characteristics that go well beyond the current materials' properties. As a result, the oil and gas industry is seeking a range of new materials to use in the design of high performance tools, equipment, sensors and instruments, seals and elastomers, as well as for drilling, drill-in, and completion and stimulation fluids, enabling them to overcome the technical challenges of extreme drilling environments. According to Amanullah and Al-Tahini (2009)[6] and Amanullah (2013)[7], the superior physicochemical characteristics and thermomechanical properties of nanomaterials and the application of nanotechnology can provide a viable avenue to overcoming those challenges.

Today's added operational complexities and environmental extremes demand radical changes in conventional tools, equipment, seals, elastomers, fluid additives, etc. For example, the changing complexity of well profiles and their increasing horizontal reach require tools that are physically lighter but mechanically stronger. Ultra HPHT drilling conditions demand equipment that has higher thermal, mechanical and chemical stability to avoid otherwise frequent failure. The seals and elastomers used in downhole tools need superior material characteristics to remain functional in extreme drilling environments. Similarly, the drilling, drill-in and completion fluids used in making a borehole require chemicals and additives that are capable of preventing their short- and long-term degradation in high temperature and high acid gas environments.

As a result, the development of extreme environment drilling and production tools and equipment is rarely possible using conventional microstructural materials due to their technical limits. Such development demands materials having characteristics that go far beyond current materials' properties. The superior physical, mechanical, chemical and thermal properties of nanomaterials suggest that they can have a significant effect on improving techniques, technologies, material properties and fluid characteristics required in extreme drilling and production environments. This article describes the application of nanomaterials and nanocomposites to overcome the limitation of conventional tools, equipment, seals, elastomers and fluid systems and to eliminate or mitigate the effect of critical factors in extreme drilling environments.

CONVENTIONAL TOOLS AND EQUIPMENT LIMITATIONS

Figure 1 shows the thermal stability limits of various tools and equipment used in current oil and gas exploration and exploitation. Figure 2 shows the range of pressures and temperatures likely to be encountered in normal and extreme drilling environments around the globe. The data presented in Fig. 1 clearly shows that most of the conventional tools and equipment available for exploration and exploitation of oil and gas resources will rarely work at temperatures above 450 °F. Analyses of current global drilling reports and activities indicate that the pressure and temperature of extreme drilling environments can exceed 25,000 psi and 500 °F in some onshore and offshore wells. Table 1 shows the drilling and completion gaps in the analysis data[8]. The data clearly shows major technology gaps in the areas of equipment limitation and fluid stability in HPHT conditions, reducing the likelihood of safe, economic

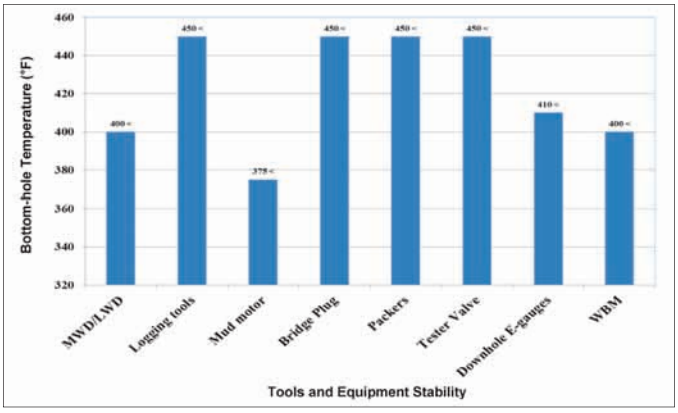

Fig. 1. Safe working temperature of conventional tools and equipment.

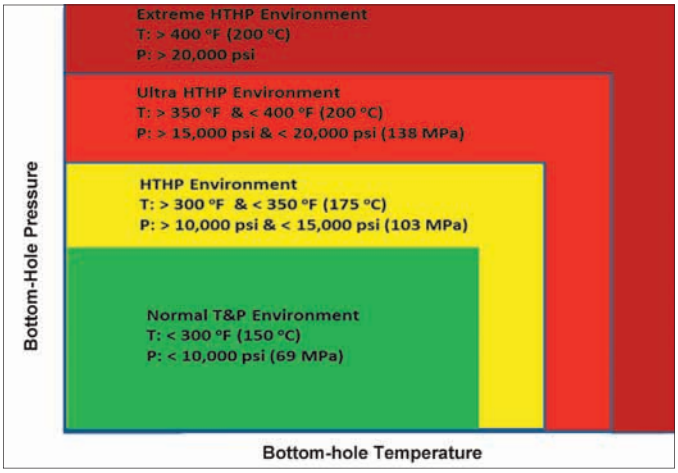

Fig. 2. Pressure and temperature regimes in normal and HPHT environments.

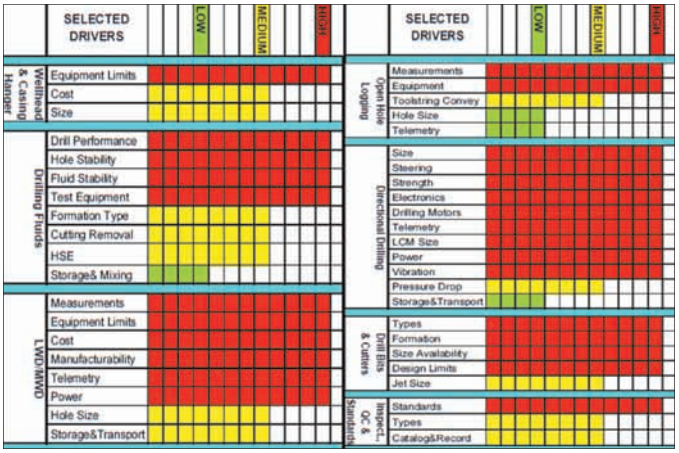

Table 1. Drilling and completion gaps in a HPHT environment[8]

and trouble-free drilling operations in such an environment.

Other than pressure and temperature, factors such as borehole profile, in situ stress regime, complexity in the subsurface geology, the nature of formation-related drilling hazards, etc., govern the performance and stability of the tools, equipment and fluid systems used in extreme drilling environments. Furthermore, field experience has shown that the actual overall stability limit of conventional tools and equipment even falls below the company supplied stability values.

At and above the mechanical, thermal, chemical, etc., stability limit, the equipment shows speedy degradation, frequent failure and eventually loss of functional capability due to the severe damage, permanent deformation and rapid wear of tools, seals and elastomers, pistons and liners, etc. The corrosion and erosion of equipment, especially severe in the presence of high concentrations of acid gases typical of extreme drilling environments, also dramatically reduces its lifetime. That is the reason why the industry needs a new generation of tools, equipment and fluid systems with superior mechanical, thermal, chemical, etc., stability limits.

The current microstructural composite-based tools and equipment used in oil and gas fields, and also the micro-size drilling and completion fluid additives, often show poor performance in extreme drilling environments, such as in ultra HPHT conditions, in deepwater and ultra-deepwater wells, in horizontal and extended reach drilling, in high acid gas environments and in areas with complex subsurface geology. Intricate geology containing highly reactive and gumbo shales, tectonically active zones, mobile formations and extremely abrasive rocks often causes serious damage to conventional tools and equipment due to the technical limits of their materials.

The need therefore is to improve the conventional material characteristics well above their current technical limits in properties such as strength, strength-to-weight ratio, torsional resistance to failure, fatigue and wear resistance, and thermal and chemical stability. The application of emerging nanotechnology, shown to dramatically improve the physical, mechanical, thermal and chemical properties in steel nanocomposite, offers a viable solution to ensure fail-safe operation of tools and equipment in extreme drilling environments.

COMPOSITE MATERIAL

Composite material is composed of two or more distinct phases of a material with each phase having different properties. The property of the composite is the combined effect of these phase properties. One phase of the composite is the continuous phase, also known as the matrix phase. Another phase of the composite is the noncontinuous phase, also known as the dispersed or reinforcing phase. Due to the joint effect of matrix and dispersed phases, the composite material has significantly different bulk properties than its constituent phases.

The dispersed phase, which is the stronger phase, is embedded in the matrix phase. Based on the particle size of the dispersed phase, a composite can be microstructural or nanostructural. A composite with a nanostructural particle size is known as a nanocomposite. According to Ajayan et al. (2003)[9], nanocomposite materials can be defined as either multiphase solid materials where one or more phases have one or more dimensions less than 100 nanometers, or solid materials that have internal structures with nano-scale repeat distances between the different phases that make up the material. The definition can be further refined: in a simple nanocomposite, the solid material has only one nanomaterial phase in the solid matrix, while in a complex nanocomposite, the solid material has two or more phases of nanomaterials in the composite material.

Nanocomposite material has physical, mechanical, chemical and thermal properties superior to those of a micro-composite material. This is the result of the incorporation of nano-sized internal phases within the bulk matrix of the solid material. It is the superior nanophase properties that cause the properties of the nanocomposite to differ so drastically from conventional composite materials. A critical size range of nanoparticles plays a dominant role in achieving a particular technical effect. According to Kamigaito (1991)[10], a size limit of less than 5 nm is needed for catalytic activity; a size limit of less than 20 nm is required to turn a hard magnetic material into a soft magnetic material; a size limit of less than 50 nm is required for altering the refractive index of the materials; and a size limit of less than 100 nm is required for achieving superparamagnetism, mechanical strengthening, matrix stiffening, deformation characteristics or dislocation behavior alterations, or movement of fabrics and structural units.

Conventional oil and gas field tools and equipment are made of microstructural-based composite materials and so have severe technical limitations for achieving safe operation in extreme drilling and production environments. Incorporation of nanophase material in a bulk matrix can significantly enhance the technical limits of composite material. As a result, the use of nanocomposite materials in the oil and gas field tools and equipment can dramatically improve their technical properties. A variety of nanomaterials with different morphological

characteristics can be used to prepare nanocomposites for different applications.

RULE OF MIXTURES

The rule of mixtures is a method to derive an approximate calculation of composite material properties; it is based on the assumption that a composite property is the volume of weighted average of the matrix and dispersed phases. Appropriate equations based on composite mixing rules were used to calculate the density, tensile strength and elasticity (the Young's modulus) of a nanocomposite, and then the percentage reduction in weight, percentage enhancement of tensile strength and percentage enhancement of stiffness (the Young's modulus) in the nanocomposite compared to the matrix phase material.

Tables 2, 3 and 4 show the dispersed phase's weight percentage (wt%) and volume in the nanocomposite material along with, respectively, the nanocomposite's density and weight reduction, its Young's modulus and stiffness enhancement, and its tensile strength enhancement, all due to the incorporation of nanomaterial into the bulk matrix. Mass concentrations of nanomaterial ranging from 5% to 25% were used in predicting the changes in the physical and mechanical properties of the nanocomposite compared to those of the original matrix phase material. Here, steel was used as the matrix phase material and a single-wall carbon nanotube (SWCNT) as the dispersed phase material to demonstrate the effect of nanos in enhancing the technical properties of nanocomposites.

NANOPHASE EFFECT ANALYSES

Based on the theoretically derived functional relations between the nanophase material concentration and several material characteristics, it can be concluded that the emerging nanotechnology and the tiny nanomaterial can have a significant effect in the design and development of superior tools and equipment to ensure trouble-free, safe and economic drilling and production operations in extreme environments. Due to the enhancement of their physical, mechanical, thermal, chemical, tribological, etc., properties, nanocomposite and nano-based additives can eliminate the detrimental effects of all of the critical factors associated with extreme drilling and production environments.

TOOLS AND EQUIPMENT WEIGHT REDUCTION

Figure 3 shows the densities of two nanomaterials (SWCNT and a multi-wall carbon nanotube (MWCNT)) and several conventional materials. This data indicates that the SWCNT had the second lowest density compared to the densities of other materials shown. Due to the lower density of the SWCNT compared to the MWCNT, it was used in the theoretical

Parameters	Dispersed Phase Weight (gm)	Dispersed Phase Volume (cc)	Nanocomposite Density (gm/cc)	Weight Reduction (%)
Steel-SWCNT 100:0	0	0.00	7.8	0
Steel-SWCNT 95:5	5	2.78	6.69	14.29
Steel-SWCNT 90:10	10	5.56	5.85	25.00
Steel-SWCNT 85:15	15	8.33	5.20	33.33
Steel-SWCNT 80:20	20	11.11	4.68	40.00
Steel-SWCNT 75:25	25	13.89	4.25	45.45

Matrix Phase Density = 7.8 gm/cc Dispersed Phase Density = 1.8

Table 2. Weight reduction based on wt% of dispersed phase in the matrix phase

Parameters	Dispersed Phase Weight (gm)	Dispersed Phase Volume (gm)	Nanocomposite Young's Modulus (GA)	Stiffness Enhancement (%)
Steel-SWCNT 100:0	0	0	208	0
Steel-SWCNT 95:5	5	2.78	317.94	52.86
Steel-SWCNT 90:10	10	5.56	400.40	92.50
Steel-SWCNT 85:15	15	8.33	464.53	123.33
Steel-SWCNT 80:20	20	11.11	515.84	148.00
Steel-SWCNT 75:25	25	13.89	557.82	168.18

Matrix Phase Young's Modulus = 208 (GA) Dispersed Phase Young's Modulus = 800 (GA)

Table 3. Stiffness enhancement based on wt% of dispersed phase in the matrix phase

Parameters	Dispersed Phase Weight (gm)	Dispersed Phase Volume (cc)	Nanocomposite Tensile Strength (GA)	Strength Enhancement (%)
Steel-SWCNT 100:0	0	0	0.4	0
Steel-SWCNT 95:5	5	2.78	5.90	1,374
Steel-SWCNT 90:10	10	5.56	10.02	2,405
Steel-SWCNT 85:15	15	8.33	13.23	3,207
Steel-SWCNT 80:20	20	11.11	15.79	3,848
Steel-SWCNT 75:25	25	13.89	17.89	4,373

Matrix Phase Tensile Strength = 0.4 (GA) Dispersed Phase Tensile Strength = 30 (GPa)

Table 4. Tensile strength enhancement based on wt% of dispersed phase in the matrix phase

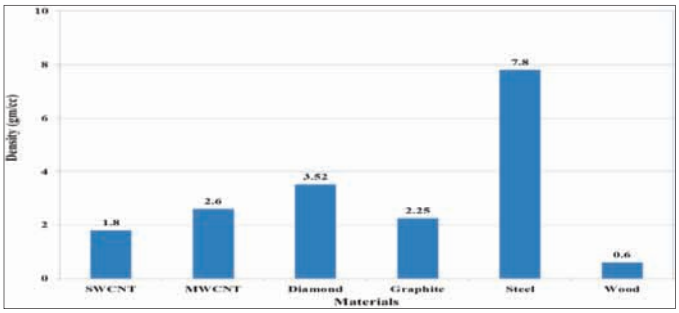

Fig. 3. Density of several conventional and nano-based materials.

blending of different wt% of nanomaterials with steel to prepare hypothetical nanocomposite samples and evaluate the tiny nano effect on the mighty steel phase of a carbon nanotube (CNT) steel nanocomposite. The mixing rule theory and equation was used for composite density calculation to determine the reduction in density due to the incorporation of a particular percentage of nanophase material into the bulk matrix of the steel.

Figure 4 shows the percentage reduction of nanocomposite weight with respect to the weight of pure steel material. The data clearly shows that the blending of different percentages of SWCNTs with steel can dramatically reduce the composite density and so can provide an avenue for manufacturing lightweight equipment, tools and tubular for oil and gas field applications, especially important for extreme drilling environments that require lighter but stronger tools and equipment. Further,

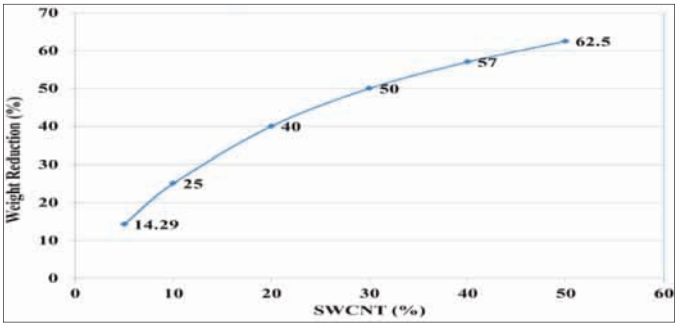

Fig. 4. Weight reduction potential of tools and equipment using nanocomposite materials.

the same application of nanomaterials in the manufacture of nanocomposites to develop lightweight but stronger casing, drillpipes, CT, surface equipment and other rig accessories will enhance the safe operational limits of these tools and equipment in extreme drilling environments. As a result, the challenges associated with using conventional tools and equipment in horizontal and extended reach drilling, HPHT drilling, deepwater drilling, casing while drilling, etc., will be removed or reduced significantly.

Figure 4 also shows the theoretical values of weight reduction due to the incorporation of specific concentrations of a nanophase SWCNT into the bulk steel matrix. The data clearly shows a progressive decrease in the weight of the SWCNT steel nanocomposite with increasing concentrations of the nanophase material. But even small concentrations are effective; the incorporation of 5% SWCNTs (w/w) into the steel matrix shows a weight reduction of more than 14%. Therefore, the designs for tools and equipment, including drillpipes and casing, measurement while drilling/logging while drilling (MWD/LWD) sensors, mud motors, CT, etc., that use the SWCNT steel nanocomposite or similar nanocomposite materials will reduce the equipment weight significantly. The data further indicates that the use of a steel matrix nanocomposite with as little as 5% SWCNT will provide tools and equipment more than 14% lighter compared to conventional tools and tubular.

The lighter weight and enhanced strength bring many benefits. For example, the nanocomposite-based drillpipe will create lower torque and drag requirement problems, along with a reduction in the frictional resistance while drilling. This type of drillpipe will also allow high weight transfer to the bit as this now will have no detrimental effect on drillpipe strength. Indeed, the nanocompsite will enhance the mechanical strength of the pipes significantly, which will be discussed later. The lighter weight and higher mechanical properties, in turn, will extend the technical limits of extended reach drilling operations, enabling longer laterals. The lower frictional resistance will improve the rate of penetration (ROP), with a positive impact on well construction cost. Moreover, the lightweight tubular will provide greater ease of handling in the assembling and

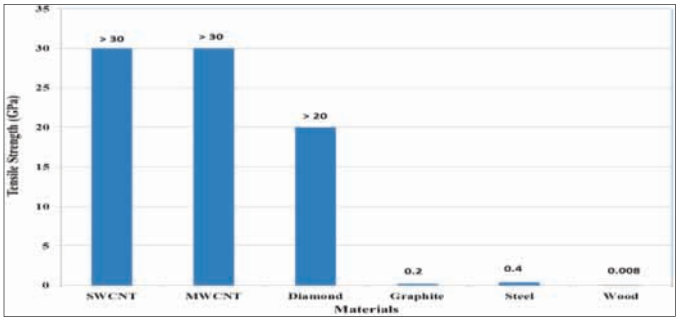

Fig. 5. Tensile strength of several conventional and nano-based materials.

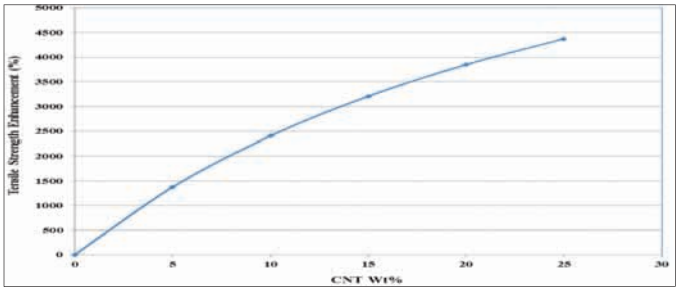

Fig. 6. Tensile strength enhancement potential of tools and equipment using nanocomposite materials.

disassembling of the different components of surface and subsurface tools and equipment. Due to the weight reduction of surface and subsurface tools and equipment, drillpipes and casings, and other auxiliary tools and equipment, operators can use a smaller rig for drilling and workover operations along with less energy.

TOOLS AND EQUIPMENT STRENGTH ENHANCEMENT

Figure 5 shows a bar graph comparing the tensile strength of the two nanomaterials and several conventional materials, including steel. The data indicates that SWCNT and MWCNT have the highest tensile strength compared to the tensile strength of other materials. (To maintain consistency with the theoretical nanocomposite preparation used in the earlier analyses of the nanophase effect, SWCNTs were used in the theoretical nanocomposite preparation here, even though the MWCNT has similar strength properties.) A different wt% of SWCNTs was used in the theoretical blending of the dispersed phase nanomaterial with the continuous phase steel to prepare hypothetical nanocomposite samples. The mixing rule theory and equation was used for composite tensile strength calculation to determine the enhancement in tensile strength due to the incorporation of a particular percentage of nanophase material into the bulk matrix of the steel.

Figure 5 also shows the percentage enhancement of nanocomposite tensile strength with respect to the tensile strength of pure steel material. The data clearly shows that the blending of different percentages of SWCNTs with steel can dramatically improve the tensile strength of the nanocomposite material and so can provide an avenue for manufacturing very high strength equipment, tools and tubular for oil and gas field applications, especially important for extreme drilling environments that require stronger, more robust tools and equipment. Further, the same application of nanomaterials in the preparation of a steel-matrix nanocomposite to develop very strong but significantly lighter casing, drillpipes, CT, surface equipment and other rig accessories will enhance the operational limits of such tools and equipment in extreme drilling environments. As a result, the challenges associated with using conventional tools and equipment in horizontal and extended reach drilling, HPHT drilling, deepwater drilling, casing while drilling, etc., will be removed or reduced dramatically.

The theoretical values of the strength enhancement of the nanocomposite due to the incorporation of specific concentrations of a SWCNT into the bulk steel matrix are shown in Fig. 6. The data clearly shows a dramatic increase in the tensile strength of the SWCNT steel nanocomposite with increasing concentrations of the nanophase material. But even small concentrations are effective; the incorporation of 5% SWCNTs (w/w) into the steel matrix shows a tensile strength enhancement of more than 1,000%. As a result, the designs for tools and equipment, including drillpipes and casing, MWD/LWD sensors, mud motors, CT, etc., that use the SWCNT steel nanocomposite or similar nanocomposite materials will improve the equipment stability dramatically in extreme drilling and production environments. The data further indicates that the use of a steel matrix nanocomposite with as little as 5% SWCNT will provide tools and equipment more than 1,000% stronger than conventional tools and tubular.

Again, the benefits of this extremely high tensile strength, compared to conventional steel-based tools and pipes, are many. The nanocomposite-based drillpipe will eliminate or significantly reduce drillstring parting, twist off, bending, etc., while drilling. In addition to the drillstring components, surface and other subsurface tools and equipment will also show considerable improvement in mechanical stability, leading to a dramatic reduction in oil and gas exploration and exploitation risk in extreme drilling and production environments. The more robust and stronger drillstring components will allow higher weight transfer to the bit without any or with only negligible detrimental effect on subsurface tools and equipment. The combined effect of very high mechanical properties with the significant drop in the weight of nanocomposite-based tools and equipment previously described will extend the technical limits of extended reach drilling operations, enabling longer laterals. The higher resistance to bending will reduce torque and drag problems, improve ROP and ensure fail-safe operation by overcoming the detrimental effects of critical factors associated with extreme drilling environments. As a result, the emerging nanotechnology and nanocomposite materials will play a pivotal role in mitigating exploration and production risk, well construction cost and nonproductive time, even as it improves operational safety while drilling in challenging environments. The enhancement of the mechanical properties of surface and subsurface tools and equipment by using

nanocomposite materials will cause a dramatic reduction in the frequency of failure for main and auxiliary rig equipment.

TOOLS AND EQUIPMENT STIFFNESS ENHANCEMENT

Figure 7 shows a bar graph comparing the Young's modulus of the two nanomaterials and several conventional materials, including steel. The data indicates that SWCNT and MWCNT have a Young's modulus nearly four times higher than that of steel. (As before, for reasons of consistency, SWCNT was used in the theoretical nanocomposite preparation for studying material stiffness, even though the MWCNT has similar properties.) Different wt% of SWCNTs was used in the theoretical blending of the dispersed phase nanomaterial with continuous phase steel to prepare hypothetical nanocomposite samples. The mixing rule theory and equation was used for the composite Young's modulus calculation to determine the enhancement in tensile strength due to the incorporation of a particular percentage of nanophase material into the bulk matrix of the steel.

Figure 8 shows the percentage enhancement of the nanocomposite's Young's modulus with respect to the Young's modulus of pure steel material. The data clearly shows that the blending of different percentages of SWCNTs with the continuous phase steel can dramatically improve the stiffness of the nanocomposite material and so can provide an avenue for manufacturing highly stiff pipes, tools, CT and other tubular for oil and gas field applications, especially important for extreme drilling environments that require very stiff material to resist the detrimental effect of associated critical factors. The

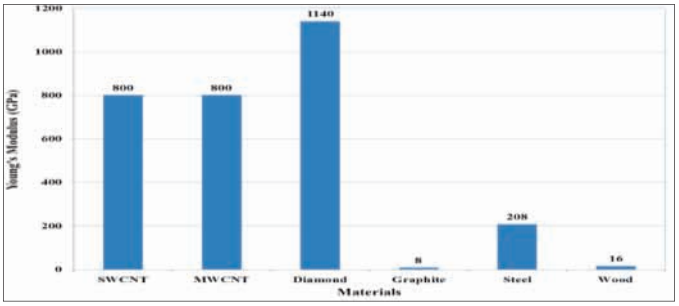

Fig. 7. Young's modulus of several conventional and nano-based materials.

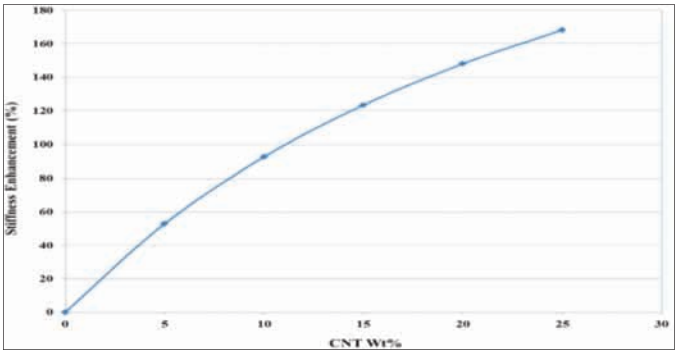

Fig. 8. Stiffness enhancement potential of tools and equipment using nanocomposite materials.

dramatic improvement of pipe and tool stiffness will enhance the technical limit, and therefore, the mechanical stability of the tools and equipment used in extreme drilling environments. Therefore, the problems associated with less stiff conventional tools and equipment in horizontal and extended reach drilling, HPHT drilling, deepwater drilling, casing while drilling, etc., will be removed permanently or reduced dramatically.

Figure 8 also shows the theoretical values of the material stiffness enhancement of the nanocomposite due to the incorporation of specific concentrations of a SWCNT into the bulk steel matrix. The data clearly shows a dramatic increase in the material stiffness of the SWCNT steel nanocomposite with increasing concentrations of the nanophase material. But even small concentrations are effective; the incorporation of 5% SWCNTs (w/w) into the steel matrix shows a stiffness enhancement of more than 50%. As a result, the designs of tools and equipment, including drillpipes and casing, MWD/LWD sensors, mud motors, CT, etc., that use the SWCNT steel nanocomposite or similar nanocomposite materials will improve the equipment stability dramatically in extreme drilling and production environments.

The benefits of the very high Young's modulus, compared to those of conventional steel-based tools and pipes, are similar to those from greater tensile strength. The nanocomposite-based drillpipe will eliminate or reduce drillstring parting, twist off, bending, etc., while drilling. In addition to the drillstring components, surface and other subsurface tools and equipment will also show dramatic improvement in mechanical stability, leading to a dramatic reduction in oil and gas exploration and exploitation risk in extreme drilling and production environments. The greater stiffness of nanocomposite-based drillpipes, tool joints, stabilizers and other components will lead to significant improvement of the drillstring stability and allow higher weight transfer to the bit without any detrimental effect on the drillstring. The combined effect of reduced pipe/tubular weight, very high material stiffness and the extremely high tensile strength of nanocomposite-based tools and equipment will extend the technical limit for safely operating the equipment to a level that is unimaginable with conventional pipes, tools and equipment. This again demonstrates the mighty effect of tiny nanos on the physical and mechanical behavior of tools and tubular. As a result, the emerging nanotechnology and nanocomposite are expected to play a pivotal role in mitigating exploration and production risk, well construction cost and nonproductive time, even as it improves operational safety and equipment reliability in an extreme drilling environment, where equipment is at perpetual war with numerous critical factors. Due to the highly positive technical effect of the nanophase material, nanocomposites will cause a dramatic reduction in the frequency of failure of surface and subsurface equipment in challenging drilling and production environments.

POTENTIAL OIL AND GAS FIELD APPLICATIONS

The examples previously mentioned discuss only the enhancement of the physical and mechanical properties of bulk steel by incorporating different percentages of nanomaterial into the bulk material matrix. Published information on nanomaterial applications in various types of nanocomposites highlights the improvement of a variety of other material characteristics, such as shock absorption and vibration dampening potential, wear resistance, intelligent response, thermal stability, chemical resistance and tribological characteristics, etc. A review of several of the nanocomposites or nanomaterials described by various authors follows to demonstrate their potential applications in the oil and gas industry.

HIGHLY STABLE CT

Conventional CT has poor buckling resistance due to the insufficient stiffness of the steel alloy used to manufacture the tubing. That is why current CT has limited performance in horizontal and extended reach drilling operations. Figure 9 shows the buckling failure of CT[11]. This buckling failure occurred under the action of compressive forces due to insufficient material stiffness. It may be mentioned that the lower the stiffness of a material, the poorer the material's resistance to buckling failure under the compressive load. Improvement of CT composite material stiffness by incorporating one or more nanophase materials will prevent the delamination tendency of CT under the action of bending forces, and so reduce the chance of buckling failure significantly.

The greater stiffness of the nanocomposite-based CT will allow a stronger push to the bottom-hole assembly while drilling ahead and a stronger pull in case of a stuck pipe condition without damaging or parting the pipe/CT. Nanocomposite-based CT having two nanophase materials can improve the tube stability dramatically due to simultaneous enhancement of compressive and tensile stiffness. For example, simultaneous incorporation of nano-sized boron fiber and tubular CNTs in a metal matrix creates a nanocomposite material that can significantly improve the compressive and tensile stiffness of the tube.

As a result, the tube will offer very high resistance to tensile, compressive and biaxial loading, leading to a dramatic improvement in the CT stability. The more than 50% increase in the stiffness of CNT steel composite described earlier highlights the potential application of nanomaterials in enhancing the mechanical properties of CT. The greater stiffness of the CNT steel nanocomposite will prevent easy delamination of CT in horizontal and extended reach wells, which can significantly improve operational safety and efficiency.

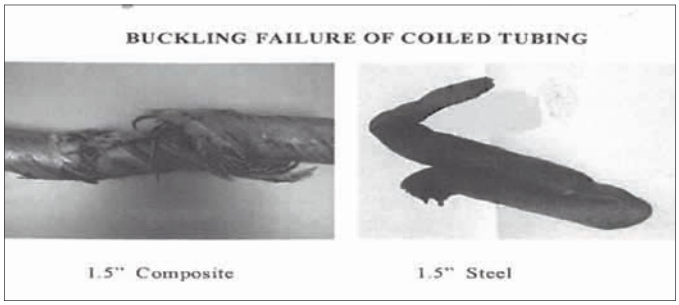

Fig. 9. Buckling failure of conventional CT under compressive force[11].

HIGH WEAR RESISTANT TOOLS AND EQUIPMENT DESIGN

The quick wear of a conventional drill bit, stabilizer, reamer, drillpipe, etc., in the presence of abrasive formations and/or extreme drilling conditions dramatically reduces the drilling performance due to the need for frequent replacement of torn out bits, stabilizers or reamers. The potential solution to this problem is improvement in the wear resistance of these tools and equipment, enough to overcome the abrasive and detrimental factors associated with extreme drilling environments. It has been demonstrated[12] that the incorporation of a nanophase material into the continuous phase of a metal, or its bulk matrix, can improve the material toughness significantly, leading to a significant increase in wear resistance, Fig. 10.

According to the experimental data presented, incorporation of only 0.5% MWCNT into the bulk matrix can significantly improve hardness and wear resistance. It again highlights the application of emerging nanotechnology to create superior tools and equipment design that can reduce wear resistance in abrasive borehole environments. The application of suitable nanocomposite materials in bit designs for extreme drilling environments can significantly improve the bit performance and can play an important role in significantly reducing well construction costs. This also highlights the importance of integrating the emerging nanotechnology in the development of superior material for highly stable tools and equipment design.

HIGH VIBRATION DAMPENING TOOLS AND EQUIPMENT DESIGN

As vibration is one of the issues causing failure of the drillstring, an improvement in the vibration dampening characteristics of the elements of the drillstring can eliminate or reduce

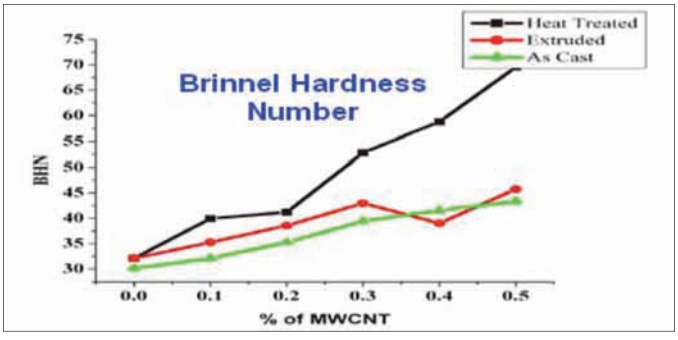

Fig. 10. Improvement in hardness due to the incorporation of MWCNT in a nanocomposite under three conditions[12].

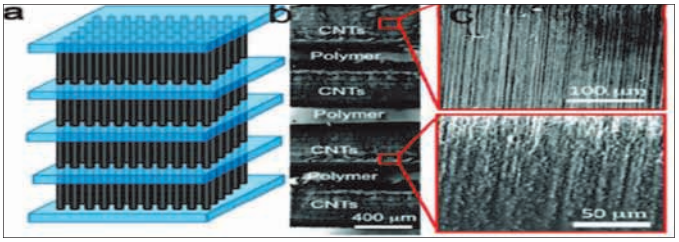

Fig. 11. Multilayer CNT polymer assembly[13]: (a) schematic of four-layer CNT polymer structure, (b) optical image of CNT polymer structure, and (c) SEM image of the CNT array.

the failure or damage associated with axial, torsional or lateral vibration of the drillstring while making a borehole. Vibration is also one of the major factors in the failure of downhole tools and equipment in extreme drilling environments, since conventional oil and gas field tools and equipment have poor vibration dampening characteristics. Incorporation of shock absorbing nanophase material in the design of tools and equipment can significantly improve their vibration dampening characteristics. As a result, the emerging nanotechnology can play an important role in the manufacturing of tools, equipment, seals, elastomers, etc., prone to failure due to vibration. Misra et al. (2011)[13] demonstrates the effect of shock absorbing CNT in the vibration dampening of a polymer CNT assembly, Fig. 11. According to the authors, the CNT polymer assembly has a shock absorbing capacity at least three times larger than that of natural and synthetic cellular foam materials of comparable densities. In addition to CNTs, inorganic fullerene, fullerene boron, silicon carbides or other shock absorbing nanomaterials can be used in improving the vibration dampening characteristics of tools and equipment.

RUBBER, SEALS AND ELASTOMER QUALITY IMPROVEMENT

Downhole pressures and temperatures likely to be encountered in current and future HPHT and deepwater environments can vary significantly, depending on the location, subsurface geology, and tectonic and volcanic activities of the areas. Conventional seals, rubbers and elastomers rarely survive the detrimental effect of extreme conditions, such as high temperature, pressure, acid gases, etc. Extreme HPHT environments place tremendous stress on any elastomeric material, leading to permanent deformation, structural distortion, a decrease in ductility and an increase in brittleness due to the poor thermal, physical and mechanical stability of conventional seals and elastomers. Therefore, improvement of the thermal, mechanical, and chemical properties of rubbers, seals and elastomers is very important to improve the life cycle of these elements in extreme drilling environments. Given the superior physical, mechanical, thermal, and chemical properties of nano-based materials, incorporation of nanophase material in the bulk matrix of seals, rubbers or elastomers can dramatically improve the technical limit of these elements.

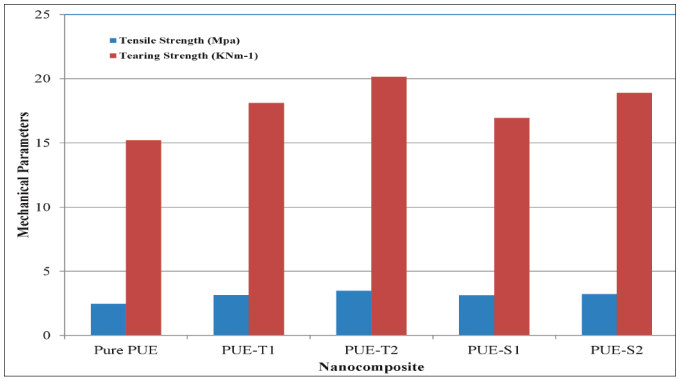

Fig. 12. Comparison of pure polyurethane (PUE) and nanocomposite polyurethane properties.

Wu et al. (2013)[14] describes the improvement in the flame retardant performance and mechanical properties of a polyurethane elastomer due to the surface modification of the elastomer by incorporating TiO_2 and SiO_2 nanoparticles. According to the authors, the surface modification of the polyurethane using nanophase materials has significantly enhanced the thermal and flame retardant characteristics of the elastomers. The authors further highlight the improvement of the mechanical properties of the composite due to the dual effect of the uniform dispersion of the nanoparticles and the hydrogen bonding between the nanoparticles and polyurethane, Fig. 12. The study demonstrates the potential application of nanomaterials in improving the technical limits of conventional elastomers, seals and rubbers to produce superior performance in extreme drilling environments.

ACID GAS ENVIRONMENTS

Corrosion is one of the main factors that can have tremendous effect on the durability of oil and gas field equipment. Very severe corrosion occurs in extreme drilling environments, such as in HPHT and high acid gas containing boreholes. As a result, conventional steel tools and equipment often show poor performance in those circumstances. A major improvement in the working life and functional ability of surface and subsurface tools and equipment dictates the elimination and/or mitigation of corrosive action as one of the critical factors in extreme drilling environments. Therefore, development of either very efficient, long-lasting and highly durable corrosion inhibitors or tools and equipment that are resistant to corrosive attack is needed to provide a viable solution to this problem. Rather than adding corrosion inhibition to special equipment design, development of highly efficient corrosion inhibitors can serve as an alternative solution. Development of nano-based corrosion inhibitors can provide a particularly efficient solution to equipment failure.

Due to the microstructural size of conventional acid gas scavengers, the specific surface area available for their interaction with, and neutralization of, harmful acid gases is very small. Therefore, the interaction kinetics is very slow, and the

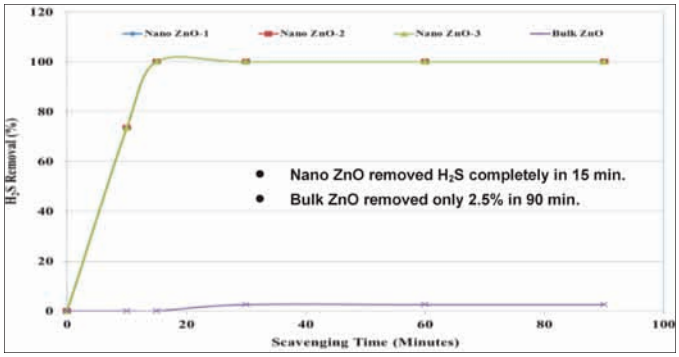

Fig. 13. Comparison of the H_2S neutralizing potential of nano ZnO and bulk ZnO[15].

efficiency of their neutralization of acid gases is very low. That is why conventional acid gas scavengers often show poor performance in neutralizing acid gases in high acid gas concentration areas. On the other hand, due to the huge specific surface area available for the interactions of nano-based materials, nano-based acid gas scavengers can quickly neutralize a huge volume of acid gases while drilling, and so provide a safe and hazard-free working environment with minimum risk of hydrogen sulfide (H_2S) exposure. Sayyadnejad et al. (2008)[15] demonstrates the dramatic effect of nano-size zinc oxide (ZnO) in neutralizing a huge volume of H_2S within a short period of time, Fig. 13. According to the experimental results described by the authors, the use of conventional ZnO in one experiment showed only 2.5% removal of H_2S in 90 minutes. On the other hand, the use of nano-based ZnO in another experiment showed complete neutralization and removal of acid gases in 15 minutes. The extremely high surface area-to-volume ratio of nanos, compared to those of micros and macros, allows nanocomposites to incorporate a huge number of functional groups for effective neutralization of the acid gases that enter the well while drilling. Therefore, the scavenging action of nanocomposites can eliminate H_2S gas totally and very quickly after its entry into the wellbore, with a drastic improvement in the working environment, the occupational health and safety of workers and the mechanical stability of the drilling equipment.

ACKNOWLEDGMENTS

The authors would like to thank the management of Saudi Aramco for their support and permission to publish this article.

This article was presented at the Abu Dhabi International Petroleum Exhibition and Conference, Abu Dhabi, UAE, November 10-13, 2014.

REFERENCES

1. Shihab-Eldin, A.: "New Energy Technologies: Trends in the Development of Clean and Efficient Energy Technologies," *OPEC Energy Review*, Vol. 26, No. 4, December 2002, pp. 261-307.
2. Amanullah, M. and Yu, L.: "Environment Friendly Fluid Loss Additives to Protect the Marine Environment from the Detrimental Effect of Mud Additives," *Journal of Petroleum Science and Engineering*, Vol. 48, Nos. 3-4, September 2005, pp. 199-208.
3. Bell, M.R.G.: "A Case for Nanomaterials in the Oil and Gas Exploration and Production Business," paper presented at the International Congress of Nanotechnology (ICNT), San Francisco, California, November 7-10, 2004.
4. Liesman, S.: "Big Oil Starts to Tap the Vast Reserves That Are Buried Far below the Waves," *Wall Street Journal*, July 3, 2000.
5. Amanullah, M. and Boyle, R.: "Experimental Evaluation of the Formation Strengthening Potential of a Novel Gel System," IADC/SPE paper 100436, presented at the Asia Pacific Drilling Technology Conference, Bangkok, Thailand, November 13-15, 2006.
6. Amanullah, M. and Al-Tahini, A.M.: "Nano-Technology — Its Significance in Smart Fluid Development for Oil and Gas Field Application," SPE paper 126102, presented at the SPE Saudi Arabia Section Technical Symposium and Exhibition, al-Khobar, Saudi Arabia, May 9-11, 2009.
7. Amanullah, M.: "Dendrimers and Dendritic Polymers — Application for Superior and Intelligent Fluid Development for Oil and Gas Field Applications," SPE paper 164162, presented at the SPE Middle East Oil and Gas Show and Conference, Manama, Bahrain, March 10-13, 2013.
8. Proehl, T.: "Drilling and Completion Gaps for HTHP Wells in Deep Water," DeepStar CTR7501, Final Report, Triton Engineering Services Company, 2006.
9. Ajayan, M., Schadler, L.S. and Braun, P.V.: *Nanocomposite Science and Technology,* John Wiley & Sons, 2003, 238 p.
10. Kamigaito, O.: "What Can Be Improved by Nanometer Composites?" *Journal of the Japan Society of Powder and Powder Metallurgy*, Vol. 38, No. 3, 1991, pp. 315-321.
11. McClatchie, D.W., Reynolds, H.A., Walsh, T.J. and Lundberg, C.: "Application Engineering for Composite Coiled Tubing," SPE paper 54507, presented at the SPE/ICoTA Coiled Tubing Roundtable, Houston, Texas, May 25-26, 1999.
12. Manjunath, L.H. and Dinesh, P.: "Development and Study on Microstructure, Hardness and Wear Properties of As Cast, Heat Treated and Extruded CNT — Reinforced with 6061al Metal Matrix Composite," *International Journal of Mechanical Engineering and Technology*, Vol. 3, No. 3, September - December 2012, pp. 583-598.
13. Misra, A., Raney, J.R., De Nardo, L., Craig, A.E. and Daraio, C.: "Synthesis and Characterization of Carbon Nanotube-Polymer Multilayer Structures," *ACS Nano*,

Vol. 5, No. 10, September 2011, pp. 7713-7721.

14. Wu, J., Yan, H., Wang, J., Wu, Y. and Zhou, C.: "Flame Retardant Polyurethane Elastomer Nanocomposite Applied to Coal Mines as Air-Leak Sealant," *Journal of Applied Polymer Science*, Vol. 129, No. 6, September 15, 2013, pp. 3390-3395.
15. Sayyadnejad, M.A., Ghaffarian, H.R. and Saeidi, M.: "Removal of Hydrogen Sulfide by Zinc Oxide Nanoparticles in Drilling Fluid," *International Journal of Environmental Science and Technology*, Vol. 5, No. 4, September 2008, pp. 565-569.

BIOGRAPHIES

Dr. Md. Amanullah is a Petroleum Engineering Consultant working at Saudi Aramco's Exploration and Petroleum Engineering Center – Advanced Research Center (EXPEC ARC). Prior to joining Saudi Aramco, he worked as a Principal Research Scientist at CSIRO in Australia.

Aman is the lead inventor of a vegetable oil-based dielectric fluid (patented) that led to the formation of a spinoff company in Australia for commercialization of the product.

He has published more than 70 technical papers and files 17 patents, with seven already granted. Aman is one of the recipients of the 2005 Green Chemistry Challenge Award, awarded by the Royal Australian Chemical Institute. He also received the CSIRO Performance Cash Reward in 2006, the Saudi Aramco Mentorship Award in 2008 and the World Oil Certificate Award for nano-based drilling fluid development in 2009. Aman is a member of the Society of Petroleum Engineers (SPE). He received the 2014 SPE Regional Service Award for his contribution to the industry.

Aman received his M.S. degree (First Class) in Mechanical Engineering from Moscow Oil and Gas Institute, Moscow, Russia, and his Ph.D. degree in Petroleum Engineering from Imperial College, London, U.K.

Dr. Jothibasu Ramasamy is a Petroleum Scientist with the Drilling Technology Team of Saudi Aramco's Exploration and Petroleum Engineering Center – Advanced Research Center (EXPEC ARC). He joined Saudi Aramco in July 2013. Prior to this, he worked as a Research Fellow with the Department of Chemistry at National University of Singapore and as a Postdoctoral Fellow with the Catalysis Center at King Abdullah University of Science and Technology (KAUST), Saudi Arabia.

Jothibasu received his B.S. degree in Chemistry from Bharathidasan University, Tiruchirappalli, India, and his M.S. degree, also in Chemistry, from Anna University, Chennai, India. In 2010, he received his Ph.D. degree in Chemistry from National University of Singapore, Singapore.

Intelligent Distributed Acoustic Sensing for In-well Monitoring

Authors: Dr. Jinjiang Xiao, Mahmoud Farhadiroushan, Andy Clarke, Rami A. Abdalmohsen, Essam M. Al-Alyan, Dr. Tom R. Parker, Dr. Janti Shawash and H. Craig Milne

ABSTRACT

Inflow control valves (ICVs) and inflow control devices (ICDs) can enable optimization of the production and injection profile along the wellbore. The ICVs are operated to increase hydrocarbon recovery and prevent unwanted fluid production. The ICVs are operated to optimize the production profile in multilateral zones. Although the operation of these devices is well understood, the optimization of these devices in situ is complex. The real-time monitoring of fluid flow along the wellbore can provide valuable information, which can then be used to set the positions of the ICVs and optimize the fluid flow in multilateral zones. In the water injector, the flow profile across ICD zones can be monitored in real-time while adjusting the surface choke.

The intelligent distributed acoustic sensor (iDAS) uniquely allows the simultaneous recording of acoustic energy along many kilometers of fiber optic cable deployed along the wellbore. The system uses a novel digital optoelectronics detection technique that captures the amplitude and phase of the acoustic waves generated and propagated along the wellbore over a wide frequency range, from 1 mHz to 100 kHz, and with a high dynamic range, >120 dB. A number of signal processing techniques have been developed for processing a large array of the acoustic data recorded along the wellbore for use in monitoring the inflow at different zones. The iDAS system can be used with both single mode and multimode fiber optic cable.

The iDAS system was retrofitted to the existing fiber optic cables already installed along several wells in Saudi Arabia to record the acoustic energy (noise) generated across the ICVs and ICDs and propagated along the wellbore tubing. The acoustic spectrum can then be used to monitor the fluid flow through the ICVs and ICDs. Further, using an array to process the data allows the speed of sound (SoS) to be determined over several sections of the tubing, which helps to identify the fluid composition.

This article reports on the results of the field trial in several wells equipped with ICVs and ICDs.

THE INTELLIGENT DISTRIBUTED ACOUSTIC SENSOR (iDAS) FIELD TRIAL SURVEY

The intelligent distributed acoustic sensor (iDAS) field trial campaign was conducted in multiple wells. These wells varied in their use, construction and the type of fiber optic cable installed. We report on the campaign's survey of the three wells outlined here.

Well-1 was a horizontal, open hole water injector equipped with inflow control devices (ICDs). This well was instrumented with multimode optical fiber.

Well-2 was a trilateral oil producer with inflow from each lateral controlled by an inflow control valve (ICV). The ICVs, along with the surface choke valve, are used to control the flow rates within the well. The well was also instrumented with a multimode fiber optic cable. The survey of this well was the first ever adoption of iDAS field measurement using a multimode fiber for flow profiling[1, 2].

Well-3 was also a trilateral oil producer with ICVs similar to those of Well-2 except that Well-3 was instrumented with only a single mode fiber optic cable, installed to monitor optical fiber gauges[3]. Also in contrast to Well-2, the laterals kick off from the motherbore much further away from their respective ICVs. This means the inflow from each lateral must flow through the annulus before entering the motherbore through the ICV. The data acquisition program in Well-3 was run alongside a seismic acquisition program.

The data was collected in three stages to ensure that each phase of the transitions between all test points was recorded. First, data was collected for a period of approximately 1 to 2 hours while the valve settings were changed. During this period, the flow regime and rate is transient, so data collected during this period is used mainly in diagnostics, ensuring the correct valves are being adjusted and indicating how the noise level within the well varies from setting to setting. Once the well had stabilized, data was collected for a further period of approximately 1 hour. This data can be used in the flow profiling analysis, using the sound generated within the wellbore from either ICV noise or the flow itself. Finally, data was collected with the well in the same condition but during simultaneous seismic acquisition. The energy put into the ground by the seismic vibration source generates tube waves within the wellbore that acoustically illuminate the production volume. A proprietary technique has been developed to process the data collected during seismic acquisition to produce enhanced measurements of the speed of sound (SoS) and calculations of the fluid velocity.

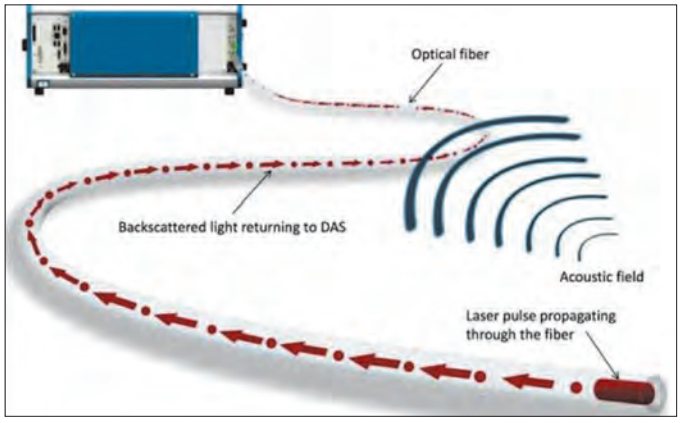

Fig. 1. Operating principle of the iDAS.

INTELLIGENT DISTRIBUTED ACOUSTIC SENSOR (iDAS)

As shown in Fig. 1, iDAS can be used to listen to the acoustic wave field at any position along a fiber optic cable[4-6]. In the case of a fiber optic cable installed in a well, iDAS can listen to the sound within the production volume along the entire wellbore. This sound can also be tracked as it travels within the production volume, which means it can be used to detect the speed at which the fluid is moving at every point within a well. At the same time, iDAS can look out into the formation and act as a seismic receiver. This means that a single fiber optic cable installation in a well can be used to both monitor the flow profile within the well and also image the surrounding formation.

We have developed a number of fast signal processing techniques to analyze the acoustic spectrum along the fiber optic cable. This enables us to characterize the acoustic energy (noise) generated along the wellbore by ICVs and ICDs. In addition, by using the array processing to analyze the propagation of the acoustic waves in space, time and frequency, we can monitor the fluid composition and calculate the fluid velocity by determining the SoS[4, 5].

DATA ANALYSIS

This section of the article will describe in greater detail the data processing techniques that were used in the analysis of this data set. The data was processed using two main approaches that treated the iDAS system: (1) as a set of many point sensors, and (2) as a distributed array of sensors. Considering each individual iDAS system on its own allows a physical quantity, such as the acoustic energy or the frequency spectrum, to be mapped along the wellbore at high resolution. In contrast, considering the iDAS system as a distributed array of sensors allows for the use of sophisticated signal processing techniques to detect things, such as the SoS for the propagating acoustic signals within the production fluid.

The first stage of processing was to correctly reference the iDAS receiver depth along the well. This can be done equally well in either the optical domain or the acoustic domain. The iDAS receiver channel corresponding to the wellhead was found by creating a controlled acoustic signal at the wellhead. Viewing the iDAS response enabled the exact receiver channel where this position calibration signal was detected to be found. In this particular well, the fiber gratings used for the flow meters installed in the well create reflections and losses in the optical signal. The detection of these features allowed each iDAS receiver channel to be accurately matched to a certain depth by checking the well completion details.

Root-Mean-Square (RMS) vs. Depth

An estimate of the amplitude of the acoustic signal over a defined period of time and at a specific position on the fiber optic cable can be made by calculating the root-mean-square (RMS) value of a single iDAS receiver channel. This analysis treats each iDAS receiver channel as an individual receiver. The RMS value is calculated using Eqn. 1:

$$RMS = \sqrt{\frac{\sum_l x^2}{l}} \quad (1)$$

where l is the length of time series in samples and x is the iDAS time series data.

The RMS levels were calculated to identify those noisy regions within the well that act as sound sources to acoustically illuminate the production fluid. The presence of a sound source within the well can greatly increase the signal-to-noise ratio (SNR) of the measurements by increasing the acoustic energy traveling within the production fluid.

Frequency Spectrum (FFT) vs. Depth

In addition to knowing the total acoustic energy measured at a specific depth in the well, it is also important to know the frequency content of that energy, again treating each iDAS receiver channel individually. The detection of propagating acoustic energy and the attenuation with distance of this energy is highly dependent on the frequency of the signal. Also, the frequency content of the noise at a specific location can be used to characterize that noise. For example, high frequency energy can be generated by high-pressure fluid passing through a small hole, such as through a perforation or a leak path. A frequency spectrum (FFT) analysis can highlight which noise sources within the well are generating the majority of the propagating acoustic energy.

The SoS is detected in the well only in regions where there is a sufficiently large distance between ICDs, which affords a greater length of continuous diameter tubing. The detected SoS, where detection is possible, is close to that expected of the SoS in water, ~4,900 ft/s. In the regions where upgoing and downgoing SoS detection was possible, the calculated flow speeds were much greater than expected and therefore do not show on the flow speed graph.

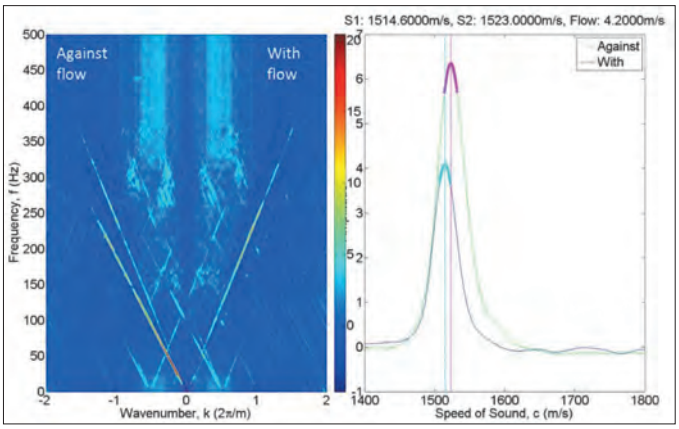

Fig. 2. SoS measurement showing upgoing and downgoing Doppler shift in the direction of the flow and f-k plot (left) and peak fit (right).

SoS and Flow

This data analysis focused on using the powerful array processing techniques made possible by the ability of the iDAS not only to measure both the amplitude and the phase of the acoustic signal, but also to provide a large number of receiver channels at a fine spatial resolution. By generating a frequency wave number (f-k) plot, it is possible to identify the speeds at which acoustic energy is traveling as it is guided within the wellbore completion. The Doppler shift, an increase and decrease in SoS induced by the fluid moving between the upgoing and downgoing SoS, can be used to estimate the fluid velocity along the wellbore.

An example of an f-k plot and the result of the line fitting algorithm that determines the SoS are shown in Figs. 2a and 2b, respectively. In Fig. 2a, it is possible to see that a "V" shape has formed where the lines correspond to the detection of sound traveling at a single speed. The result of a line fitting algorithm applied to the plot in Fig. 2a is shown in Fig. 2b. This plot shows a peak correlating to the speed of propagation of the sound detected in Fig. 2a. The exact SoS is found from the location of this peak.

This SoS determination is dependent on two factors: The theoretical SoS through oil in an infinite medium, and the effect of the particular completion details on this basic sound speed. The speed of acoustic propagation within the fluidic production volume is dependent on flow speed. This phenomenon is known as the Doppler shift. Measuring the SoS in both directions within the well allows the speed of the flow to be calculated using Eqn. 2:

$$v = \frac{c_u - c_d}{2} \quad (2)$$

where v is the flow speed and c_u and c_d are the SoS up and down the well, respectively.

The actual speed of the sound propagation in a well is affected by both the fluid composition and the completion materials and structure. The interaction between the sound propagation and these factors is very complex and depends on a number of variables, such as the compliance of the pipe and formation. Changes in the cross section dimensions will lead to changes in the SoS.

ACQUISITION SURVEY

The iDAS system was retrofitted to the existing fiber optic cables already installed along several wells in Saudi Arabia. These wells varied in their use, construction and the type of fiber

Condition	Surface Choke
Base	0
1	100
2	80
3	50
4	40
5	35
6	25

Table 1. Well-1 test matrix

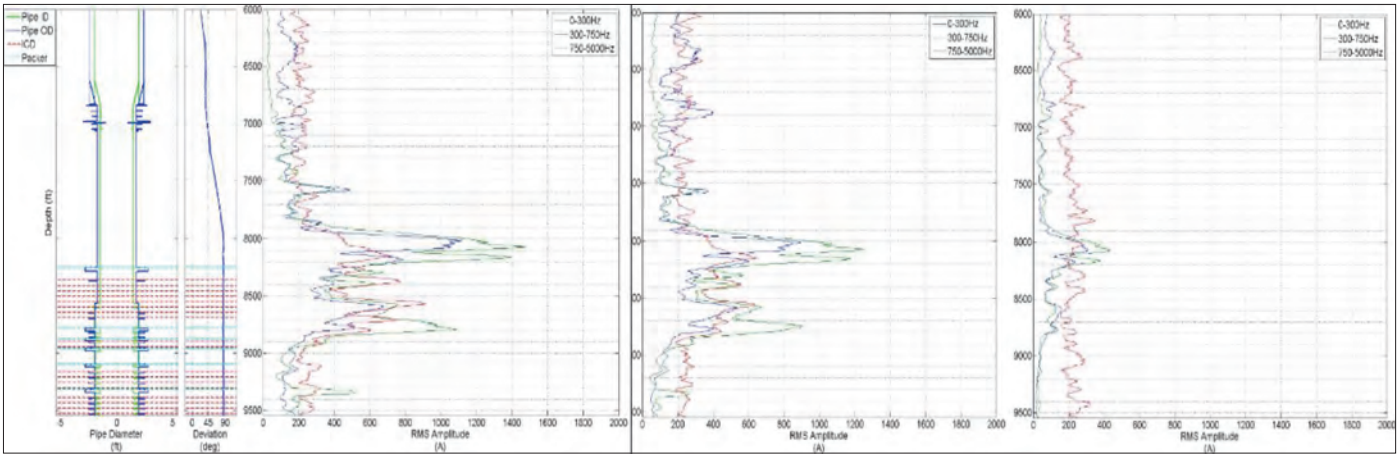

Fig. 3a. Schematic diagrams and deviation of Well-1 together with the RMS amplitude of the acoustic energy at different frequency bands for 100%, 50% and 25% injection rates, respectively.

optic cable installed. During the data acquisition program for each well, the ICVs and/or surface choke settings were altered to produce a range of different flow rates, as described next.

Well-1 — Water Injector with ICDs

Well-1 was a water injector well featuring a single tubing construction in open hole with ICDs. This well was instrumented with multimode fiber. In this case, the surface choke was adjusted to change the rate of water injection, Table 1.

Figure 3a shows a schematic of the lower completion of Well-1, a water injector with ICDs, along with graphs showing the RMS amplitude of the acoustic energy at different frequency bands, indicated along the well trajectory. The acoustic amplitude can be used for dynamic profiling of the injection profile. Figure 3b shows the calulated water injection profile from the acoustic energy.

As previously mentioned, the SoS was calculated using f-k array data processing, Fig. 4. The SoS is detected in the well only in regions where there is a sufficiently large distance between ICDs, which affords a greater length of continuous diameter tubing. The major feature seen in the data is that SoS detection was only possible where a spacing of at least 100 ft was present between the ICDs. The detected SoS, where detection was possible, was close to that expected of the SoS in water, ~4,900 ft/s.

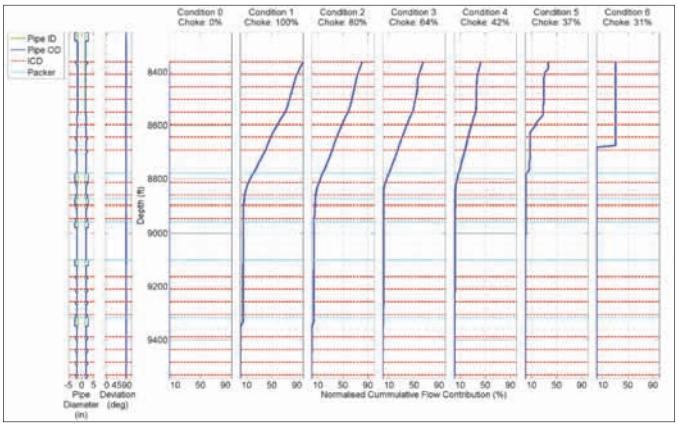

Fig. 3b. The water injection profile across the ICD zones. The majority of the water injection is taken by the upper compartment.

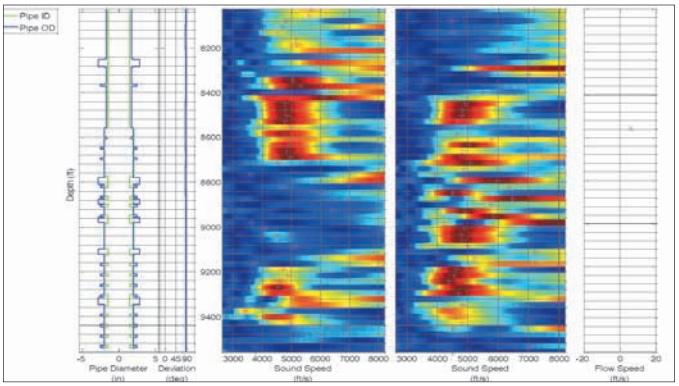

Fig. 4. SoS and flow analysis for Well-1, test point 4.

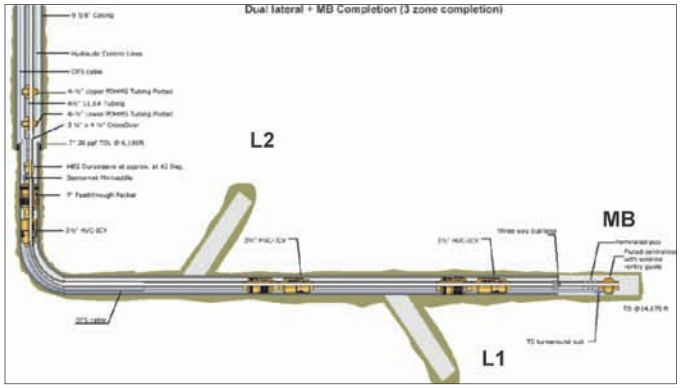

Fig. 5. Intelligent well completion diagram of Well-2 with the multimode fiber optic cable originally installed for a distributed temperature sensor[7].

Test Point	Settings			
	L2	L1	MB	SC
Base	0	0	10	64
1	3	0	10	64
2	3	3	10	64
3	10	10	10	64
4	10	10	0	64
5	10	10	3	64
6	0	10	3	64
7	0	3	10	64

L1 = Lateral 1 and L2 = Lateral 2, MB = Motherbore and SC = Surface Choke

Table 2. Well-2 test matrix

The changes in pipe diameter and the turbulence flow across the ICDs resulted in rapid changes in the calculated SoS. In this case, we did not attempt to measure the flow rate using the Doppler shift, although improving the spatial resolution of the system would make it feasible to measure the SoS between each ICD interval and so directly measure the injection profile.

Well-2 — Trilateral Oil Producer with ICVs and Multimode Fiber Optic Cable

Well-2 was a trilateral oil producer with inflow from each lateral controlled by an ICV, Fig. 5. The well was also instrumented with a multimode fiber optic cable. The survey of this well was the first ever adoption of iDAS field measurement using a multimode fiber for flow profiling[1].

The ICVs, along with the surface choke valve, are used to control the flow rates within the well, as indicated in Table 2. Figure 6 shows a schematic diagram of the well completion and the spectrogram of the acoustic energy along the wellbore. ICV locations show the highest acoustic energy, centered around 500 Hz. In addition, the ICVs are quiet when set in a fully open position of 10, Fig. 6e.

Using the f-k analysis, we can separate coherent acoustic energy propagating in both directions. The SoS can be determined by measuring the slope of the ridges in the f-k plot. The SoS

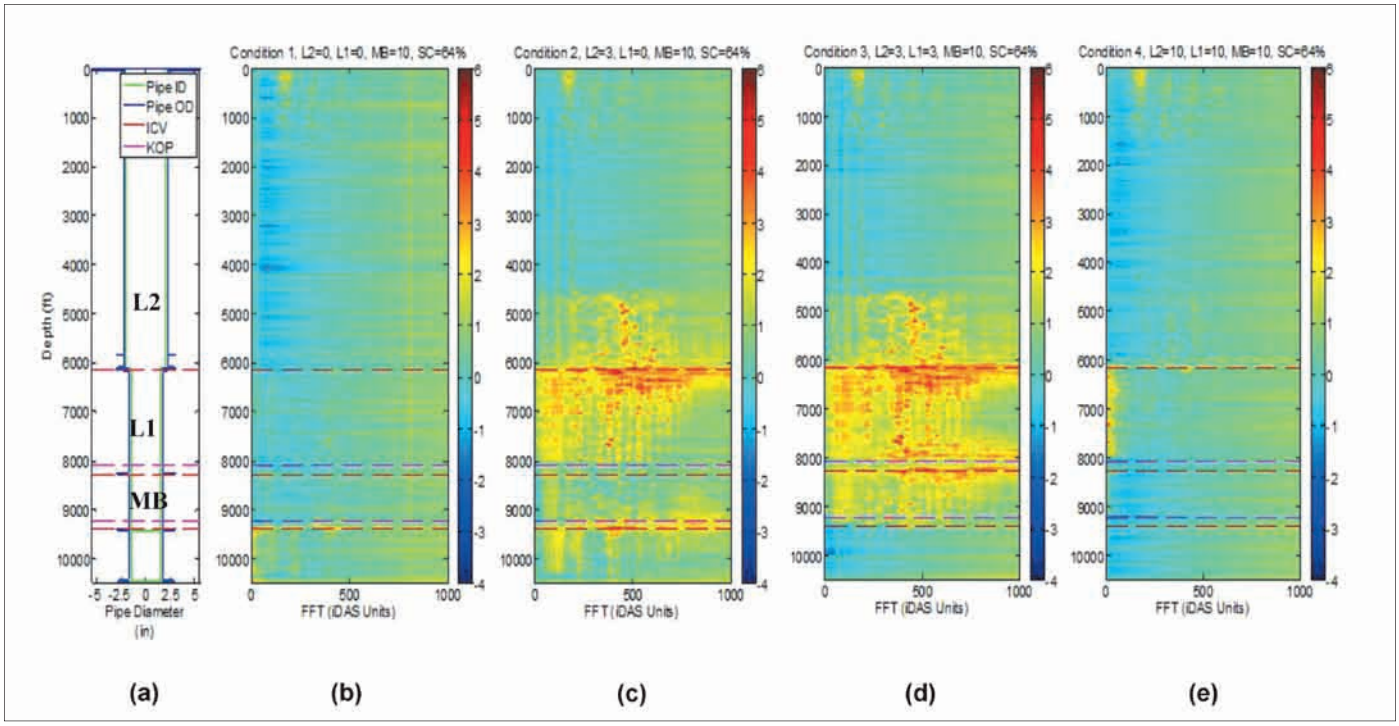

Fig. 6. Spectrogram of the acoustic signal vs. depth for different ICV settings in Well-2: (a) well schematics, (b) base, (c) test point 1, (d) test point 2, and (e) test point 3.

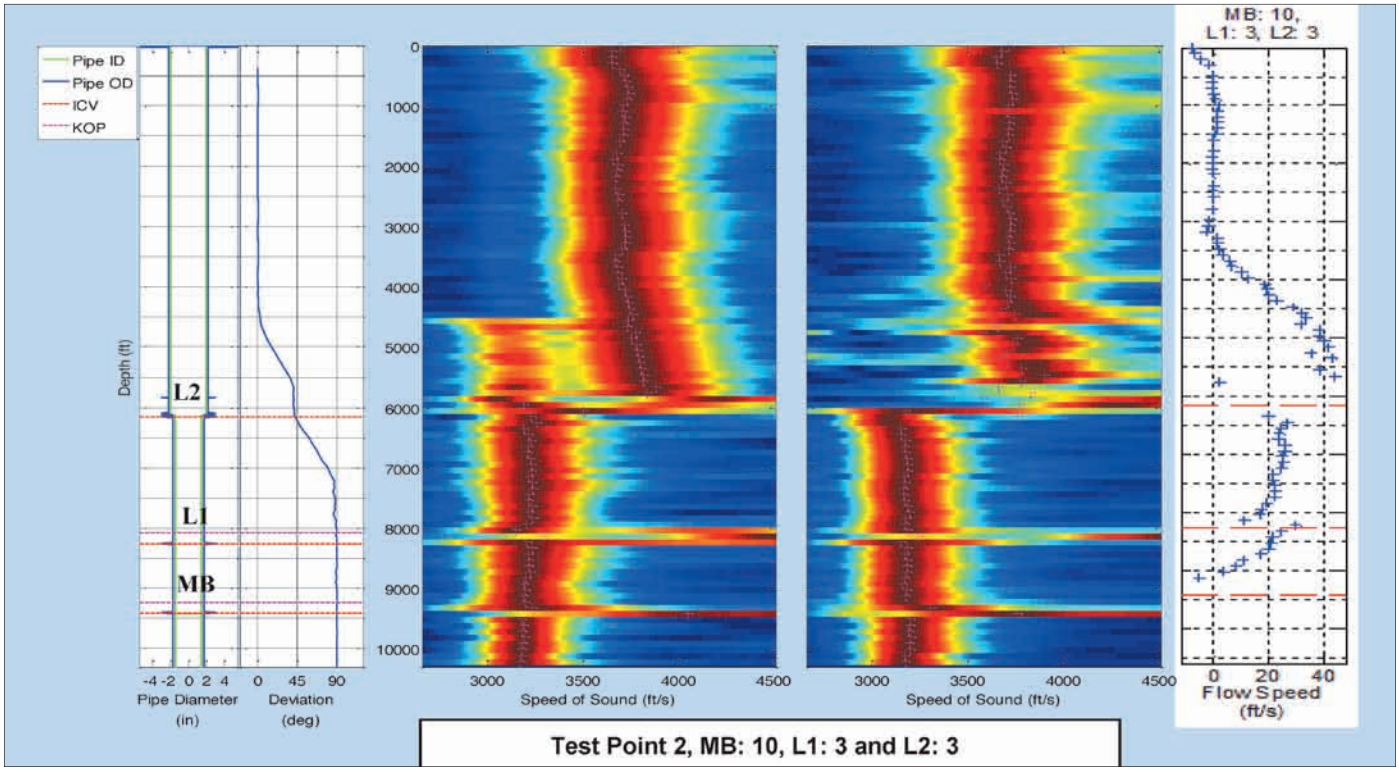

Fig. 7. SoS and the fluid velocity along the wellbore for Well-2, test point 2.

along the wellbore is determined as indicated in Fig. 7 for test point 2, where the ICVs generated a strong acoustic energy for both upgoing and downgoing waves. The SoS is about 3,000 ft/s to 3,500 ft/s. A shift in the SoS can be seen around 6,000 ft.

The fluid velocity was then calculated using Eqn. 2. Average values — around 20 ft/s — were obtained between the lateral 1 and lateral 2 ICVs, which corresponds to the typical production rates. The fluid velocity near the surface was measured at close to zero. This can be explained by acoustic energy coupling to the annulus fluid in the vertical section of the well that is not flowing.

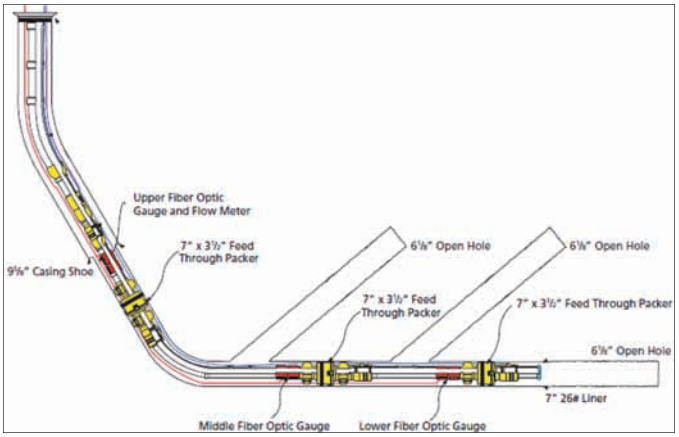

Fig. 8. Intelligent well completion diagram of Well-3 with the single fiber optic cable originally installed for fiber optic sensors[6].

Test Point	L2 ICV %	L1 ICV %	MB ICV %	Surface Choke %
1	12	12	0	43
3	6	0	0	100
4	3	0	0	100
5	0	12	0	100
6	0	6	0	35
8	0	3	0	65
9	0	0	20	100
10	100	100	20	43

MB = Motherbore, L1 = Lateral 1 and L2 = Lateral 2.

Table 3. Well-3 test matrix

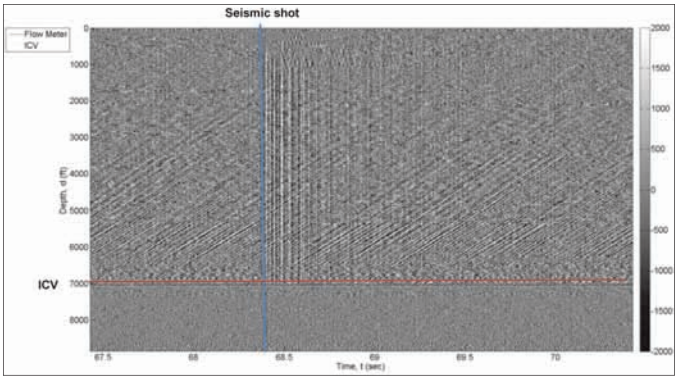

Fig. 9. Well-3, test point 9, acoustic amplitude (far right) vs. depth vs. time during a single seismic shot, showing the up going and down going waves before and after a single shot.

Well-3 — Trilateral Oil Producer with ICVs and Single Mode Fiber Optic Cable

As shown in Fig. 8, Well-3 was also a trilateral oil producer with ICVs similar to Well-2 except that it was instrumented with only a single mode fiber optic cable for monitoring optical fiber gauges[3]. Also, in contrast to Well-2, the laterals kickoff from the motherbore much further away from their respective ICV. This means the inflow from each lateral must flow through the annulus before entering the motherbore through the ICV.

The data acquisition program in Well-3 was run alongside a seismic acquisition program. A summary of the test matrix for Well-3 is provided in Table 3.

Figure 9 shows the acoustic amplitude time data as recorded byeach iDAS receiver channel within the well for test point 9. Inthis case, the two upper lateral ICVs were shut and the motherbore ICV was partially open. The depth of the iDAS receiver channel is plotted on the y-axis, and time is along the x-axis. The plot shows that this particular seismic shot occurred just 68 seconds into the iDAS recording file. The plot shows 1 second of data prior to the shot and 2 seconds of data after the shot. Also of note is the presence of the diagonal lines between 4,000 ft and 7,000 ft. These lines register the presence of propagating acoustic signals. The direction of the lines shows that this signal is propagating up the well. It can also be seen that these lines are not present below 7,000 ft and that the overall signal amplitude is lower, as indicated by the lack of high amplitude information in that region. The location where propagation ceases coincides with the location of both the ICVs and the optical fiber gauge.

Prior to the seismic shot, within the top 500 ft of the well, some more diagonal lines are visible. This shows that some acoustic energy is being created at the surface and propagating a short distance down the well. The seismic shot then creates more energy at the surface, which can be seen to propagate much further down the well, indicated by the bright diagonal lines that start after 68.5 seconds. The plot also shows two features in this region traveling at different speeds. The steeper lines that propagate in a zigzag nature are traveling faster and can be seen to reflect back up the well at approximately 1,200 ft. These waves continue to bounce up and down this section of the well for about 1 second. The lines signaling the slower feature show energy propagating down the well only, reaching approximately 2,500 ft to 3,000 ft in about 1 second. The vertical stripes are an artefact of the correlation processing and do not represent a physical feature within the data.

Figures 10 and 11, respectively, show the analyses before the seismic shot and 0.5 seconds after the single seismic shot illumination, each taking a time window of 0.5 seconds. The sections were chosen so that the windows did not overlap. Figure 11 also shows acoustic seismic energy propagating in the wellbore.

The left-hand plot provides a schematic of the completion diagram, showing the internal and outer diameters of the production tubing as well as the depths of the ICVs and flow meter. It can be seen that the tubing size changes at approximately 6,300 ft. The second plot from the left shows the well deviation survey as a function of depth. The well is vertical until approximately 5,000 ft and then deviates to be horizontal from 7,100 ft onwards.

The results from the FFT analysis and RMS analysis are shown, respectively, in the third and fourth plots. The color

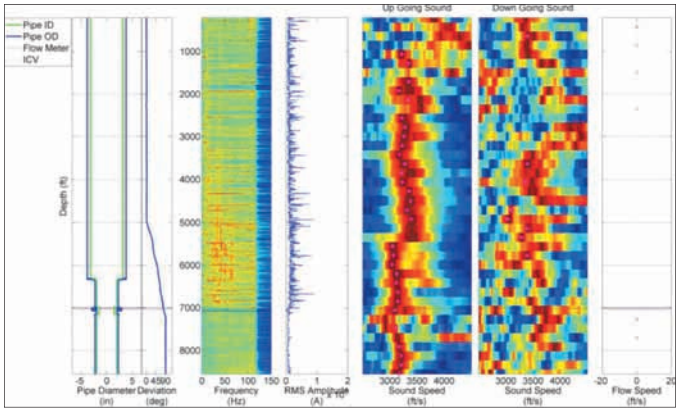

Fig. 10. Well-3, test point 9, FFT, RMS and f-k data analysis before the seismic shot for a time window of 0.5 seconds.

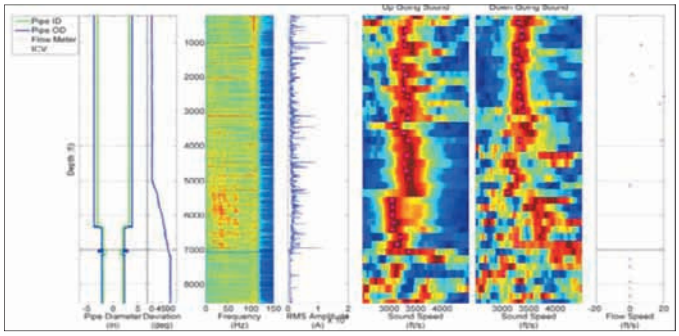

Fig. 11. Well-3, test point 9, FFT, RMS and f-k data analysis 0.5 seconds after a single seismic shot illumination for a time window of 0.5 seconds.

FFT plot has frequency along the x-axis and shows the signal amplitude at each frequency for each sensor depth, blue being the minimum and red being the maximum amplitudes. The plot shows an increased broadband acoustic energy between a depth of 4,000 ft to 7,000 ft, indicated by the increase in yellow color in this region — as opposed to below 7,000 ft, for example. This region also shows the presence of single frequency, tonal, and energy at approximately 40 Hz and again at approximately 50 Hz. The RMS graph shows that the overall signal level is much lower below 7,000 ft than above, although this is difficult to show on the graph due to the large amplitude ranges. Above 7,000 ft, the graph is very spiky due to the effect of clamping the cable against the production tubing, which creates points that are coupled more firmly to the production tubing than other points directly adjacent to them.

The plots show that, for this test point, there is an upgoing acoustic signal from about 7,000 ft, which corresponds to the location of the lateral 2 ICV. This signal propagates up the well to approximately 2,000 ft at between 3,000 ft/s and 3,400 ft/s. The SoS is the most stable between 6,500 ft and 4,000 ft, with the highest SNR and the smallest variation between depth windows. The SoS can be seen to gradually decrease slightly in this region before increasing more significantly between 4,000 ft and 3,000 ft, and then increasing again from 3,000 ft to 2,500 ft. The SoS varies by up to 300 ft/s over the range of propagation. There is also a weak downgoing acoustic signal that propagates from the surface to approximately a depth of 1,000 ft.

The final graph on the far right plots the calculated flow speed using Eqn. 2. In this distance and time window, an upgoing and downgoing acoustic signal was not detected at the same depth, and meaningful flow results could not be calculated. In situations where the peak fitting algorithm cannot find a peak in the data, it returns a value of 0 ft/s as the SoS. If this occurs for both the upgoing and downgoing case, then the flow speed calculated will be 0 ft/s. This can be seen in the region below 7,000 ft where no propagating acoustic signal was detected in either direction, giving a default flow speed of 0 ft/s.

The immediate feature that stands out in Fig. 11, showing the results 0.5 seconds after the seismic source shot is fired, is the increased energy between the surface and approximately 1,500 ft depth. The FFT and RMS graphs show the increased energy level in this region, with the measured energy mostly concentrated in the 80 Hz to 110 Hz region. This energy can also be seen to propagate to approximately 2,000 ft depth, as shown in the downgoing SoS plot. This is further than was seen for the data window before the seismic shot was fired. The SoS detected is stable at around 3,400 m/s over the 2,000 ft range.

The SoS detection region is similar for each Well-3 test point, all showing good detection of the SoS between a depth of approximately 3,000 ft and 7,000 ft. This depth range can be split into three further regions based on the characteristics of the data seen in the graph. As indicated in Fig. 12, between 7,000 ft and approximately 5,750 ft, the SoS for test points 5, 8 and 9 cluster together around 3,100 ft/s, whereas for test points 1 and 6, the speeds collect at a higher value of around 3,200 ft/s. There is also a slight trend in this region for the SoS to decrease as we move up the well. At approximately 5,750 ft, the group of test points with the lower SoS sees that speed increase significantly to approximately 3,400 ft/s and stay at this speed up to around 4,000 ft depth. Test points 1 and 6 continue on the same trend as between 7,000 ft and 6,000 ft, with the SoS gradually decreasing to almost 3,000 ft/s at 4,000 ft depth. This creates a large difference between the two groups

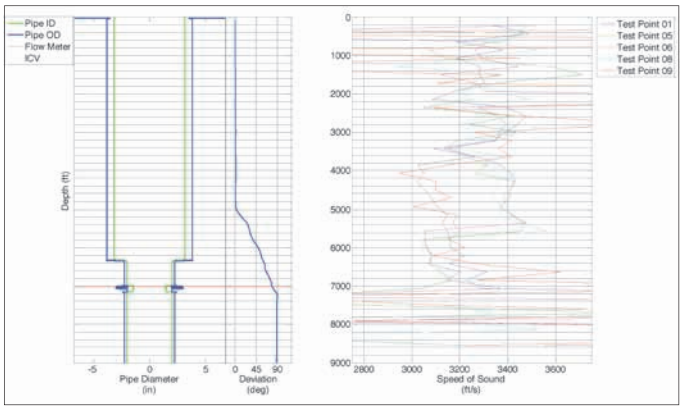

Fig. 12. ICV and surface choke settings for Well-3 test points with up going acoustic energy.

Valve	Settings				
	Test Points with SoS ~3,100 ft/s		Test Points with SoS ~3,400 ft/s		
	1	6	5	8	9
Surface Choke	43	35	100	65	100
L2 ICV	12	0	0	0	0
L1 ICV	12	12	6	3	0
MB ICV	0	0	0	0	20

L1 = Lateral 1, L2 = Lateral 2, MB = Motherbore and SoS = Speed of Sound

Table 4. ICV and surface choke settings for Well-3 test points with up going acoustic energy

of test points in this region. At the 4,000 ft depth, test points 1 and 6 show a step increase in the detected SoS: Test point 1 jumps to about 3,200 ft/s while test point 6 jumps to 3,400 ft/s. The other test points, which were already at around 3,400 ft/s, show a dip in the SoS at approximately 3,500 ft depth, dropping down to 3,200 ft/s before returning back up to 3,400 ft/s by 3,000 ft depth. That the SNR in the region above the 4,000 ft depth is lower than at deeper parts of the well is shown by the detection of an erroneous SoS outside the range of the plot.

The ICV and surface choke settings for each of these test points are shown in Table 4. The test points are grouped by their approximate SoS, between a depth of 4,000 ft and 5,750 ft.

The table shows that the test points that did not produce the step increase in the SoS around 5,750 ft depth both had lower surface choke settings, 43% and 35%, than the other test points of 100%, 65% and 100%. The other ICV settings do not show any other obvious trends.

Effect of Stacking Seismic Shots Illumination

Multiple seismic shots were recorded at a single location for each test point in Well-3. In standard seismic data processing, averaging the shots together (stacking) is used to improve the SNR of the final result. The same technique can be applied to the flow data used here.

Figure 13 shows a stack of 123 shots performed at a single location near Well-3 during test point 9. The plot demonstrates how the stacking has increased the SNR significantly, making the seismic shot energy much clearer. The plot shows two features caused by energy from the seismic shot propagating to the fiber optic cable in different ways. The curved line, seen most clearly at 0.1 seconds and at a depth of 3,000 ft, can now be seen to propagate further down the well to an approximate depth of 6,500 ft. This energy is the first arrival from the energy propagating through the formation — this signal is important in seismic imaging analysis[7], but since it propagates within the formation, it does not contain any information about the fluid within the well.

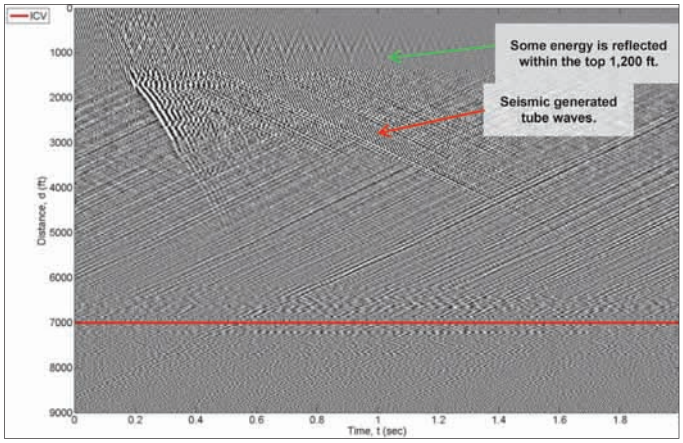

Fig. 13. Well-3, test point 9, stack of seismic shots along with the position of the ICV.

Arriving after this formation energy is a series of straight lines, seen between 0.3 and 0.4 seconds at a depth of approximately 3,000 ft. This energy is propagating as a tube wave within the well completion structure and so contains information about the fluid within the well. This energy is the same as that seen for the single seismic shots presented earlier, where downgoing energy was detected. In this case, however, the stacking has improved SNR enough that it is possible to see that this energy propagated much deeper into the well, reaching approximately 6,500 ft instead of around the 2,500 ft to 3,000 ft detected from a single shot.

The same data processing techniques to determine SoS were applied to this data as were applied to the single seismic shot records. The results of this processing are shown in Fig. 14. The downgoing acoustic energy can be seen to propagate almost the full length of the well, with a peak in the SoS measurements shown as deep as nearly 8,000 ft. This is even further than first seen in the depth-time plot, since the processing steps extract the downgoing energy that was not visible to the naked eye due to noise or the presence of energy propagating in other directions. Since upgoing and downgoing SoS has been detected over most of the well depth, it is possible to calculate a flow speed estimate. In this case, the values obtained for the flow speed were not representative of the expected flow speed within the well in all regions.

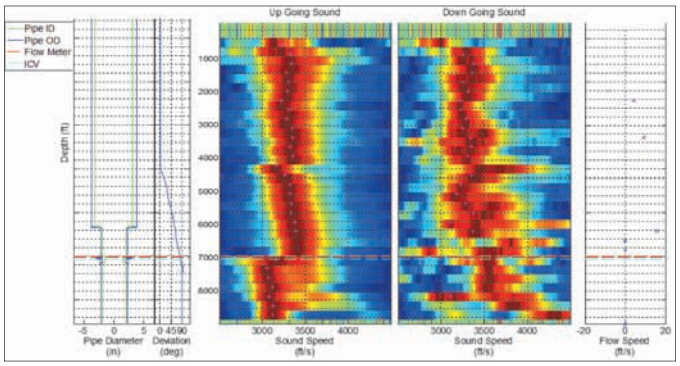

Fig. 14. Well-3, test point 9, KW data analysis with the seismic shots attached.

Many variables can affect this result, and these issues are discussed along with the rest of the results next.

DISCUSSION

The selection of the data processing performed on the data set from these trials, presented earlier, was made to highlight a representative selection, one showing all the features and characteristics of the data.

This data shows that varying the ICV and surface choke settings has a significant effect on the acoustic energy propagation within the well; those settings therefore had a very significant effect on the results obtained for each test point. This data also shows that certain ICVs can be noisier than others, and that certain settings for a single ICV can be noisier than other settings. This is to be expected due to a combination of factors affecting the fluid inflow velocity through the ICV.

The inflow through an ICV can be described as fluid flowing from an area of high-pressure to an area of lower pressure through a small aperture. Noise is generated when this happens through two mechanisms. The highly turbulent flow that is generated as the fluid passes through the small aperture, which forces it to speed up, causes eddies to form, which generates acoustic energy. The second mechanism involves very large pressure differences or very small apertures, which can cause cavitation to occur where tiny bubbles are formed within the fluid, which then collapse and release a large amount of acoustic energy. In both these mechanisms, the noise generated is a factor of the fluid properties, the pressure difference and the aperture size. If the fluid properties are considered to be relatively constant, then the pressure difference and aperture size are the key variables that influence the acoustic energy created. A large pressure difference and a small aperture size will generate the largest velocity for fluid passing through the ICV, which will generate the most acoustic energy. A smaller pressure difference or a larger aperture will generate less acoustic energy since the fluid will not flow as fast through the ICV. In the specific case of this data, the overall pressure drop was greatly influenced by the surface choke setting. A higher setting (more open) will tend to reduce the pressure within the motherbore and create a larger pressure difference between that and the lateral. A lower setting (more closed) on the ICV means that there is a smaller aperture size for the fluid to flow through. It would therefore be expected that wells with the highest surface choke setting and the lowest ICV setting would generate the most acoustic energy. All the upgoing acoustic energy detected during this analysis was seen to propagate from the position of the ICVs.

The accuracy and precision of the SoS calculation is increased as the number of recording channels within the array is increased; to achieve that precision can mean increasing the overall length of the array or reducing the distance between each recording channel. Another factor affecting this calculation is the underlying SNR in the acoustic data. The iDAS used in these trials was capable of sampling the fiber every 0.512 m, approximately 1.7 ft, and the array length was optimized based on the data from each well. For example, to obtain the required SoS calculation precision for the Well-3 data, an array of 256 channels was used. This corresponds to an overall array length of approximately 430 ft. To build a picture of the SoS profile over the whole well, this array was shifted along the fiber by half the array length for each iteration. The spacing between each SoS measurement was therefore approximately 215 ft. It is possible in some circumstances to reduce the number of sensors within the array, e.g., the Well-2 data processing used an array length half of that used during the Well-3 analysis — 128 channels — since the SNR of the acoustic data was higher for this well.

CONCLUSIONS

The iDAS system was used in this trial to monitor the acoustic signal both within a well and in the surrounding formation using a fiber optic cable installed on the outside of the production tubing for the purposes of simultaneous flow monitoring and seismic imaging. The iDAS has been shown to be capable of measuring the SoS within a well when sufficient propagating acoustic energy is present.

The results presented here, which utilized existing, already installed fiber optic cable, have also helped us to better understand the acoustic energy propagation in both multilateral and single tubing well completions with ICVs or ICDs. Further improvements are required for quantitative distributed flow measurements. These include improving the detection sensitivity and the spatial sampling of the acoustic energy in particular sections of interest, such as across ICVs and ICDs. This would require optoelectronics detection sensitivity enhancements, improved data processing resolution, the acoustic modeling of the well completion geometry, optimizing of the fiber optic acoustic sensing cable and the deployment configurations that can lead to direct flow measurements.

ACKNOWLEDGMENTS

The authors would like to thank the management of Saudi Aramco for their support and permission to publish this article.

This article was presented at the SPE-SAS Annual Technical Symposium and Exhibition, al-Khobar, Saudi Arabia, April 21-24, 2014.

REFERENCES

1. Xiao, J.J., Farhadiroushan, M., Clarke, A., Khalifa, Q., Mulhem, A., Foreno Reyes, H., et al.: "Inflow Monitoring in Intelligent Wells Using Distributed Acoustic," SPE paper 167447, presented at the SPE Middle East Intelligent Energy Conference and Exhibition, Manama, Bahrain, October 28-30, 2013.

2. Hembling, D., Berberian, G., Carter, N. and Naldrett, G.: "Enabling Efficient Permanent Production Monitoring of Advanced Well Completions in Saudi Arabia Using Fiber Optic Distributed Temperature Sensing," SPE paper 115255, presented at the SPE Annual Technical Conference and Exhibition, Denver, Colorado, September 21-24, 2008.
3. Al-Arnaout, I.H., Al-Buali, M.H., Al-Mubarak, S.M., Al-Driweesh, S.M., Zareef, M.A. and Johansen, E.S.: "Optimizing Production in Maximum Reservoir Contact (MRC) Wells with Intelligent Completions and Optical Downhole Monitoring System," *Saudi Aramco Journal of Technology*, Summer 2009, pp. 22-30.
4. Farhadiroushan, M., Parker, T.R. and Shatalin, S.: "Method and Apparatus for Optical Sensing," Patent WO/2010/136810A2, 2009.
5. Parker, T., Shatalin, S.V., Farhadiroushan, M., Kamil, Y.I., Gilles, A., Finfer, D., et al.: "Distributed Acoustic Sensing — A New Tool for Seismic Applications," SPE paper presented at the 74th EAGE Conference and Exhibition incorporating SPE EUROPEC 2012, Copenhagen, Denmark, June 4-7, 2012.
6. Johannessen, K., Drakeley, B.K. and Farhadiroushan, M.: "Distributed Acoustic Sensing — A New Way of Listening to Your Well/Reservoir," SPE paper 149602, presented at the SPE Intelligent Energy International, Utrecht, The Netherlands, March 27-29, 2012.
7. Madsen, K.N., Dümmong, S., Parker, T., Finfer, D., Travis, P.N., Bostick, T., et al.: "Simultaneous Multiwell VSP Using Distributed Acoustic Sensing," paper presented at the 2nd EAGE Workshop on Borehole Geophysics, St Julian's, Malta, April 21-24, 2013.

BIOGRAPHIES

Dr. Jinjiang Xiao is a Petroleum Engineering Specialist working with the Production Technology Team of Saudi Aramco's Exploration and Petroleum Engineering Center – Advanced Research Center (EXPEC ARC). His interests are well productivity improvement and water management.

Prior to joining Saudi Aramco in 2003, Jinjiang spent 10 years with Amoco and later BP-Amoco, working on multiphase flow, flow assurance and deepwater production engineering.

He received both his M.S. and Ph.D. degrees in Petroleum Engineering from the University of Tulsa, Tulsa, OK.

Mahmoud Farhadiroushan co-founded Silixa in April 2007, where he is the Chief Executive Officer. Mahmoud has many years of experience in designing and developing optical fiber sensors. He previously co-founded Sensornet in 1998.

Mahmoud is the joint winner of two DTI SMART awards, the prestigious Manufacturing Metrology for World-Class Manufacturing Award (Frontier Science and Measurement) in 2000 and the British Telecom Innovation Award in 2001.

In 1984, he received his B.S. degree (with honors) in Electrical and Electronic Engineering from Queen Mary University of London, London, U.K. In 1985, Mahmoud received his M.S. degree (with honors) in "Microwaves and Modern Optics" in Electrical and Electronic Engineering from University College London, London, U.K.

Andy Clarke joined Silixa in 2010 and is a Senior Development Engineer.

In 2008, he received his M.Eng. degree in Acoustical Engineering from the University of Southampton, Southampton, U.K.

Andy is a member of the European Association of Geoscientists and Engineers (EAGE).

Rami A. Al-Abdulmohsen joined Saudi Aramco in 2001. Currently, he is working as a Production Engineer handling oil production in the Southern Area of Ghawar reservoir.

Rami received his B.S. degree in Computer Engineering and his M.S. degree in Petroleum Engineering, both from King Fahd University of Petroleum and Minerals (KFUPM), Dhahran, Saudi Arabia.

Essam M. Al-Alyan joined Saudi Aramco in 2005 as a Reservoir Engineer working in the Reservoir Management Department. He has worked in different assignments as a Production Engineer and Reservoir Engineer, handling fields of different maturity and complexity. Essam worked as a Reservoir Engineer for the Haradh Increment-III, the world's largest field development with advanced well completions and intelligent field infrastructure. Currently, he is working with Reservoir Management looking after Haradh Increment-I, one of the most challenging areas in the super giant Ghawar field.

Essam received his B.S. degree in Petroleum Engineering from King Saud University, Riyadh, Saudi Arabia.

Dr. Tom R. Parker co-founded Silixa in 2007 and is Silixa's Chief Technology Officer (CTO). As CTO, he takes the lead in the development of Silixa's iDAS and ULTIMA DTS range of instruments and oversees Silixa's application-specific development projects.

Tom's awards include the Metrology for World-Class Manufacturing Award and British Telecom Technological Innovation Award.

He completed his first degree at University College London, London, U.K., and was awarded a Ph.D. in Physics from Imperial College London, London, U.K.

Dr. Janti Shawash has been working on distributed acoustics and temperature sensors and a multitude of their applications at Silixa for the past 5 years. His research interests include digital signal processing, image processing, pattern recognition and the design of heterogeneous real-time computing systems.

Janti received his M.S. degree in Telecoms and a Ph.D. degree in Electronics Engineering focusing on real-time machine learning, both from University College London, London, U.K.

H. Craig Milne is the Vice President of Oil and Gas at Silixa. Craig joined Silixa in 2012 following a 15-year career in the Wireline division of Schlumberger Oilfield Services. While at Schlumberger, he held operational and management positions in Asia, the Middle East and Europe.

Craig received his B.S. degree in Electrical and Mechanical Engineering from the University of Strathclyde, Glasgow, U.K.

New Generation Inflow Control Device to Maximize Well Productivity during Every Phase of a Well's Life

Authors: Hemant K. Sharma and Abdulrahman K. Al-Mulhim

ABSTRACT

In a carbonate reservoir, oil production from long horizontal wells is typically a challenge due to reservoir heterogeneities and the presence of fractures. The result is an imbalanced production profile, leading to early water breakthrough. Once water coning occurs, oil production may be severely decreased due to resistance to oil flow by the water contributing zone. To eliminate this imbalance, passive inflow control devices (PICDs) are placed in compartments across the entire lateral length of the horizontal, which compensates for permeability variation. The compartments are separated from each other using open hole packers and constrictors. The PICDs are always opened to production. In cases where specific inflow control devices (ICDs) start to contribute to undesired water production, water shut-off of the length below this ICD has to be performed, leaving much of the oil behind.

A new generation of active ICDs was installed in an open hole horizontal producer, where they could be selectively opened/closed by a setting tool to control water production. For the well using this completion, oil production has increased by more than 200% with a consequent decrease in water production by 50%. The traditional water shut-off techniques of using cement plugs, inflatable packers, gel plugs or chemical plugs, etc., are no longer needed with this kind of completion.

To operate the new generation of ICDs, a new generation modular anchor and universal shifting tool (UST) is used. The downhole application of this tool for selective shifting of the ICDs in the horizontal wellbore was the first in the world. The tool uses hydraulic pressure created by an electric motor to generate force. It provides setting assurance via real-time monitoring with controlled setting force, distance and speed. Using the signature from the log to confirm the position of the ICD sleeve — whether opened or closed — eliminates the need to have additional production logging runs to confirm sleeve position.

This article details the design and advantages of the new generation of active ICDs in horizontal wells and how the new modular anchor and UST is being effectively used for selective operation of the ICDs.

INTRODUCTION

Over the past 30 years, advances in drilling technology have made it possible to drill horizontal wells for maximum reservoir contact, providing optimal sweep with lower drawdown. Horizontal drilling enables engineers to increase the production of the wells and give wells increased longevity. The increased wellbore length, however, leads to various production related issues, depending on the heterogeneity of the reservoir. Higher pressure drawdown around the heel section as a result of the frictional pressure drop of the fluid in the wellbore can cause nonuniform fluid influx along the length of the wellbore. An extended length of contact with the reservoir also results in encounters with a higher variation of the reservoir properties, which means heterogeneity becomes a critical factor in the reservoir and well performance. Both problems can lead to early breakthrough of water or gas at the higher drawdown, which causes reduction in the oil recovery and uneven sweep of the drainage area. Recovering the unswept oil in the reservoir at a later stage of production requires substantial investment, which might not be economical in most cases.

To eliminate these problems, wells are completed with advanced well completion (AWC) to avoid water coning/cresting through the matrix, which involves isolating the high permeability streaks/fractures using open hole packers and chemicals. The basic objective of AWC is to equalize the influx into the wellbore. AWC consists of inflow control devices (ICDs) separated by open hole packers/constrictors. Swell packers are also used, as they were in the recent completion, to provide extra inflation in the case of wellbore enlargement during production or due to acid stimulation. In addition, water adaptive ICDs and autonomous ICDs (AICDs) have recently been introduced to control water production in the wellbore automatically as the water cut increases.

ICD TYPES AND COMPLETION

ICDs are permanent hardware installed in both new and sidetracked horizontal/deviated wells upon completion of the well. Their use is based on the initial reservoir condition and the simulation prediction of reservoir performance. An ICD is part of the completion base pipe (liner/casing) with a differently

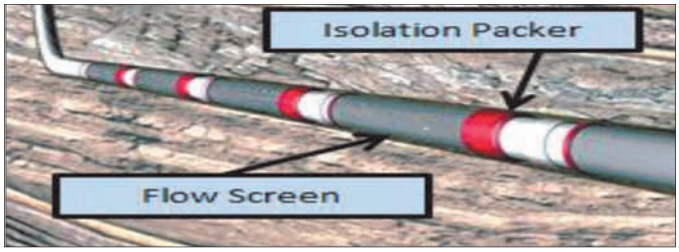

Fig. 1. PICD in a passive completion.

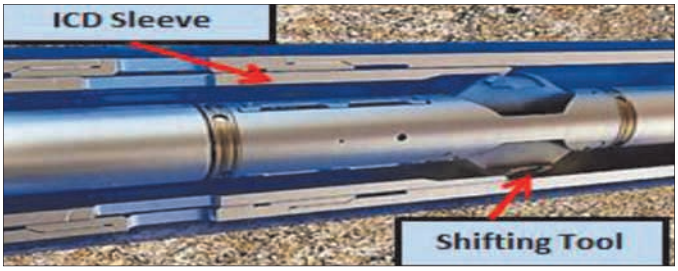

Fig. 2. ICD in an active completion.

designed flow path to create additional frictional pressure, thereby restricting the flow through the path. The purpose is to equalize the flow along the length of the wellbore regardless of the location of a given section and reservoir permeability variation. ICDs enable the entire length of the wellbore to contribute to the total production, which optimizes and maximizes hydrocarbon recovery[1]. ICDs in general are choking devices, restricting flow for the section of the lateral with higher permeability; this allows the less permeable lateral sections to contribute to production, which in turn balances the contribution along the wellbore. NetTool software is used in determining the number of port/channels required in each compartment of the wellbore before installation of the ICDs. The design applies specific differential pressure at certain flow rates; as a rule of thumb, 25 psi differential pressure is assumed across each compartment[2]. The ultimate objective for the installation of the AWC system is to increase well productivity, prolong well life, and ultimately improve reservoir sweep and recovery.

The ICD is designed to take care of changes in fluid viscosity, density and velocity, which occur with time, without creating an inflow imbalance and a negative effect on production. Therefore, the dynamic conditions of the reservoir make ICD selection and design an important factor in determining the subsequent productivity from a well.

Based on the completion design, there are two kinds of AWC: passive completion and active completion.

Passive Completion

The passive completion consists of passive ICDs (PICDs) and annular isolation packers, Fig. 1. These PICDs cannot be adjusted as changes occur in the reservoir condition. To change a PICD's location/number of ports, the whole completion has to be pulled out and reinstalled after making the desired changes.

Active Completion

Figure 2 shows the active completion featuring an integral, premium, inner sliding sleeve with a shifting profile incorporated into the ICD joint. It provides the option of setting the ICD to a fully open or fully closed position by using a mechanical intervention tool as required.

Two basic pressure drop mechanisms currently are being used in designing the ICDs: restrictive or frictional. The restrictive mechanism relies on a contraction of the fluid flow path to generate an instantaneous pressure across the device, whereas the frictional device creates pressure by directing fluid flow along the length of a channel or tube[3].

The result is three primary types of ICDs: (1) Helical-Channel/Labyrinth type (frictional), (2) Orifice/Nozzle type (restrictive), and (3) Hybrid Design type (combination of frictional channel and restrictive nozzle).

Helical-Channel/Labyrinth Type ICDs

This type of ICD uses surface friction to generate pressure drop. It uses a number of channels with preset diameters and lengths, Fig. 3a. The produced fluid flows through a multilayer screen into the annulus between the screen and the solid base pipe, where it is then forced to flow through the channels before getting into the wellbore. The design forces the fluid to change directions numerous times, which creates a pressure drop along the longer channel path. This has proven advantageous because it generates lower flow velocities, which reduce the chances of erosion and plugging. The disadvantage of using friction to generate pressure drop is that the ICD becomes viscosity dependent, which can cause problems in maintaining uniform influx in wells where larger differences exist between the viscosities of the oil and those of the produced water. These kinds of ICDs are generally used in sandstone reservoirs.

Orifice/Nozzle Type ICDs

These ICDs use fluid constriction to generate a desired pressure drop. Fluid is forced through a preconfigured set of small diameter nozzles before entering the pipe to create a flow resistance, Fig. 3b. The pressure drop across this ICD occurs instantaneously as it is highly dependent on fluid density and velocity and not

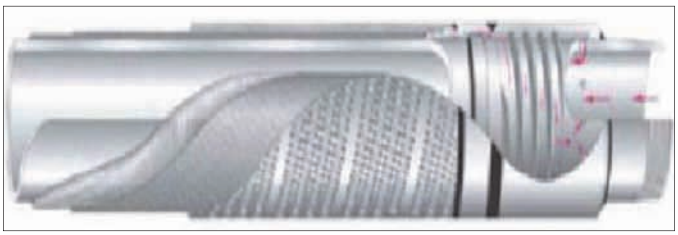

Fig. 3a. Helical-Channel/Labyrinth type ICD.

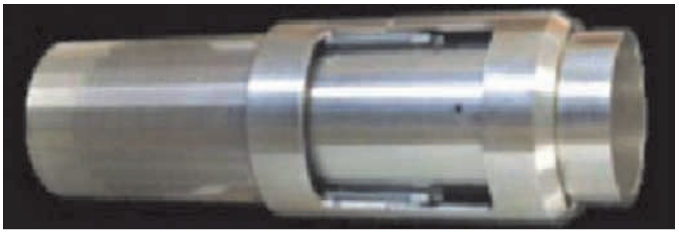

Fig. 3b. Orifice/Nozzle type ICD.

on viscosity. One of the advantages of this ICD is its simple design, however, because it is dependent on fluid velocity, it is prone to erosion during production. These kinds of ICDs are used in carbonate as well as sandstone formations.

Hybrid Design Type ICDs

This combination ICD uses multiple bulkheads that form chambers and flow slots 180° apart, Fig. 3c. Fluid flows through each successive chamber and each incurs a pressure drop. The primary pressure drop mechanism is restrictive, but flow paths are in a distributive configuration. The ICD here also incorporates a simple adjustment feature capable of altering the ICD flow resistance immediately before running in a well, which is useful should real-time data collected during drilling indicate the need to change flow resistance settings. The adjustability comes from having multiple discrete chambers on board, each with a different number of stages. Therefore, the user may select the desired setting — with more stages for higher resistance or fewer stages for lower resistance.

New Technology in Active ICDs

The latest additions to the active ICD completion are the water adaptive ICD and the AICD.

- **Water Adaptive ICD:** The water adaptive ICD works on the principle of restricting the entry port/nozzle as water production increases. The idea is to use relative permeability modifiers (RPMs) inside a screen. RPMs are typically hydrophilic polymers used in downhole applications. The ability to create a variable choking option is provided by different RPM polymers. As the water cut increases, the entry port of the ICD reduces in size until it is completely closed with water cut above 70%. The polytetrafluorethylene (PTFE) called Teflon is found to be suitable for this application. Teflon is a porous material that has the ability to create a variable choking option, and it is nonsensitive to salinity, acid or fine plugging.

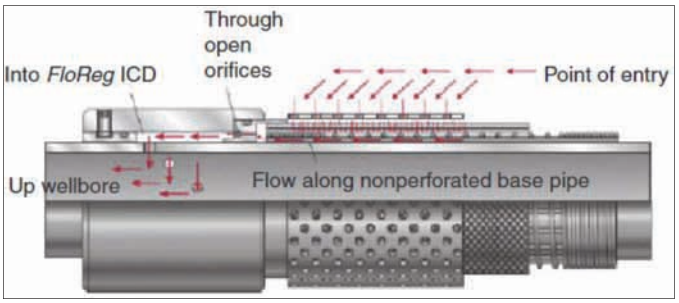

Fig. 3c. Hybrid Design type ICD.

Fig. 4. ACID.

- **AICD:** The AICD utilizes dynamic fluid technology to differentiate between the viscosities of the fluid flowing through the device. To maximize oil production, the AICD technology employs an engineered system of flow paths and channels to control fluid flow, Fig. 4, restricting water production by means of "identifying" the viscosity contrast between the oil and water. All fluid enters the side ports and exits the hole in the center. Oil, which has a higher viscosity, is able to turn the corner and travel through the side passages, giving it a short, direct path to the exit. Water cannot achieve this path as easily. This results in a low-pressure differential and high total flow rate. The AICD has three individual dynamic fluid components — a viscosity selector, a flow switch and a flow restrictor — which function together to allow the restricted or unrestricted flow of fluids. The viscosity selector utilizes a system of flow paths, which, based on fluid viscosity, density and velocity, "identifies" the fluid that is flowing through the AICD and then divides the total flow into two fluid paths. Based on the viscosity selector's output, the flow switch, or "fluid crossroad," directs the selected fluid down one of the two separate paths according to its properties. Finally, the fluid restrictor restricts the flow of unwanted fluid (water/gas) from entering the wellbore, yet provides very little restriction to the flow of the desired fluid (oil).

The mechanical designs of the various types of ICDs vary, but the operating principle remains the same — using additional pressure drop to redistribute flow along the horizontal wellbore.

TYPICAL DESIGN OF AN AWC

Figure 5 shows the typical design of an AWC using active ICDs. The design is based on the formation analysis log and

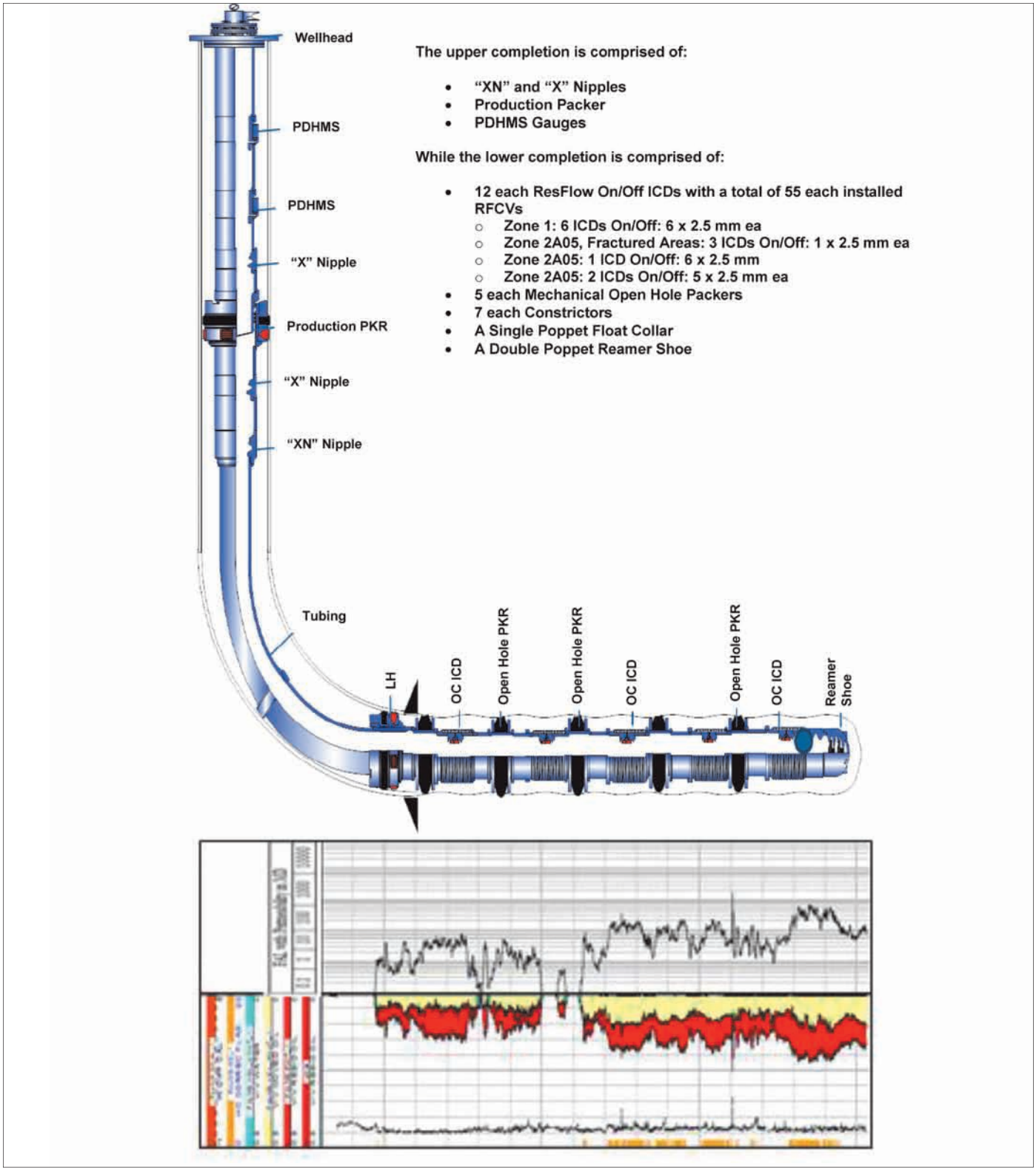

Fig. 5. Typical design of AWC.

image log, including the loss circulation zone that results from drilling the well. NetTool software is generally used to determine the location of the ICDs and isolation packers. The wellbore is divided into compartments depending on the permeability of the reservoir, including the intervals showing high permeability contrast/fractures. Generally, more ICDs are placed in compartments recovering oil from less permeable intervals. In contrast, the high permeability streak/fracture intervals are generally isolated using two open hole packers with blank pipe. Sometimes the fracture zones are allowed to produce with ICDs having a lower number of ports.

Based on the simulation of this particular well, the decision was made to use an equalizer completion in five compartments, consisting of 12 active ICDs separated by the five MPas packers

and seven constrictors. The constrictors are mainly oil swellable inflatable packers that will inflate as per the wellbore condition. Since the well is drilled in two different reservoirs with variations in bottom-hole pressure (BHP), the reservoir with the lower pressure is allowed to produce more, achieved with an increased number of ICD ports. This will make the production in the wellbore uniform.

The active ICDs can be opened/closed as needed using the shifting tool run by wireline or coiled tubing (CT). The closed position of the ICD is shown in Fig. 6a, and the open position in Fig. 6b.

Wells completed in two different zones with different BHP in the reservoirs risk the possibility of cross flow between the reservoirs. To mitigate the issue of cross flow, the ICDs are provided with a check valve, Fig. 6c, which will allow flow in one direction only, i.e., from the formation into the wellbore/liner and not vice versa. The check valve allows closed system pumping with the sleeve in the open position.

The active ICDs are run in the closed position. They are (shifted up to the open position to be able to:

- Circulate from the bottom of the completion during installation without the use of a wash pipe.
- Set the liner hanger and the mechanical open hole packers.

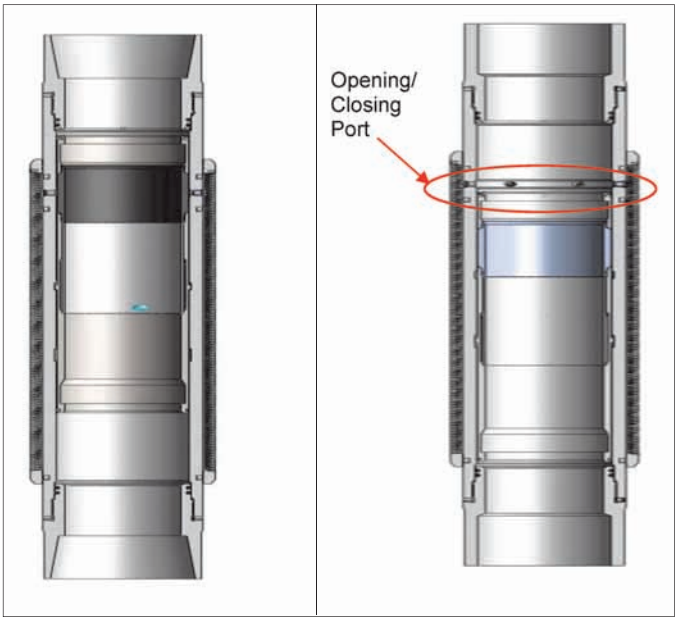

Fig. 6a. Closed position of the ICD (left).
Fig. 6b. Open position of the ICD (right).

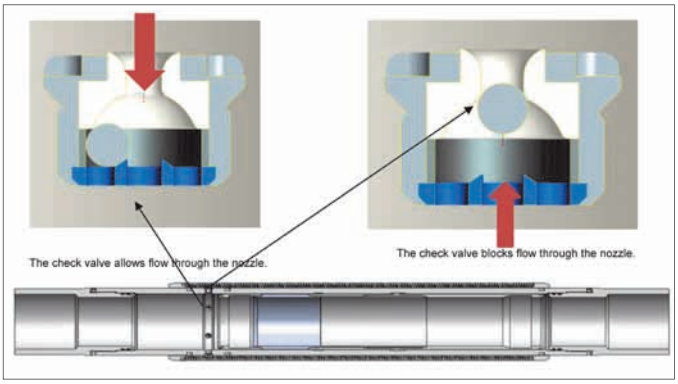

Fig. 6c. Active ICDs with check valve in opened and closed positions.

Advantages of Active Completion

1. Future water shut-off can be performed by closing the water producing ICD using the shifting tool run by wireline or CT.
2. Cross flow between zones and/or branches can be prevented using the check valve in the ICDs.
3. Future matrix acid stimulation can be performed selectively by closing the ICDs where the acid is not desired and stimulating the intervals having open ICDs.

Note: The installed check valve is acid dissolvable, so it can be dissolved if required. Therefore, care is needed while per forming any kind of acid job as this might disable the check valve and lead to cross flow between the reservoirs.

4. Reservoir management is enhanced.
5. The mechanical sleeve in the active ICD is designed to provide reliability and longevity.
6. Completion time is reduced (no inner string required for open hole packet setting).
7. Hole displacement is possible prior to setting the lower packer.
8. Drillers can get underbalance wells safely in place prior to landing the hanger.

The disadvantage of using this completion is that in case of well control issues, the completion proves to be a major hurdle in regaining control, as it is a closed system. The ICDs can also be deformed if the differential pressure at the check valve is above 1,000 psi.

To mitigate this issue of well control in the completion for the horizontal producer, the check valves of three ICDs in the higher permeability zone were dissolved with 10% hydrochloric (HCl) acid using CT. The injectivity after dissolving the check valves was more than 2 barrels per minute at 1,000 psi.

An enhanced ICD design, which provides the required functionality to eliminate the inner string for open hole packer setting, has been developed. This incorporates a series of hydro-mechanical delayed opening valves and designated multitasking valves into the ICD, which effectively allows the ICDs to act as solid, pressure containing, inner components, Fig. 7. This provides the flow-through capabilities required for circulating through the liner and the pressure integrity for setting the packers. Once the packers are set, all the ICD valves in the well are tripped open by simply applying pressure above a predetermined triggering pressure. The valves open when this applied pressure is bled off, resulting in fully functional ICDs.

Additionally, the option exists to postpone opening these

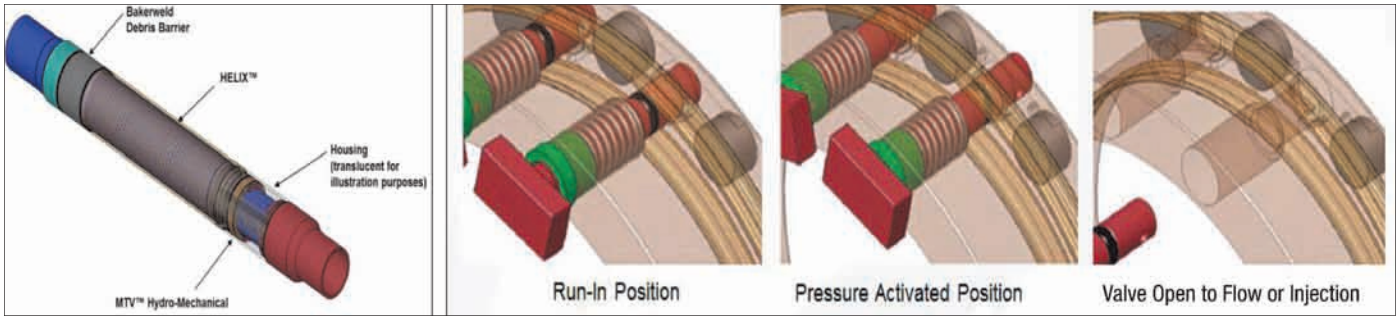

Fig. 7. ICD with multitasking valve.

valves until after the upper completion is installed, thereby isolating the open hole until after the well has been fully completed and surface equipment has been installed. This results in a higher level of well control, similar to using a formation isolation valve in the liner[4].

MODULAR ANCHOR AND UNIVERSAL SHIFTING TOOL (UST) FOR ACTIVE ICD SLEEVE OPERATION

The wireline conveyed modular anchor and UST brings precision to well intervention operations, eliminating the reliance on estimates and assumptions. The bidirectional, high speed telemetry system provides precise control from the surface, resulting in a dynamically controlled modular tool that proves flexibility during intervention operations. The sensors incorporated into the tool enable the operator to monitor the tool and the progress of the downhole operation while responsively controlling the tool for optimal performance.

To open or close a well component, such as the sliding sleeve, the UST radially extends profile keys to engage the completion equipment. The keys are extended with specified preload force, but remain compliant to navigate varying well geometry. The keys can fully retract into the UST to enable the tool to pass any restrictions.

The modular anchor and UST, Fig. 8, used in combination with a wireline conveyed UST, Fig. 9, provides setting assurance via real-time monitoring with controlled setting force,

Fig. 8. Modular anchor and UST.

Fig. 9. Wireline conveyed UST.

distance and speed. The tool provides data for assessing anchoring force, anchoring diameter, axial force and displacement, plug setting force, wellbore pressure and temperature, and the casing collar locator. The system uses hydraulic pressure created by an electric motor to generate force.

The tool uses linear actuator modules to apply controlled axial force to the shifting tool. First, the anchor module opens to anchor the tool in the well, then the linear actuator extends or retracts multiple times to apply the force required for the shifting tool to perform the opening/closing action. The linear actuator can be extended up to 20", and it delivers continuous measurement of displacement along the force applied to validate the operation. The speed, force and displacement of the anchor and linear actuator are controlled automatically downhole according to the parameters set by the operator at the surface.

The signature of the movement of the linear actuator can be closely monitored. Before the operation of the job, the actual signature of the modular anchor and UST is obtained in the workshop while opening/closing the ICD while in the position of the latching profile. This signature is for reference, and the same will be verified later while the linear actuator is opening/closing the ICDs. Figure 10 shows the signature of the tool while opening the active ICD.

Benefits of using the modular anchor and UST are:

- Real-time monitoring of the sleeve of an ICD can be maintained from the surface using the tool.
- With the signature from the log, the position of the ICD sleeve can be confirmed (whether opened/closed).
- Additional production logging runs are not needed to confirm the position of the sleeve.
- The tool can be used in conjunction with a tractor for horizontal wells.

The downhole application of the modular anchor and UST in this horizontal producer for use in selective shifting of the ICDs was the first in the world.

OPERATION SUMMARY AND JOB EXECUTION

After ICD completion of the horizontal well, the modular anchor and UST used in conjunction with the tractor were able

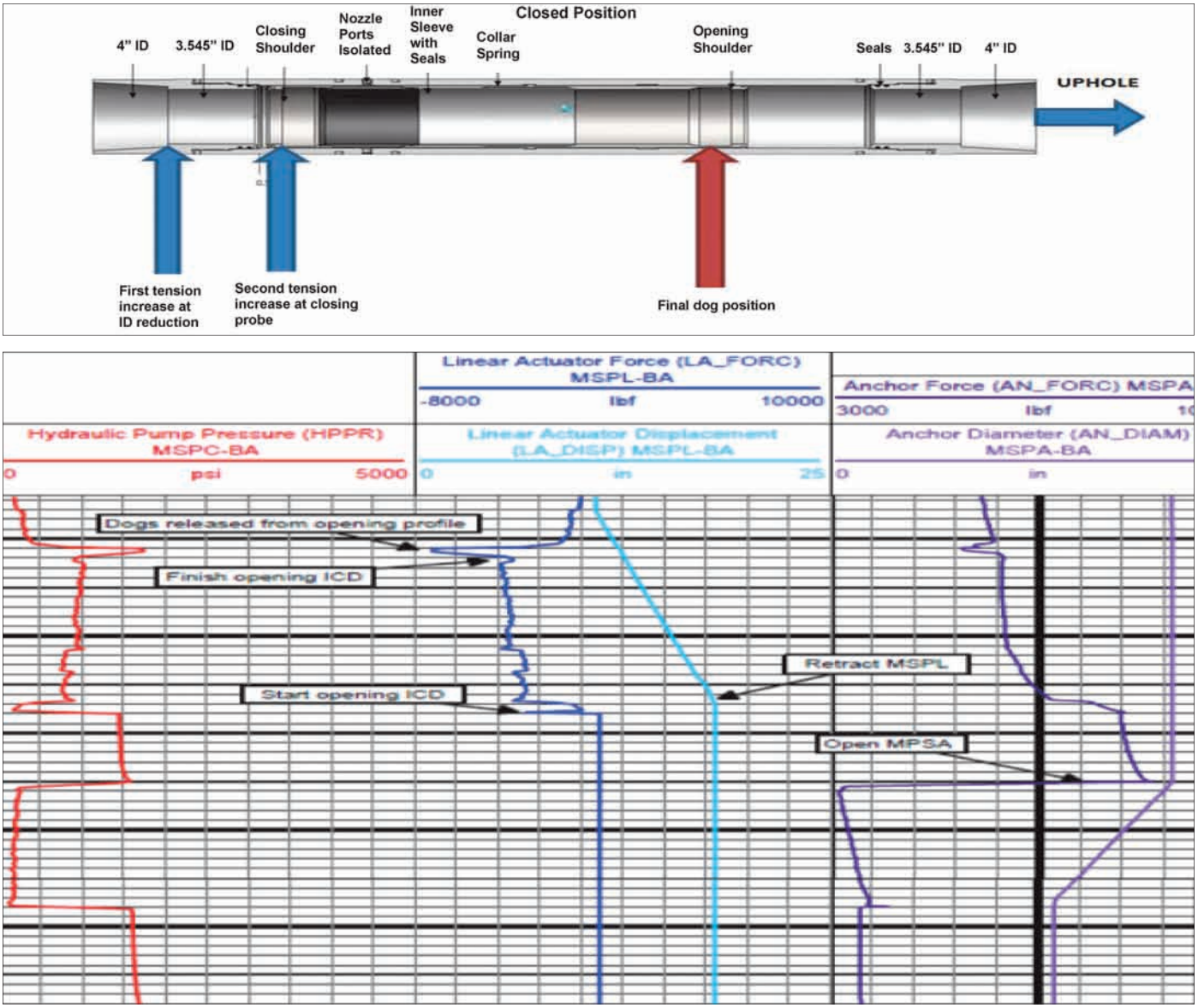

Fig. 10. Signature while opening the ICDs, used for reference.

to selectively engage each of the ICDs and obtain the signature profile while performing each job, Fig. 11. The anchor and the linear actuator secured the system, then pulled to shift open the ICDs. The force vs. the displacement signature was captured for each shifting operation and was compared with the reference signature, as previously seen in Fig. 10, to confirm that the ICDs were fully opened. From Fig. 11, it is clear that ICDs 1, 3, 4, 5, 6, 7, 9 and 10 clearly replicated the signature obtained while testing the tool in the workshop. The signature for ICDs 11 and 12 is not exactly as per the reference signature; however, the signature trend clearly indicated that the ICDs were opened using the tool.

PRODUCTION EVALUATION

The production results before and after completing the well clearly show that the active ICDs substantially helped to decrease water production, from 30% to 16%, with an increase in oil production from 1,200 barrels per day (bpd) to 3,700 bpd, an increase of 208%. The production results are tabulated in Table 1.

The production evaluation made using the NETool simulation model to compare the inflow production profile of the ICDs against the open hole completion is shown in Fig. 12.

It can be seen from Fig. 12 that there is a contribution from all of the opened ICDs; however, due to one section's higher permeability and reservoir pressure, the ICDs completed in this section have a higher contribution. Later, the sections of the completion with lower permeability and lower reservoir pressure were also able to contribute to the production (which was not the case when the well was completed as open hole). The plot in red shows the contribution from the reservoir while the completion was open hole, and the plot in blue shows contribution when the well was completed with active ICDs.

Comparing the well performance with the formation analysis log clearly shows that the zones that previously were

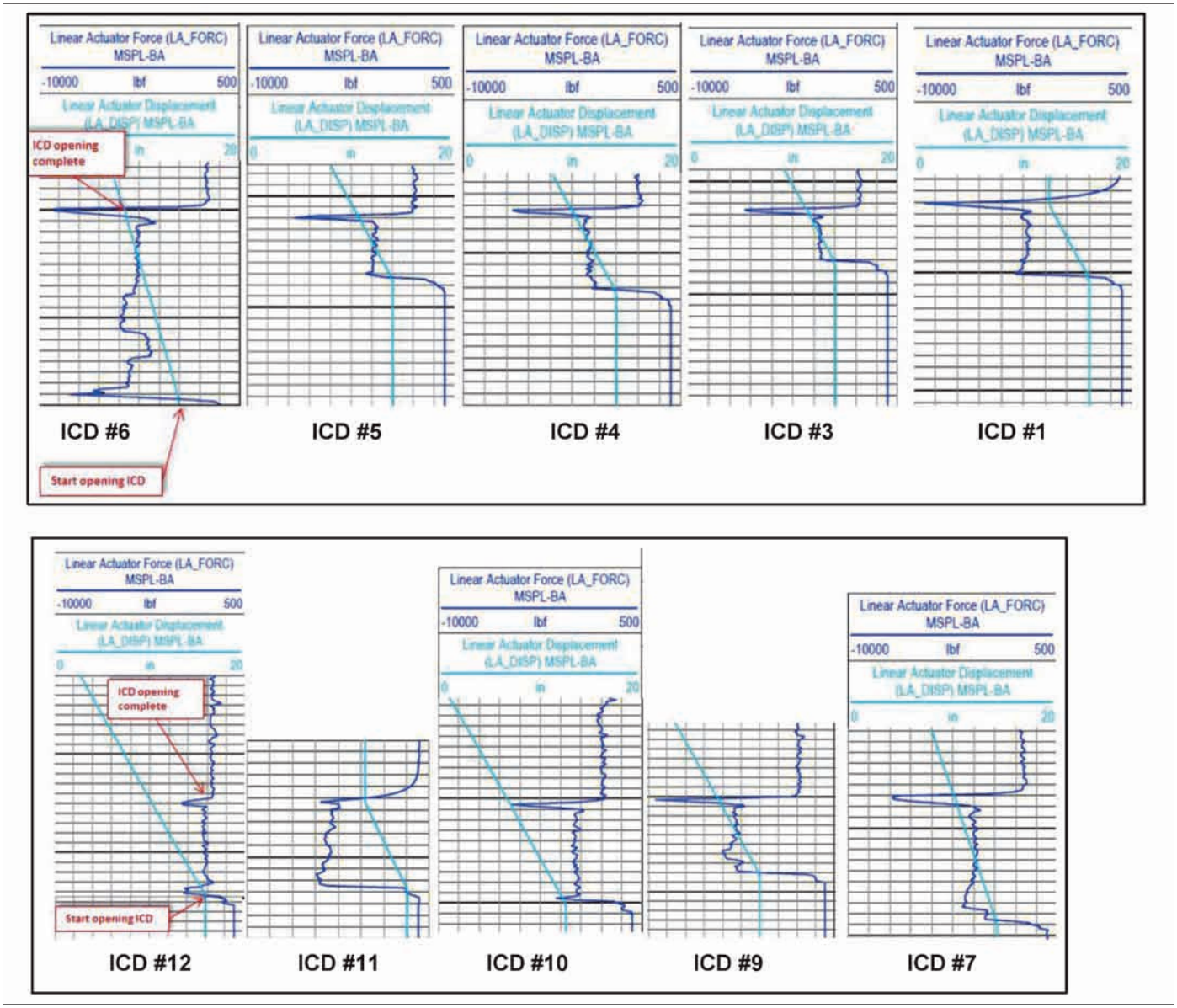

Fig. 11. Actual signature of the tool while opening the ICDs.

Type	Liquid Rate (MBD)	Oil Rate (MBOD)	W/C%	% Increase in Oil Production
Rate test with open hole completion	1.7	1.2	29.7	208%
Rate test with active ICDs completion	4.4	3.7	16.0	

Table 1. The tabulated production results

contributing to production due to a high permeability streak, leading to water coning, have been restricted. In fact, with the installation of the ICDs, all the zones have started to contribute to the production in the wellbore. Since the number of ports in each active ICD is dependent on the permeability variation and required contribution to the wellbore, the contribution from each ICD is now showing the desired variation.

CONCLUSIONS AND RECOMMENDATIONS

Below are the conclusions and recommendations following installation of the new generation active ICDs and use of the modular anchor and UST to open the closed ICDs.

- Installation of the new generation ICDs helps to control oil and water production.
- Because installation of the new generation of active ICDs provides the flexibility to close and open the ICDs

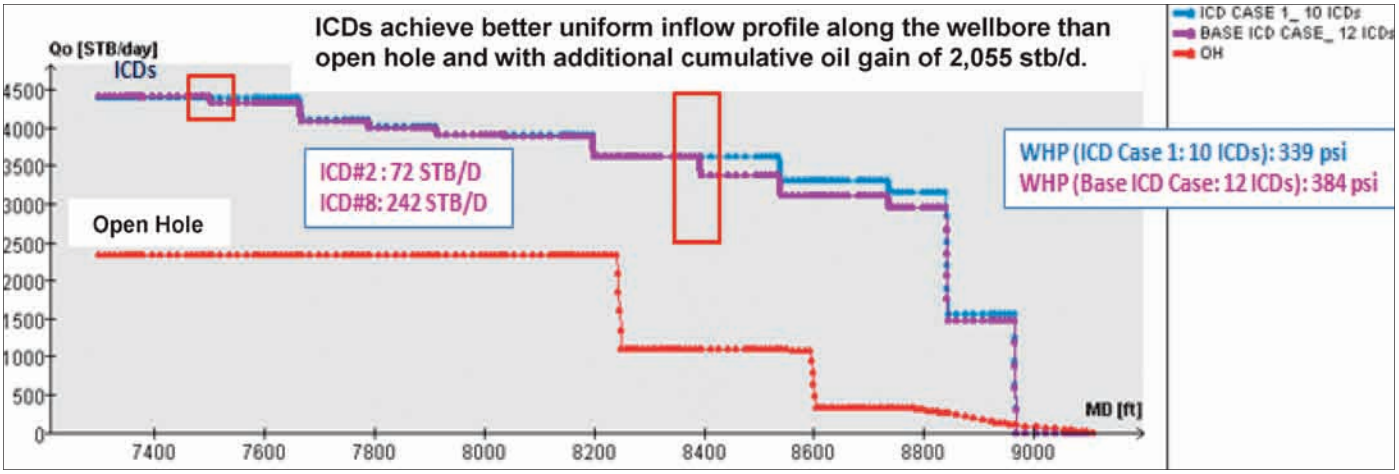

Fig. 12. Production comparison with open hole and active ICD.

as required, there is no need to perform an additional water shut-off job in wells completed with the active ICDs, as the ICDs producing water can be closed using the UST.

- Using the modular anchor and UST provides a clear signature of the sleeve position, which confirms the open/closed status of the ICDs, realizing cost savings since there is no need to run an additional production log for confirmation of the sleeve position.
- Using new generation ICDs minimizes well intervention as the production logging along with subsequent action to open/close the ICDs can be performed in one run.
- Flow from more than one zone is possible using wells completed with AWC even with different BHPs, while the cross flow between reservoirs/zones is avoided with check valves.
- Wells completed with AWC are able to minimize the water coning effect, leading to increased well life. The economics of completing the well with AWC are favorable, as the well life is increased substantially.
- The need for well maintenance is minimized, including workover for isolating and sidetracking in another direction when the water production increases. The sweep efficiency is also enhanced by use of this technology.
- Possibilities exist for expanding the utilization of new generation active ICDs for future drilling/workover completions in horizontal wells susceptible to water production.

ACKNOWLEDGMENTS

The authors would like to thank the management of Saudi Aramco for their support and permission to publish this article and to the management of Schlumberger and Baker Hughes for providing support while preparing this article.

This article was presented at the SPE Annual Technical Conference and Exhibition, Amsterdam, The Netherlands, October 27-29, 2014.

REFERENCES

1. Peterson, E.R., Coronado, M.P., Garcia, L.A. and Garcia, G.A.: "Well Completion Application for the Latest Generation Low-Viscosity Sensitive Passive Inflow Control Device," SPE paper 128481, presented at the IADC/SPE Drilling Conference and Exhibition, New Orleans, Louisiana, February 2-4, 2010.
2. Al-Mulhem, N.I., Sharma, H.K., Al-Zain, A.K., Al-Suwailem, S.S. and Al-Driweesh, S.M.: "A Smart Approach in Acid Stimulation Resulted in Successful Reviving of Horizontal Producers Equipped with ICD Completions, Saudi Arabia: Case History," SPE paper 127318, presented at the SPE International Symposium and Exhibition on Formation Damage Control, Lafayette, Louisiana, February 10-12, 2010.
3. Garcia, L.A., Coronado, M.P., Russell, R.D., Garcia, G.A. and Peterson, E.R.: "The First Passive Inflow Control Device That Maximizes Productivity during Every Phase of a Well's Life," IPTC paper 13863, presented at the International Petroleum Technology Conference, Doha, Qatar, December 7-9, 2009.
4. Coronado, M.P., Woudwijk, R., Infra, M., Al-Mumen, A.A. and Al-Baggal, Z.A.: "Latest Generation Inflow Control Technology Provides Added Functionality during Completion with Improved Well Control Features," IPTC paper 13862, presented at the International Petroleum Technology Conference, Doha, Qatar, December 7-9, 2009.

BIOGRAPHIES

Hemant K. Sharma is Senior Production Engineer with more than 23 years of experience in the upstream oil and gas industry, which includes onshore and offshore technical support. His experience and knowledge includes production enhancement and sustainability, formation damage diagnosis and remediation, well stimulation, water shut-off, well surveillance and monitoring, well completion and wireline, long-term planning/forecasting and construction/commissioning of large oil and gas complexes. Currently, Hemant is working as a Senior Production Engineer in the Southern Area Production Engineering Department.

He is a member of the Society of Petroleum Engineers (SPE) and has published many technical papers related to production engineering.

In 1990, Hemant received his M.Eng. degree from Bhagalpur College of Engineering, Bihar, India, and in 2005, he received an MBA from Indira Gandhi National Open University, Delhi, India.

Abdulrahman K. Al-Mulhim is a Senior Petroleum Engineering Consultant working in Saudi Aramco's Southern Area Production Engineering Department. He has 30 years of experience within Saudi Aramco and has worked in various upstream organizations — production engineering, reservoir engineering, production facilities, drilling engineering and well completion. During the development of the giant Khurais field, Abdulrahman was assigned the responsibilities as Superintendent of the Khurais and Central Arabia Well Services division from March 2007 through September 2010.

He is an active member in the Society of Petroleum Engineers (SPE) and has authored, coauthored and presented various SPE technical papers.

Abdulrahman received his B.S. degree in Petroleum Engineering from King Fahd University of Petroleum and Minerals (KFUPM), Dhahran, Saudi Arabia.

Technology Test Site: Value Proposition for a "Live Field Laboratory"

Authors: Modiu L. Sanni, John T. Allen, Scott S. Jennings, Dr. Michael A. Jervis, Christopher B. Ayadiuno, Razally M. Ali and Husain N. Al-Najrani

ABSTRACT

To accelerate the development, early uptake and deployment of new technologies being developed in-house by Saudi Aramco's EXPEC Advanced Research Center (EXPEC ARC) and technologies being developed in collaboration with industry service providers and academia, Saudi Aramco started constructing a Technology Test Site (TTS) in a producing oil field. The TTS, when completed, will be a "live field lab" where many emerging technologies and innovative ideas can be tested and tried under normal reservoir conditions.

To date, six wells have been drilled and completed. Extensive and comprehensive geoscience and engineering data were acquired for detailed reservoir characterization and description, including over 11,000 ft of core data. Preliminary results from the ongoing elaborate data analyses, including dual energy X-ray computed tomography (CT) scans, geomechanical data and log data, have yielded some intriguing insights into the often ignored nonhydrocarbon-bearing Upper Cretaceous and Tertiary formations. The ongoing data analyses show why certain intervals are unable to withstand mud weight of 8.33 pounds per gallon (ppg), equivalent to fresh water, while drilling. Attempts are being made to extract requisite information that may help to resolve some of the challenges, e.g., the lost circulation while drilling and near surface seismic anomalies that are frequently encountered across the Tertiary and Cretaceous shallow formations.

This article highlights the value proposition for the live field lab technology test site, lessons learned during the first phase of the TTS development, some results of ongoing analyses and some of the best practices that were developed.

INTRODUCTION

Saudi Aramco's EXPEC Advanced Research Center (EXPEC ARC) is responsible for upstream oil and gas technology development. The center carries out cutting-edge upstream research and development of innovative, high impact solutions and technologies that will help expand Saudi Aramco's reserves base and improve hydrocarbon recovery. From a humble beginning as a technology department, the center has become an incubator of groundbreaking technologies and a cradle for unique and leading technologies designed to meet the challenges of current and future world energy demands.

The Technology Test Site (TTS) was conceived as a world-class field laboratory within a producing oil field where new ideas, concepts, subsurface/surface tools and technologies from EXPEC ARC can be tested, proved, calibrated and qualified to expedite the development and deployment of pertinent technologies to address some of the company's business needs, including:

- Improved seismic acquisition and processing practices.
- Enhanced reservoir management practices.
- Improved drilling and completion practices.
- Reduced costs and increased recovery factors.

The site not only will act as a catalyst to accelerate the development and deployment of new technologies from EXPEC ARC, but will also provide a companywide location/platform for the integration of multidisciplinary research projects focusing on oil and gas "discovery and recovery" related challenges. In addition, the TTS will also undertake Saudi Aramco approved projects that may be proposed by partner companies, service companies, agencies, research institutes and universities.

SITE SELECTION

The TTS is situated in a designated 5 km x 10 km area in the

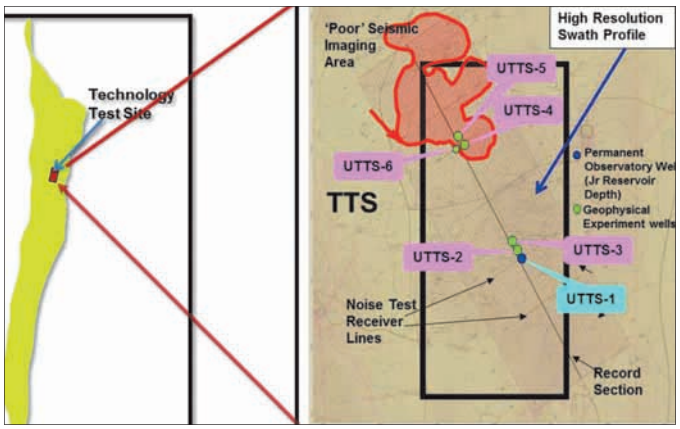

Fig. 1a. Location of the TTS on the Ghawar structure (left).
Fig. 1b. TTS well location (right).

mid-northern part of the world's biggest onshore field, Fig. 1. The site was carefully chosen to include a variety of geologic and reservoir conditions that are representative of challenges in terms of future reservoir development and data acquisition quality. Other factors considered in the location decision were to find an area of active oil and gas production with little or no changes to its reservoir conditions in the forseeable future, with low density of major surface facilities (existing and planned), and with no major topographic challenges (scarps, wadi drainages, etc.).

Furthermore, the area's preexisting seismic data, which straddles both good and poor seismic data areas, Fig. 2, would help to address some of the challenges relating to the effect of near surface anomalies on seismic interpretation, an issue that is prevalent across the onshore fields in the Arabian Peninsula.

GEOLOGY OF TTS/CANDIDATE FORMATIONS

The TTS was planned to be a well-characterized site targeting the Upper Jurassic (Arab-D reservoir) to the Tertiary sedimentary section, Fig. 3a, of the Arabian Peninsula. According to Powers et al. (1966)[1] this section is naturally dominated by gross characteristic carbonate and siliciclastic lithologies separated by significant breaks in the geologic record. The formations range from mostly carbonate but with alternating evaporite-normal marine cyclic deposits near the end of the Jurassic through the dominantly coarse clastic rocks with thin basal carbonate units of the Cretaceous, which include some evaporites, but mostly sandy limestone and sandstone of the Pliocene.

The Upper Jurassic and early Lower Cretaceous rocks, almost entirely shallow water limestone facies, are composed of predominantly calcarenitic limestone — lime sand admixed with a lime mud matrix — although thick, often laterally persistent beds of calcarenite — clean washed lime sand and gravel — are common at many levels. Lime sands are of various origins, but skeletal debris and aggregate pellets are most common.

With the exception of a thin, albeit persistent, basal limestone, the late Lower Cretaceous rocks in central Arabia are mainly continental sandstone. Fine-grained sandstone is interbedded with carbonate in the upper part, and the unit shows gradational contact with the overlying continental series. Shale is commonly interbedded, and thin dolomite and limestone layers are locally present. Upper Cretaceous to Eocene rocks are for the most part limestone and dolomite with a few very thin interbeds of marl and shale, which are separated from beds above and below by a hiatus.

Tertiary rocks are mostly of shallow water to nonmarine origin. These deposits are a heterogeneous assemblage of sandy limestone, calcareous sandstone, sandy clay and a sandstone blanket in the Eastern Province. Unconsolidated sand and gravel, presumably for the most part of Quaternary and Recent periods, are erratically superimposed on the Miocene and Pliocene sequence.

Given the heterogeneity of the lithofacies and the unconsolidated nature of the younger rocks, especially in the Cretaceous and Tertiary sequences, one can begin to appreciate the difficulty of drilling through this section and the attendant massive lost circulation often encountered in these zones, as shown by the caliper log plots, Fig. 3b.

NEAR SURFACE SEISMIC ANOMALY CHALLENGES

This area presents many challenges for acquiring and processing seismic data. The near surface layers in particular present difficulties for seismic imaging due to varying weathering depths, near surface low-velocity zones, velocity inversions, karsting, topographic variations, buried wadis (dry riverbeds) and surface sand[2]. A series of tests was planned to help characterize the near surface as well as act as a test bed for new seismic technologies, such as single sensor high channel acquisition. As previously seen in Fig. 2, the TTS was designed to cover areas

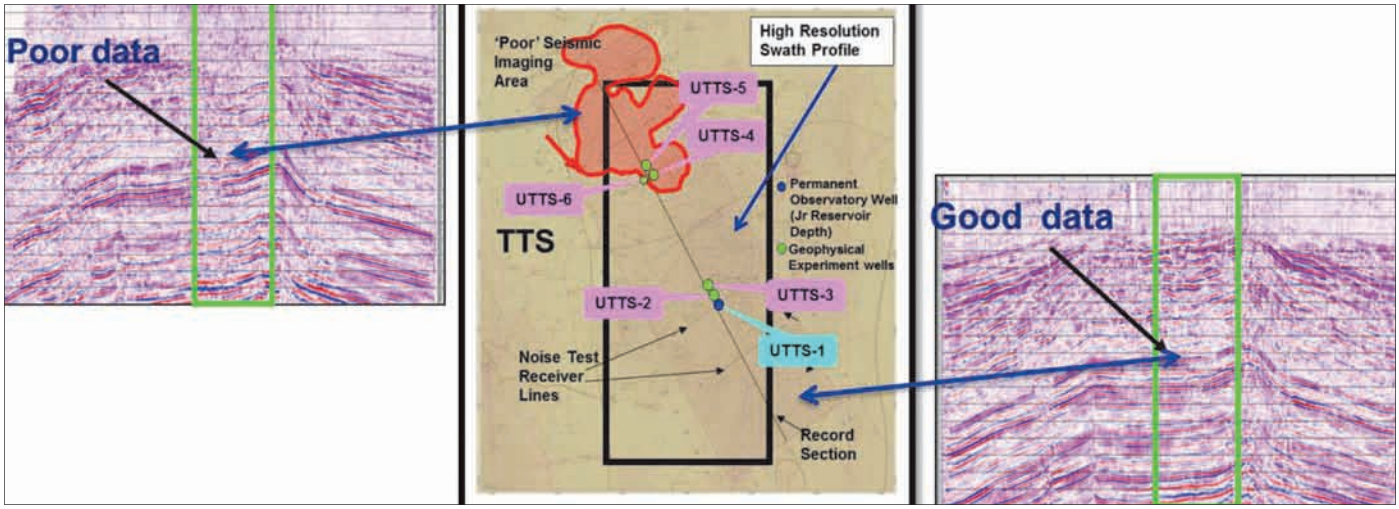

Fig. 2. Quality of seismic data across the TTS area.

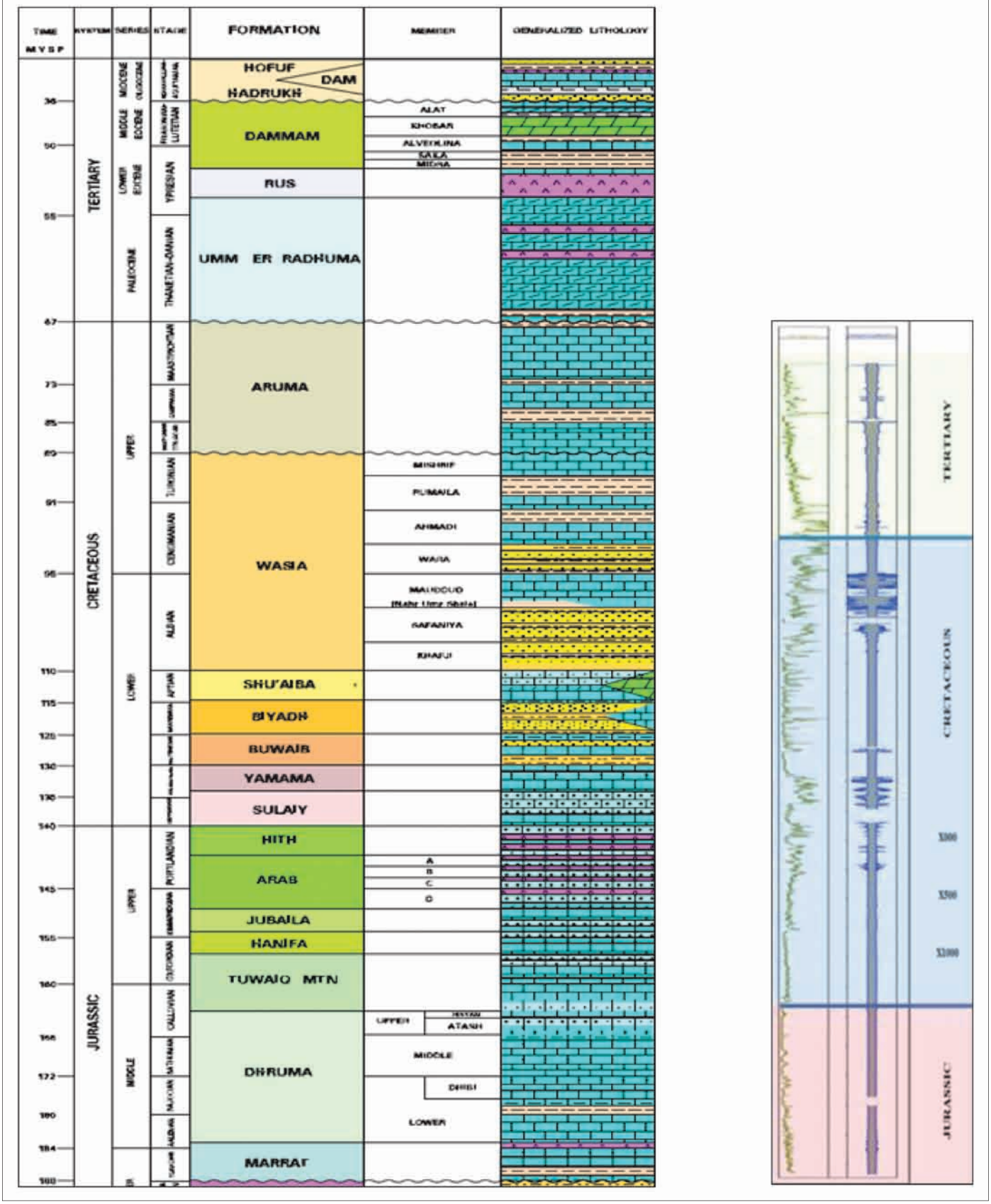

Fig. 3a. Stratigraphic column of the TTS area (left).
Fig. 3b. Sections of interest and typical caliper readings (right).

of both good and bad seismic data quality. These variations provide an opportunity to better understand the factors affecting seismic signal-to-noise ratio in this desert environment.

The initial seismic tests included the following:

- Designing and recording an uncorrelated, bunched geophone ambient noise spread (microspread) for the test site — the objective being to characterize the noise levels. We performed a set of sweep tests in a circle around the microspread at a constant azimuthal increment to give an idea of anisotropy over a fixed spatial subsurface region.
- Designing a very high resolution, uncorrelated, multiple 2D line test where we could group data from different crossline and inline receiver/source arrays. Each channel needed to be a very small array or bunched geophones to aid in development of acquisition/processing strategies and algorithms for point source/receiver acquisition. This high resolution line can also be used to determine where future "smart" upholes — those with multiple logging suites along with conventional velocity profiling — might be drilled for calibration purposes.

One of the goals of the high resolution line is to produce a very detailed near surface model. Indeed, the actual "weathering layer" for the test site is not well-defined. The uphole log data will be used to help evaluate the seismic resolution limitations as well as define the lower base of the weathering or near surface zone. Factors, such as the effects of near surface velocity inversions and saturated layers (open or confined aquifers) on depth estimation in refraction statics, also need to be understood. Finally, these two tests will be used to investigate how the ambient noise limits seismic processing resolution in this area.

SITE DEVELOPMENT PLAN

The development plan for the TTS comprises subsurface and surface facilities that serve as key enablers for the site to fulfill its objectives as a catalyst to accelerate the development and deployment of new technologies. The TTS has two parts, namely the southeast and northwest. The southeast portion will serve as the main operational base of the TTS, with a few shallow wells having their total depth (TD) in the nonhydrocarbon-bearing Upper Cretaceous formation and a few Upper Jurassic wells that penetrate the hydrocarbon-bearing Arab-D reservoir. Here, a few state-of-the-art surface facilities will be built. The northwest part — with poor seismic data — will have a few shallow wells with TD (about 2,500 ft) in the Upper Cretaceous formation.

To date, six wells have been drilled, three on either side of the TTS. It is worth noting that a few more shallow wells may be drilled in the northwest part of the TTS. Furthermore, in the southeast part, other Jurassic deviated and horizontal wells — up to and below the Arab-D reservoir — will be drilled for drilling and completion tools related tests that can't be conducted in Well UTTS-1.

WELL DESIGN AND CONSTRUCTION

Each of the six wells drilled to date has its unique design and data acquisition objectives. A description of each well and the primary function of each well are provided next. The wells were not drilled in a sequential order. Well UTTS-1, being the deepest well, was drilled first by a heavier rig, and then Wells UTTS-4, UTTS-3 and UTTS-6 were drilled by a lighter rig. Wells UTTS-5 and UTTS-2 were drilled last because of their fiberglass casings.

SOUTHEAST WELLS

Data Well-1 (UTTS-1)

The first well drilled at the site, UTTS-1, is currently the only well penetrating the hydrocarbon-bearing Jurassic reservoir. UTTS-1 was drilled to a depth of about 7,000 ft, Fig. 4a. The well was drilled primarily to test tools intended for 5⅞" to 6⅛" open hole sections across the Arab-D reservoir. We needed to be able to do this with a completion string in place for better pressure control and safety. The well was extensively logged and cored virtually from surface to TD to establish a "ground truth" for incontestable comparisons between new logging tools and previously proven technologies tested under a similar environment. This meant that killing the well to run the open hole tools, as would normally be done, would affect the "sand face" and compromise the validity of our baseline data. The well therefore had to be designed to run open hole tools on hepta-cable into a live well. This led to a choice between two designs.

The easier and less expensive option was a monobore completion using the final cemented 7" drilling liner in the last hole section above the reservoir as the completion, with 7" completion tubing tied back to the surface above it. This design would have resulted in the ability to downsize all overburden hole sections.

The other alternative was a conventional design used in most Saudi Aramco Jurassic oil wells. Usually in this design, if the reservoir section is going to be 6⅛", the drilling liner in the previous section will be 7" and the completion tubing will be a smaller size, i.e., 4" or 4½". Since this would restrict entry into the reservoir section of larger tools, UTTS-1 would need a 7" completion inside of a 9⅝" drilling liner, necessitating increasing the size of all previous hole sections. This is no trivial matter for Saudi Aramco as our surface hole sections are already very large; due to the unresolved hole integrity problems we face on the onshore part of the Arabian Peninsula, we usually have four casing/hole sections plus a surface conductor above the reservoir in our Jurassic oil wells.

One of the aquifers immediately above the reservoir is overpressured in this particular part of the field. This has led to compromised cement jobs and premature failure of the drilling liner in a number of wells in this area. We developed a plan to prevent this in the test well; however, we knew that if we suffered such a failure in any case, we would have to perform a cement squeeze and then cement a smaller piece of tubing

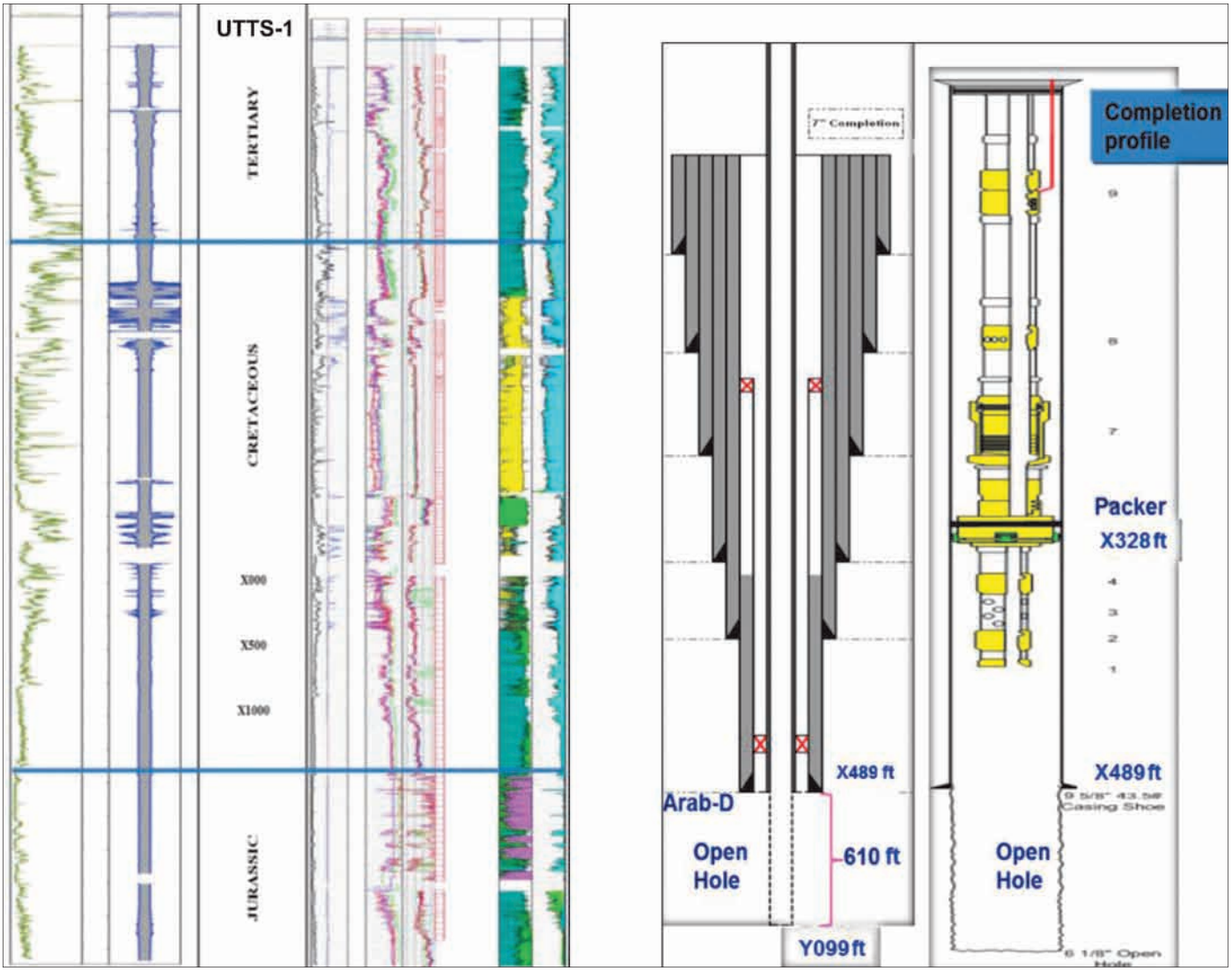

Fig. 4a. Well UTTS-1 log data; this is one of the most extensively cored wells (left).
Fig. 4b. Well UTTS-1 completion with over 600 ft of open hole (right).

across the damaged liner section. If we chose the easier, less expensive monobore design, this failure and remedy would reduce our ability to run the very tools that we were constructing the well to test.

We therefore chose to go with the more expensive completion well design to allow for workover in the event of liner failure.

The mechanism of liner failure in this part of the field was found to be related to the interplay of the characteristics of cement as it sets and the large pressure differential between two adjacent reservoirs. As cement enters its gel phase during setting, it loses most of its ability to transmit hydrostatic pressure. Therefore, if there is a large pressure differential between two zones in the cemented section, a flow will develop between them during the gel phase, washing permanent channels in the cement. We attempted to prevent this by placing inflatable packers in the open hole above and below the overpressure section and inflating them as soon as we finished pumping the cement, before the cement could begin to gel. Figure 4b shows the completion status of UTTS-1.

Data Wells -2 and -3 (UTTS-2 and UTTS-3)

The other two wells, UTTS-2 and UTTS-3, were drilled in the southeast area of the TTS for testing cross-well related tools, such as seismic and electromagnetic tools. The wells' TD ended at the Upper Cretaceous formation, Fig. 5a. UTTS-3 was extensively cored, and UTTS-2 was cored to fill a few gaps of poor or low data recovery in UTTS-1 and UTTS-2. UTTS-2 was completed with a fiberglass casing to provide transparency to electromagnetic signals. Figure 5b shows a typical completion for the shallow wells — they were completed with inhibited diesel in the casing.

NORTHWEST WELLS (UTTS-4, UTTS-5 AND UTTS-6)

Three wells have been drilled in the northwest area of the TTS. We initially planned to drill only two wells (UTTS-4 and UTTS-5) for cross-well technology related testing purposes. But after severe lost circulation led to a large washout, Fig. 6, which invariably affected the cement bond and led to poor

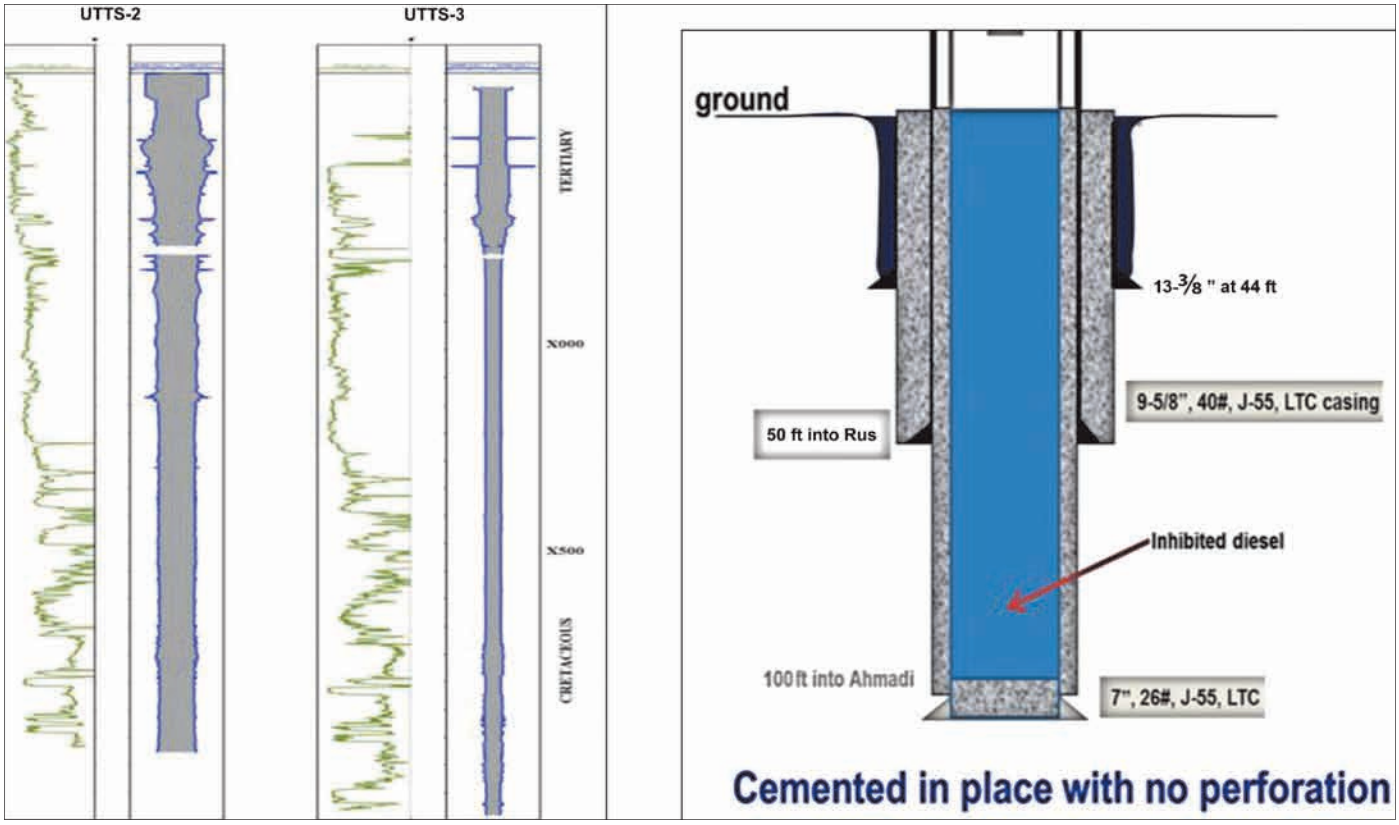

Fig. 5a. Shallow wells UTTS-2 and UTTS-3 (left).
Fig. 5b. Typical completion diagram for shallow wells (right).

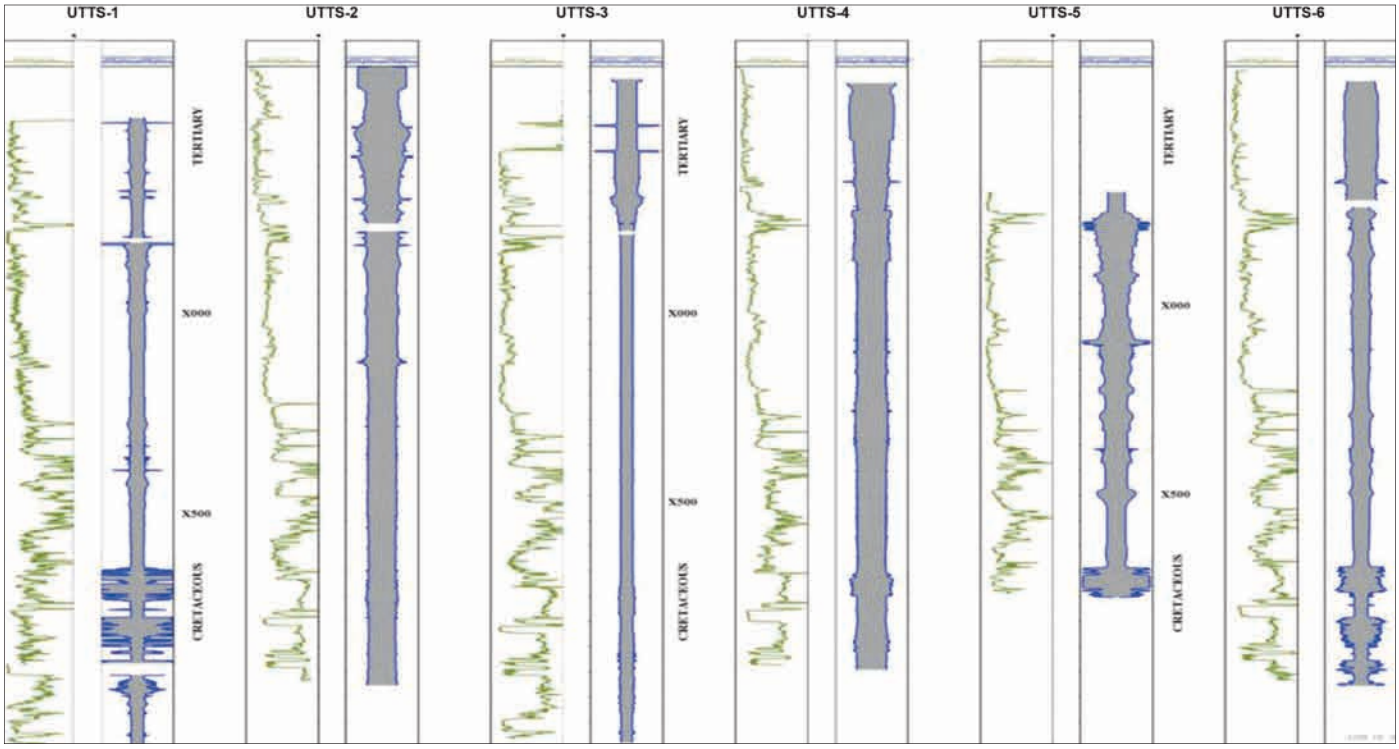

Fig. 6. Borehole sizes for all the wells across the Tertiary and Cretaceous formations, showing the effect of curing lost circulation. Well UTTS-6 was drilled as a replacement well for UTTS-4 because of severe washout and bad cement bond.

acoustic coupling in UTTS-4, a replacement well, UTTS-6, was drilled. The lost circulation cure using "downhole concrete" was initiated and applied in both UTTS-5 and UTTS-6. This ensured a reasonably gauged hole for good data quality and a decent cement bond. UTTS-5 was completed with fiberglass casing, while UTTS-6 was completed with metal casing. Both

wells were completed with inhibited diesel in the casing, similar to UTTS-2 and UTTS-3.

CURING SEVERE LOSSES IN THE UMM ER RADHUMA (UER) — A SEAT-OF-THE-PANTS APPROACH

Complete mud losses in the UER are quite common and to be expected while drilling in this area. These losses are considered incurable, so loss of circulation (LOC) treatment is generally not attempted for normal oil wells. Previous attempts to cure these losses with many types of conventional and unconventional lost circulation material (LCM) treatments had proven ineffective. The standard procedure to deal with losses in this interval is to drill ahead blind with water and gel sweeps; however, the presence of shales that react with water below the loss zone often necessitates stopping and setting casing as soon as possible after the shale is encountered.

In normal operations, there would be very little or no cement behind the casing, and therefore no effective acoustic coupling, above the loss zones. This isn't critical for normal oil wells; however, a good cement bond for proper acoustic coupling from casing to formation was required in these geophysical test wells to ensure good vertical seismic profile (VSP) data acquisition. This VSP logging-driven requirement for acoustic coupling necessitated a fresh look at this "insurmountable" drilling hazard.

Very little geological and geomechanical data had ever been gathered for the non-reservoir (Tertiary and Cretaceous) intervals in the test well area. The paucity of pertinent geomechanical data necessitated a robust, brute force approach. During the drilling campaign for the TTS wells, a logical protocol evolved, and reliable operational procedures were developed in curing or largely mitigating severe lost circulation. The practice used to cure these losses was a "let the well talk to you" approach. This seat-of-the-pants approach was used to successfully construct these wells. The only well that experienced severe washout and invariably poor cement bond at the early part of the drilling campaign was UTTS-4.

EXPERIMENTS CONDUCTED DURING THE DRILLING PHASE

Cementing experiments to cure losses were developed during the drilling of the producing wells. Complete losses were dealt with during the drilling of the hole section, which included the UER formation. Of the attempts to cure the losses, some were successful, while others were not. Lessons learned while dealing with curing these losses are shown at the conclusion of this article. Several cementing attempts to gain circulation follow:

Development of Downhole Concrete

- Typical oil well cement pumping equipment cannot pump large aggregate due to the opening of the suction and exhaust valves. To develop a "downhole concrete," we dumped some bridging material consisting of a series of sized aggregate down the hole. The largest was approximately 2½" in length and approximately ½" in thickness. The smallest was medium calcium carbonate ($CaCO_3$). Two more intermediate sizes of aggregate were placed inbetween the large aggregate and the medium $CaCO_3$. These were finally followed by medium sized mica.
- Cement was then pumped in the well via a drillpipe. The cement flowed through the aggregate/mica bridging material to form the downhole concrete.
- Generally, this method worked, so drilling could resume until losses occurred again. Sometimes these losses occurred almost immediately after drilling out the downhole concrete. On other occasions, drilling continued for several feet while in the UER formation before experiencing losses.

Cementing Bridging Material Overtreating

- An early attempt at developing a bridging material began with the above formulation of various sized aggregate, but was followed by cottonseed hulls. When running in hole with drillpipe, however, the cottonseed hulls were tagged too high and made a bridge above the previously dumped material. The question on the rig was whether perhaps the cottonseed hulls were dumped too rapidly. The rig had to pull out of hole and run back in with a clean out assembly to remove the bridged cottonseed hulls. This was another lesson learned.

Development of a Floating Cement Plug

- A floating cement plug was developed in the lab. The drilling fluid density in the well was 65 pounds per cubic feet (pcf). The cement developed in the lab contained hollow glass spheres with a downhole density of 65 pcf. The objective of developing and pumping this floating cement plug was to try a different cementing system to determine if the cost-effectiveness — in reduced rig time, cementing materials and cured LOC — would be beneficial to well construction.
- After the cement was designed in the lab, preparations were made to pump the new floating cement plug. During the batch mixing of the cement, the rig only had neat class G cement on location, so it was decided that other additives would be placed into the mixing water.
- During the mixing of the mix water, when adding the hollow glass spheres, it was discovered that they were of low quality, with a specific gravity of 0.75 to the water

specific gravity of 1.002. The resulting density, measured by the pressurized density balance, was not below 65 pcf. At that point, it was obvious that with the materials available to us, we could not make a floating cement plug. At that point, a quick decision was made on the rig to add enough cement to bring the density to 70 pcf. Therefore, the floating cement plug was never really pumped. This information was added to the lessons learned. During this project, this cement system was not attempted again.

Logging Experiments

- The uniqueness of the Jurassic well (UTTS-1) provided the opportunity to conduct a mud logging comparison between different local service providers.
- In addition, a new mud gas technology, being promoted by one of the service providers at that time as the best-in-class solution to accurately measure gas composition in the reservoir, was tested, Fig. 7[3].

DATA ACQUISITION

The TTS is expected to be a fully characterized and well understood environment that will serve as a "ground truth" for establishing incontrovertible comparisons between new logging tools and previously proven technologies tested under a similar environment. Therefore, comprehensive sets of log data were acquired in each well to establish "reasonable baseline data." All the wells were logged from surface to TD. In addition, over 11,000 ft of cores were acquired in all the wells.

DATA ANALYSIS

Critical to developing a competent geological model of the TTS is a robust and comprehensive reservoir characterization.

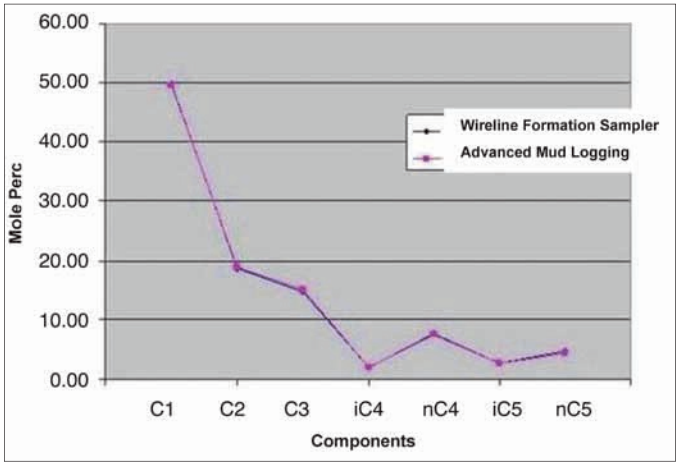

Fig. 7. Results of advanced mud logging in Well UTTS-1 show a perfect match between the composition derived from mud logging and from the modular formation dynamics tester sample analysis.

This requires identifying all the main stratigraphic zones, lithofacies and petrophysical properties, such as porosity and permeability, to be used as input into the geo-cellular model. Following this underpinning objective, a comprehensive logging and coring program was put in place as part of the drilling campaign. Data acquired in the six wells include advanced mud logging, wireline logs and over 11,000 ft of core data.

In one of the experiments/tests conducted while drilling, a new mud gas technology, being promoted by one of the service providers at that time as the best-in-class solution to accurately measure gas composition in the reservoir, was tested. The results were compared to the gas compositional analyses derived from the formation tester — modular formation dynamics tester samples. It is worth highlighting that the results showed a perfect match.

Three major service providers were involved in the wireline data acquisition work. The logging program was an extensive and comprehensive undertaking that went far beyond a typical logging program for any well. This was necessary to ensure that all relevant geological and engineering input data for a robust geological earth model was captured at this stage. Wireline logs acquired included, but were not limited to, spectral gamma ray, vertical and horizontal resistivity, neutron, density, full wave sonic, magnetic resonance, mineralogy — such as elemental capture spectroscopy — formation tester and borehole image logs. Given the sheer volume of data acquired, a systematic workflow was required for achieving effective formation evaluation results.

A preliminary log analysis was performed on all six wells, which provided an initial understanding of the lithofacies encountered and the petrophysical properties used in the geological model. The lithofacies comprise both siliciclastic and carbonate rocks of the Upper Jurassic (Arab-D) and Tertiary formations of Saudi Arabia. The shallow stratigraphic interval encountered in all six wells is predominantly devoid of hydrocarbon charge in this field. Subsequently, the lithostratigraphic framework was determined to be varied and heterogeneous, due to the highly variable geological processes that may have taken place, resulting in a complex depositional and diagenetic footprint that is often the hallmark of these formations at all scales. Porosity values range between 10% in tight zones to over 40% in unconsolidated sections. There is abundant evidence of karsts and thief zones, responsible for lost circulation in many intervals. Log quality was severely affected across these zones, which made data interpretation challenging at best. The image data, CT data and nuclear magnetic resonance (NMR) data gave some indications of why certain intervals are unable to withstand a mud weight of 8.33 parts per gallon (ppg), equivalent to fresh water, while drilling, Fig. 8.

These stratigraphic intervals are not typically logged in this field because they are never a target of interest during conventional exploration campaigns. This analysis therefore was aimed at providing vital standardized lithostratigraphic, petro-

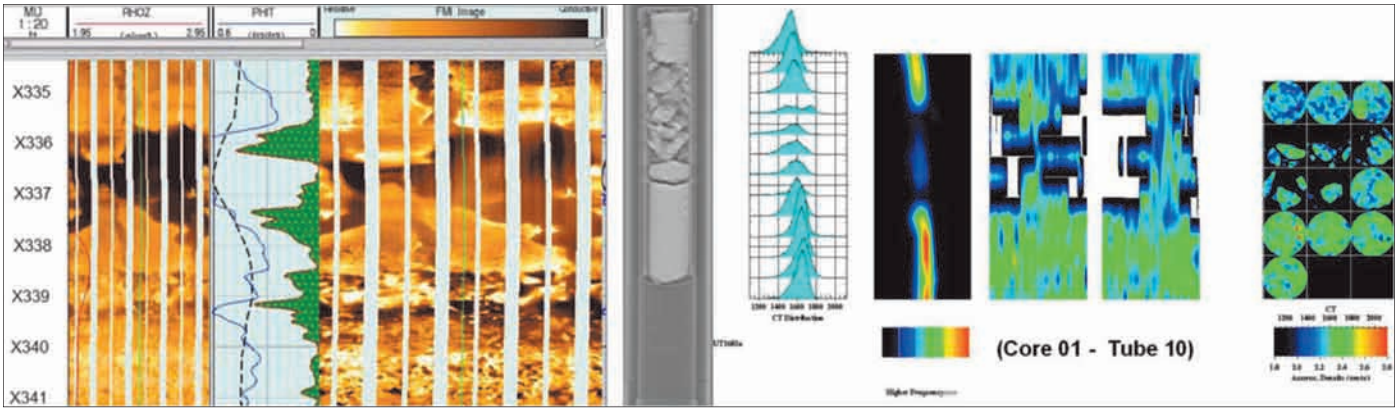

Fig. 8. CT scan and formation micro-imager data showing intervals that are prone to severe washout.

physical and other engineering parameters for improved understanding of the geology of the drilled sections.

Furthermore, over 11,000 ft of core was cut during the drilling campaign. Comprehensive core analysis is currently ongoing. Figure 9 shows the core analysis workflow being used. A dual energy CT scan has been carried out on some of the cores, both in-house and by an external service provider. Core log integration is ongoing, and extensive integration with other data will be done when significant sets of the core analysis data become available.

The result will be integrated into the analysis routine. Preliminary log analysis results highlight the internal geological heterogeneity and complexity of the formations. A cross section of the six wells covering the first 2,600 ft TVD is shown in Fig. 10.

SURFACE FACILITIES

Given the anticipated high number of trial tests that will be carried out at the TTS and its distance from the head office, it was planned to have state-of-the-art surface facilities at the southeast part of the test site. The surface facilities plan includes the construction of about 1,140 m^2 of dedicated buildings. These include office space for personnel working at the test site, a central control room to operate and control subsurface experiments with real-time data transfer capability, a multipurpose room, a conference area for planning experiments and for holding technology transfer meetings, an equipment shed and a storage facility. Other facilities at the site include a maintenance workshop consisting of three bays: mechanical, hydraulic and electrical/electronic. The workshop will serve as a field maintenance and repair shop for prototypes or production downhole logging tools; wireline and formation evaluation while drilling tools and other electronic tools that may require minor repair or maintenance during the trial tests. This will eliminate the need to ship such tools out of the area — or the country — for repair. The site will also have a radioactive source bunker, located at some distance from the work area, for temporary storage of radioactive sources that may be needed for some downhole tools.

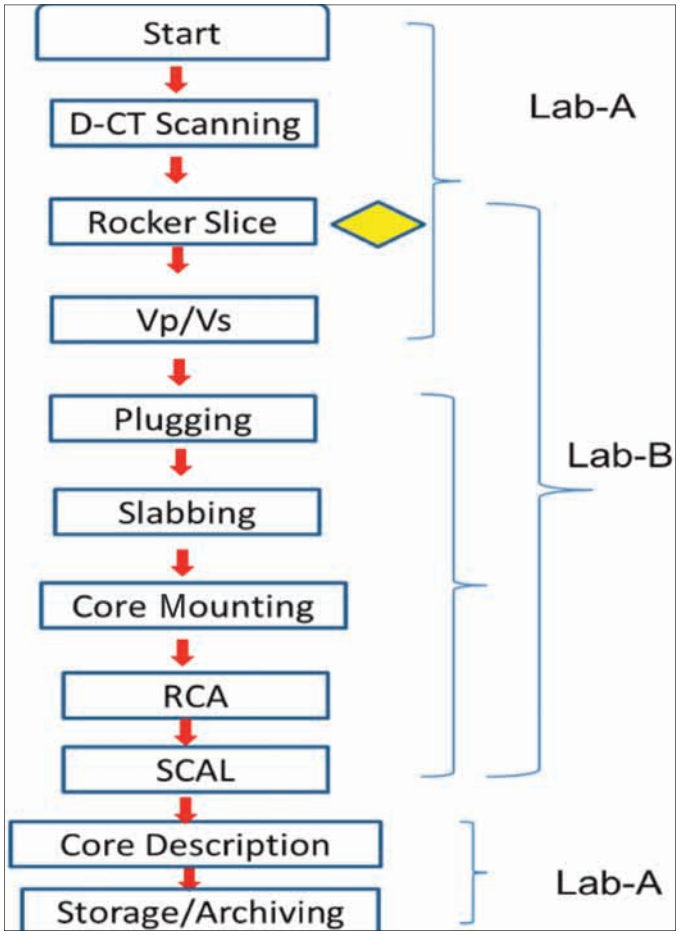

Fig. 9. Core analysis workflow.

In addition, the site will also have its own permanent hoist (a modified drilling rig) for safe deployment of logging tools into the test wells. The hoist will have a substructure, an elevated work floor and a sliding mechanism that will allow it to skid from one wellhead to another wellhead within the same row of cellars, if needed. It is anticipated that the hoist's derrick floor will be wider than that of a normal drilling rig to accommodate the many researchers and scientists who may want to witness an interesting trial test.

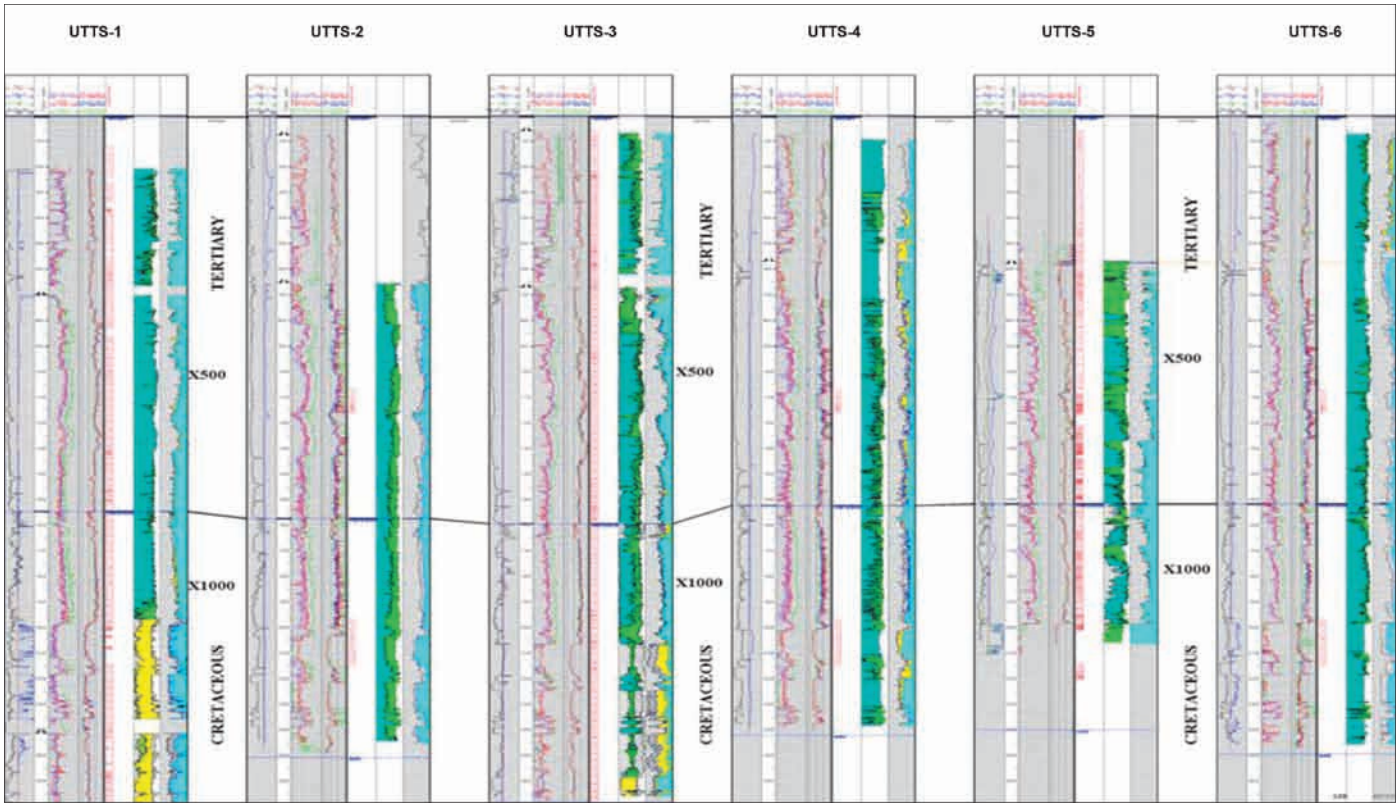

Fig. 10. Log sections across the Tertiary and Cretaceous formations in all the wells (from south to north).

LESSONS LEARNED AND BEST PRACTICES

To develop a knowledge base of best practices in constructing wells and developing a well test site required many lessons learned, as documented here.

Well Construction

- The upper hole LOC can be cured. To achieve this, many attempts are required, using sizing technology to achieve a bridging medium, for which cement is dehydrated, to form downhole concrete.
- Cement with no fluid loss control or expansion additives is successful when following the dumped LCM to create 100% circulation.
- The cooperation of rig personnel with drilling engineering expertise and lab support is extremely important in developing a wellbore that has excellent acoustic coupling properties.
- Many nonstandard procedures can be necessary on the rig floor to regain circulation.
- The choice of high quality cementing service companies and chemical packages can make or break a successful cement plug job.

TTS Value

From a broader perspective, successful implementation of the TTS as envisioned will be of substantial benefit to Saudi Aramco and the oil and gas industry at large. Experiences from existing test centers, with similar but fewer facilities, which are run by service companies, have shown that the return on investment can be huge if all the key elements are put in place. When completed as planned, the value proposition of the TTS for Saudi Aramco includes, but is not limited to:

- Faster and more reliable testing, qualification and validation of new technology, equipment and processes.
- Acceleration of technology deployment. It is envisaged that significant time — months to years — can be shaved off the current field deployment time of new technologies, eliminating the constraints of rig time, costs, oil production deferral and safety issues.
- A key enabler for creating and developing new technology as Saudi Aramco transits to becoming a "creator of value added E&P technology instead of just a end user of technology." Many emerging technologies and innovative ideas can be swiftly tested and tried under normal reservoir conditions.
- Provider of a "ground truth" for establishing incontestable comparisons between new logging tools and previously proven technologies tested under similar environments.

- Enhanced internal R&D capabilities, and external research and technology development partnerships.
- An oasis for reliability tests, from component tests through system integration testing in a controlled and well-characterized environment.
- A companywide location and platform for the execution of multidisciplinary research projects focusing on oil and gas "discovery and recovery" related challenges.
- An excellent educational facility for training the next generation of engineers and scientists — especially as the Kingdom moves toward a knowledge-based economy.
- Promotion of international collaborations and joint industry projects. With the gamut of geoscience data collected and its well-characterized test wells, the TTS can serve as a certification center for new tools and equipment.
- A method to cure lost circulation across the troublesome Cretaceous and Tertiary formations. When fully implemented, the method developed at the TTS could lead to a significant reduction in the number of casing strings deployed in the normal Arab-D oil well. This will lead to huge savings in the drilling and completion costs for such wells, especially for the very deep gas reservoir wells.

FUTURE WORK

To realize one of the key aspirations of the TTS — its goal to be a fully characterized and well understood environment for testing technology — significant effort is being made to fully analyze and integrate the wealth of subsurface data acquired to date. Conventional and special analyses of some of the data are ongoing. Appropriate reservoir models will be built for each geological zone of interest: Tertiary, Cretaceous and Jurassic formations. In addition, efforts are being made to build state-of-the-art surface facilities on the site to expedite the utilization of the current subsurface assets (wells). Special hoist/mast and dual downhole lubricators will be deployed in UTTS-1 to enable safe, convenient and economically feasible deployment of experimental tools into and out of the wellbore.

CONCLUSIONS

The TTS is a laudable project, which when completed as envisioned will be a unique facility with a huge potential for benefiting Saudi Aramco and the oil and gas industry at large. No stone was left unturned in acquiring pertinent data for full characterization of the site to make it a "ground truth" for faster and reliable testing, qualification and validation of new technology. Significant efforts are being made to finalize the description and data analyses for this full characterization of the site and also to install state-of-the-art surface facilities. Once properly equipped, the TTS will be able to undertake technology tests proposed by Saudi Aramco, partner companies/agencies, such as service companies, research institutes and universities, thereby expediting the development and deployment of many future tools and technologies.

ACKNOWLEDGMENTS

The authors would like to thank the management of Saudi Aramco for their support and permission to publish this article.

This article would not have been possible without the contributions and efforts of many current and ex-colleagues and continuous support from Saudi Aramco. In particular we would like to acknowledge and thank Shiv Dasgupta, Jim Tucker, Jim Funk, Ton Loermans, Bob Greaves, Richard Palmer, Emmanuel Nwosu, Eid Al-Enezi, Ayedh Al-Dossary, Jason Hubbard, Sinan Caliskan, Alberto Marsala, Clemons Van Dijk and many others for their contributions.

This article was presented at the Abu Dhabi International Petroleum Exhibition and Conference, Abu Dhabi, UAE, November 10-13, 2014.

REFERENCES

1. Powers, R.W., Ramirez, L.F., Redmond, C.D. and Elberg Jr., E.L.: "Geology of the Arabian Peninsula: Sedimentary Geology of Saudi Arabia," U.S. Geological Survey Professional Paper 560-D, U.S. Geological Survey, 1966.
2. Keho, T.H. and Kelamis, P.G.: "A New Era in Land Seismic: The Near Surface Challenge," SEG paper 2009-3421, presented at the SEG Annual Meeting, Houston, Texas, October 25-30, 2009.
3. Loermans, T., Bradford, C.M., Kimour, F., Karoum, R., Meridji, Y., Kasprzykowski, P., et al.: "Advanced Mud Logging (AML) Aids Formation Evaluation and Drilling, and Yields Precise Hydrocarbon Fluid Composition," SPE paper 141277, presented at the SPE Middle Oil and Gas Show and Conference, Manama, Bahrain, September 25-28, 2011.

BIOGRAPHIES

Modiu L. Sanni is the Focus Area Champion for Saudi Aramco's Technology Test Site (TTS) development initiative. He is a Petroleum Engineering Consultant with the Reservoir Engineering Technology Division of Saudi Aramco's Exploration and Petroleum Engineering Center – Advanced Research Center (EXPEC ARC). Prior to joining Saudi Aramco in 2004, Modiu worked for Shell for about 15 years in Africa, Europe and the Middle East in various capacities. In addition to TTS, he is also involved in research efforts relating to enhanced oil recovery and formation evaluation.

Modiu received both his B.S. and M.S. degrees in Mechanical Engineering from the University of Ibadan, Ibadan, Nigeria.

Scott S. Jennings is the Group Leader for cementing at Saudi Aramco's Exploration and Petroleum Engineering Center – Advanced Research Center (EXPEC ARC). He has 32 years of experience in cementing. Prior to joining Saudi Aramco in 1987, Scott assumed duties that included stimulation, cementing and sand control with Halliburton Co. in East Texas and the Middle East region. His areas of interest are developing standards and test equipment, well construction, gas migration prevention and long-term cement durability. Scott is the Saudi Aramco voting member of the American Petroleum Institute Subcommittee 10 and a long-term member of the Society of Petroleum Engineers (SPE).

In 1980, he received his B.S. degree in Chemistry from Angelo State University, San Angelo, TX.

Dr. Michael A. Jervis is currently Group Leader Reservoir Geophysics with the Geophysical Technology Team in the Exploration and Petroleum Engineering Center – Advanced Research Center (EXPEC ARC) where he has been for the past 12 years.

His first job was as a field geologist in Australia, but he has since worked as a geophysicist in various companies based in the U.S., including Exxon, Western Atlas Logging and TomoSeis. Life as a geophysicist has carried Michael to Canada, Mexico, Venezuela, Tunisia and Egypt, working in both well logging and seismic service companies.

He received his B.S. degree in Geology from the University of Western Australia, Crawley, Western Australia, an M.S. degree in Apllied Physics from Curtin University of Technology, Perth, Western Austrailia, and his Ph.D. degree in Geophysics from the University of Texas at Austin, Austin, TX.

Christopher B. Ayadiuno is currently a Petrophysicist with the Geology Technology Team of Saudi Aramco's Exploration and Petroleum Engineering Center – Advanced Research Center (EXPEC ARC). He has over 23 years of oil and gas industry experience covering business development, information technology support, exploration geological operations and research.

Chris received his B.S. degree in Applied Geophysics from the Federal University of Technology, Akure, Nigeria. He is an active member of many professional organizations.

Razally M. Ali is a Reservoir Engineer with Saudi Aramco's 'Uthmaniyah Reservoir Management Unit. He has 18 years of industry experience. Prior to joining Saudi Aramco in 2006, Razally worked as a Reservoir Engineer for Petronas Carigali in Malaysia and for Brunei Shell Petroleum, and with Shell Expro in Aberdeen, Scotland, and Woodside Petroleum in Perth, Australia. He also spent 4 years with Schlumberger (Consulting Services) formulating integrated field development plans and production optimization projects for operators.

Razally received his B.Eng. and M.S. degrees in Petroleum Engineering from the Imperial College London, London, U.K.

He is a member of the Society of Petroleum Engineers (SPE).

Husain N. Al-Najrani is a Petroleum Engineer in Saudi Aramco's Reservoir Description and Simulation Department. Since joining Saudi Aramco in 2002, he was worked as an Operational Petrophysicist in the Southern Area Petrophysical Unit.

Husain received his B.S. degree in Petroleum Engineering from Montana Tech of the University of Montana, Butte, MT. He is a member of the Society of Petroleum Engineers (SPE).

Intelligent Field Real-Time Data Reliability Key Performance Indices

Authors: Abdulrahman A. Al-Amer, Naser A. Al-Naser, Muhammad M. Al-Gosayir and Waleed Y. Al-Awadh

ABSTRACT

The dependence on intelligent field real-time data for oil and gas operations has significantly increased in the past few years. High frequency real-time data is the baseline of critical analysis and decisions that can lead to maximized oil and gas recovery, increased revenue and reduced environmental impact. Acquiring that data is a complex process. A massive amount of intelligent field real-time data is acquired continuously from numerous instruments and transmitted through several distributed systems located in different area networks.

The challenge that is facing oil and gas companies is to keep the continuous data flow reliable. To achieve this objective, it is mandatory to continuously monitor the health of the field data quality and flow, the field's instruments and the communication systems. In addition, any unreliable data or communication failure must be addressed immediately and treated as a high priority item if companies are to ensure the full availability of reliable data, ready to be processed and analyzed.

This article will highlight Saudi Aramco's experience in improving intelligent field data reliability by developing key performance indices (KPIs). These indices classify the assessment of data reliability into three main categories: Data Definition and Configuration, Data and Systems Availability, and Data Quality. Each category consists of a group of indices that contribute to the main category, and each category contributes to the overall data reliability KPI.

INTRODUCTION

As intelligent field technology evolves in the upstream oil and gas industry, the need to have a continuous and reliable feed of real-time data has significantly increased. Measuring the data acquisition efficiency across various intelligent field infrastructure nodes remains a challenging task, especially for large oil and gas companies. Without a clear key performance index (KPI) measurement across various intelligent field nodes, the tracking of infrastructure deployment progress — compared to the original plan — becomes a very difficult task. Therefore, identifying infrastructure reliability, performance and value becomes even more difficult.

Establishing KPIs against best practices helps the company not only to realize the full potential value from the investment, but also to build an infrastructure foundation that is flexible and reliable. This is essential if systems are to feed the integration and optimization layers in the intelligent field projects with quality data that can be converted into knowledge. Production and reservoir management engineers are required to make and immediately implement decisions to prolong the reservoir, the wells and the instruments' lives. These decisions must be made based on reliable data, which comes from the instruments in the field and well sites. Saudi Aramco has developed and implemented several intelligent field standards, specifications and guidelines to follow when treating and managing the enormous real-time data flow in terms of enhancing integrity, quality, availability and reliability. The ultimate goal for these measures and enforcements is to ensure the high availability of reliable intelligent field real-time data[1]. Intelligent field network implementation consists of two major components. The first component is the real-time data capturing and transmission systems, which include instruments, remote terminal units (RTUs), supervisory control and data acquisition (SCADA) systems, etc. The second component is data management and reliability assurance[2].

INTELLIGENT FIELD NETWORK INFRASTRUCTURE

Real-time data at Saudi Aramco traverses multiple zones of instrumentation, networks and data servers before it reaches the corporate database and an engineer's desktop. Data captured by a sensor is transmitted to the RTU, which collects all the well's sensors and equipment data and sends it to the SCADA control system in the plant. Then the real-time data passes through several plant information (PI) systems, after which it gets processed and pushed by the complex event processing (CEP) agents. It eventually resides in the upstream corporate database.

ROOT CAUSE ANALYSIS

As previously mentioned, the intelligent field network is complicated and has several nodes, which presents challenges for the monitoring and detecting of any data delivery failures. Over time, different real-time data transmission and reliability

issues have been captured and analyzed. A knowledge base has been built from experiences in such an environment. It classifies the common data problems into two main categories, each with subcategories, as follows:

- **Data Transmission Failures:** This failure could occur due to a control systems transmission failure, such as a failure in the RTU, SCADA, De-Militarized Zone (DMZ), PI and CEP systems.
- **Data Reliability Issues:** Reliability comes under question if the data doesn't meet the quality checks that are defined by Saudi Aramco standards, guidelines and specifications.

DATA TRANSMISSION FAILURES

This category deals with monitoring the data transmission system's health and identifying any data delivery interruptions. As the network consists of multiple nodes — namely RTU, SCADA, DMZ and PI systems and CEP agents — it is difficult to identify in which node the data stopped when a data transmission interruption occurs. An innovative solution is needed to monitor and detect the root cause of data transmission failures.

DATA RELIABILITY ISSUES

Even if the real-time data reaches the upstream database without interruption, it has to be reliable and trustworthy for the petroleum engineers to make correct decisions. The data has to pass several reliability checks to be considered reliable. These checks are:

1. **Data Configuration and Integrity:** The required sensor data has to be configured in all layers of the intelligent field data flow network to be transmitted to the upstream database. Configuration has to follow the tag configuration standards, including naming conventions, data identifications, data types, equipment types, installation locations and many more parameters, all of which must meet internal Saudi Aramco standards[3, 4] based on ISA-5.1.
2. **Data Availability:** Data availability here refers to the partial data flow interruptions that occur because of instrument, interface or communication problems, rather than data transmission system failure. Sometimes, the sensor stops sending data due to a defective instrument, cabling issues or a communication disconnection. This check is to ensure the required data is always available to the data users who need it to monitor, diagnose and analyze the reservoir or well performance. This check also includes the so-called stale readings, where the data has time issues, either delayed or futuristic.
3. **Data Quality:** This check is to ensure the received data is of good quality and ready to be used by petroleum engineers in making their decisions. The data quality check consists of several standards the data has to meet before it is labeled as good data. Data is considered unrealible in the following cases:
   - **Out of Range Data:** Each data type has its own value ranges, which are defined during the data configuration process. The received data has to fall into the normal range for that data. Otherwise, the data is labeled as unreliable.
   - **Negative Data:** None of the upstream data is expected to have a negative value. Pressure readings, rate value frequencies and all other values should be positive values. Any negative data is labeled as unreliable.
   - **Frozen Data:** The received data should be changing over time, responding to the variables in the reservoir, well and surrounding conditions. Any stuck values that are not changing over time are labeled as unreliable.
   - **Cross Checking Failure:** Data changes should make logical sense if they are viewed together. For example, any increase of the oil production rate should come with an increase in the wellhead pressure and temperature. Data that doesn't pass cross checking is labeled as unreliable data.
   - **Noisy Data:** Noisy data refers to data that is fluctuating across a very large range, indicating that the gauge needs to be calibrated. This type of data is labeled as unreliable.

Figure 1 shows some examples of data quality assessments, including readings of normal data, frozen data and out of range data.

Figure 2 summarizes the three data reliability categories.

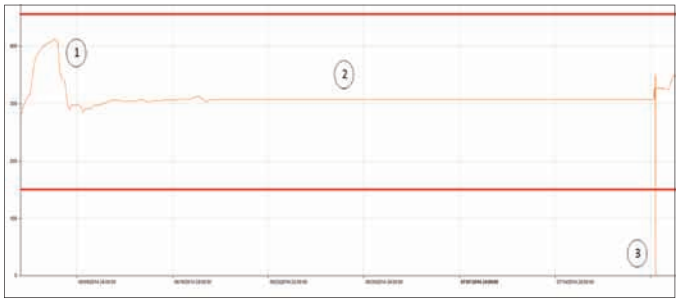

Fig. 1. Data quality case study, showing readings for (1) normal data, (2) frozen data, and (3) out of range data.

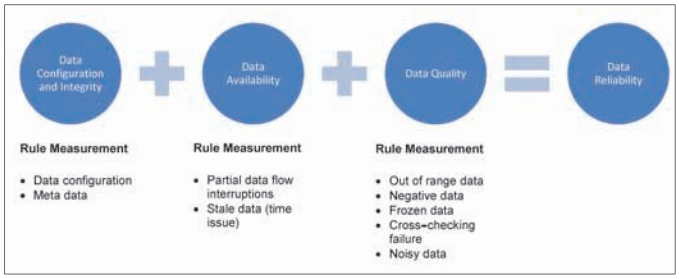

Fig. 2. Data reliability KPIs.

PROPOSED SOLUTION

One objective of the implementation of the intelligent field concept in Saudi Aramco is to provide petroleum engineers with reliable real-time data that will help them to optimize the reservoir and well performance as well as optimize the cost of attending to a remote well's activities. Because unexpected events can affect the data reliability, the objective of this proposed solution is to develop an integrated solution that consists of several utilities. Each utility addresses one or more of the reliability measures that contribute to the overall data reliability KPI.

Data Transmission Monitoring

To monitor the real-time data from/to transmission systems and detect any data availability issue, an engine was developed that uses innovative logical data flow grouping techniques to detect the root cause of the data transmission failure. This methodology detects the health of each transmission system, including the sensors and the equipment. The engine is capable of providing the historical status of each node to evaluate its performance over time, Fig. 3.

Data Configuration and Integrity

To monitor the data configuration status and detect any discrepancy between the equipment as installed and the data configuration in the upstream database, this utility was designed to integrate multiple data sources to provide a comprehensive overview of the field instrumentation's health status. The output of this utility is a report showing the instruments in the field, from the time the equipment is installed until it transmits the real-time data, including the commissioning and connectivity stages. Not only this, it also signals whether the equipment is transmitting reliable data or not, using the other reliability checks, Fig. 4. This engine has the potential to be integrated with other solutions to automate maintenance request activities and measure the maintenance team's performance[5].

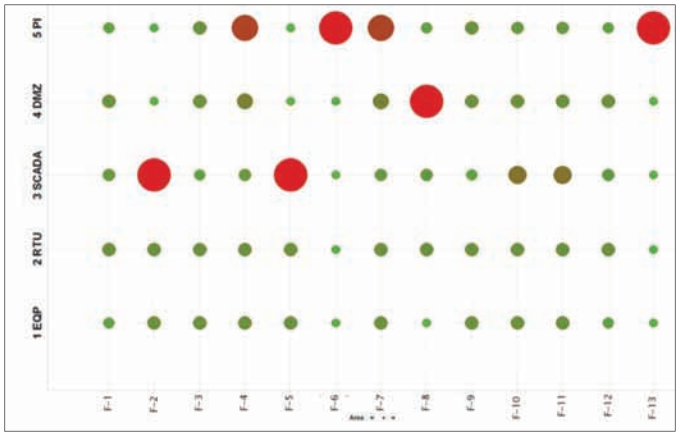

Fig. 3. Data transmission monitoring report.

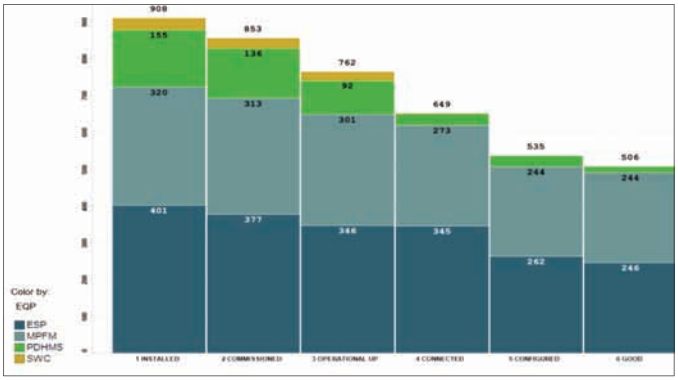

Fig. 4. Intelligent field equipment status report.

Data Availability

To monitor the sensor data availability in the upstream database and map it to its equipment, this utility produces a detailed report and list of sensors that are not transmitting data and sends it to the engineer's desktop. In addition, the utility is capable of grouping the sensor's data by its field and providing an overall field performance status in terms of data availability over a period of time.

Data Quality

To detect data quality issues, this utility labels the received data as good quality if the data passes all quality checks previously described. Briefly, the good data should be within the defined ranges, not frozen, make sense and fluctuate in a stable manner. The output of this utility is a detailed report of the data quality issues in selected fields, Fig. 5.

IN-HOUSE DEVELOPED SOLUTION

The goal is a comprehensive integrated solution that monitors the data transmission and reliability, and detects any failure or discrepancy. Therefore, in addition to the engines and utilities that were previously mentioned, more features have been developed and added to the solution to enable support organizations with the necessary tools and functionalities to respond proactively. The additional features include:

Remedial Workflows. In the case of real-time data transmission failure, a remedial workflow is submitted automatically to the control system's support organizations to take corrective actions to fix the issue, whether it is software, hardware or communication related. The data transmission systems should be up and running 24/7. If the system is not fixed within a defined time frame, the workflow will be escalated to a higher management level.

Data Recovery Monitoring. During the data transmission system downtime, the collected data should be backed up and then restored to all transmission systems upon resolution of the problem. Therefore, a utility has been developed to monitor the data flow after resolution of the problem. The output of

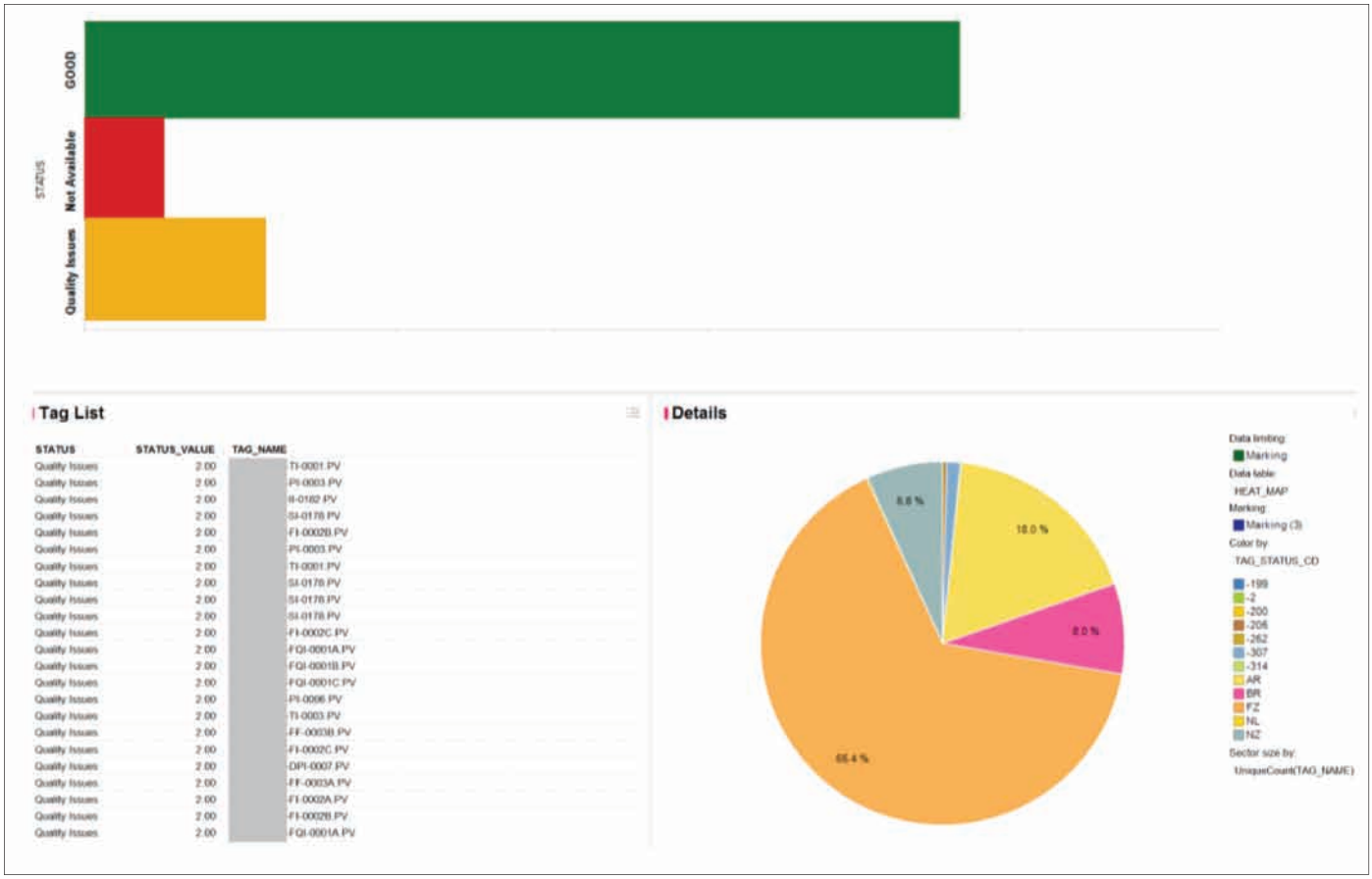

Fig. 5. Data reliability status report.

this utility is a comparison chart for the data availability before and after the problem's resolution. These charts help data users to identify the missing data and the period when that happened, Fig. 6.

Data Reliability Analysis (Heat Map). This feature of the system provides petroleum engineers and other data users with tools to analyze the data transmission and its reliability over a period of time and so to identify the best period to conduct an analysis or case study. Figure 7 shows the data transmission and reliability readings in a color-coded format. From this chart, the engineer can find the best periods, i.e., periods with good data, to conduct his/her case study; an engineer can also identify and investigate the bad periods.

BUSINESS IMPACT

The purpose of developing this data monitoring solution is to improve the data transmission systems and data reliability for petroleum engineers and other data users who rely on the data to make their decisions. This solution helped to increase the real-time data transmission system availability by 33% in seven months as teams tackled the issues highlighted and reported by the system. Moreover, the solution helped to improve the data reliability in the upstream database by 23% in the same period. The comprehensive in-house developed solution provides an interactive environment for the petroleum engineers to use to monitor, visualize and maintain the intelligent field components' health.

CONCLUSION

Saudi Aramco has been investing in intelligent field infrastructure to provide petroleum engineers with real-time data at their desktops for better management of oil and gas fields. To maintain the data integrity and reliability, Saudi Aramco established a comprehensive solution that enables engineers to monitor the data quality and transmission reliability from their offices. This solution consists of several components that monitor data transmission reliability, the integrity of data definitions and configuration, data availability and data quality in addition to initiating remedial workflows that are tracked when a data problem occurs. This solution improves the intelligent field reliability, safety and efficiency.

The solution also provides a one-stop shop solution for all reliability indices, which minimizes the assigned engineer's efforts to detect any transmission failure or data quality issue. The system allows users to monitor one or more fields at the same time. This solution provides real-time alerting and alarming in case of any data discrepancy or interruption, thereby maximizing safety and increasing data accuracy and reliability.

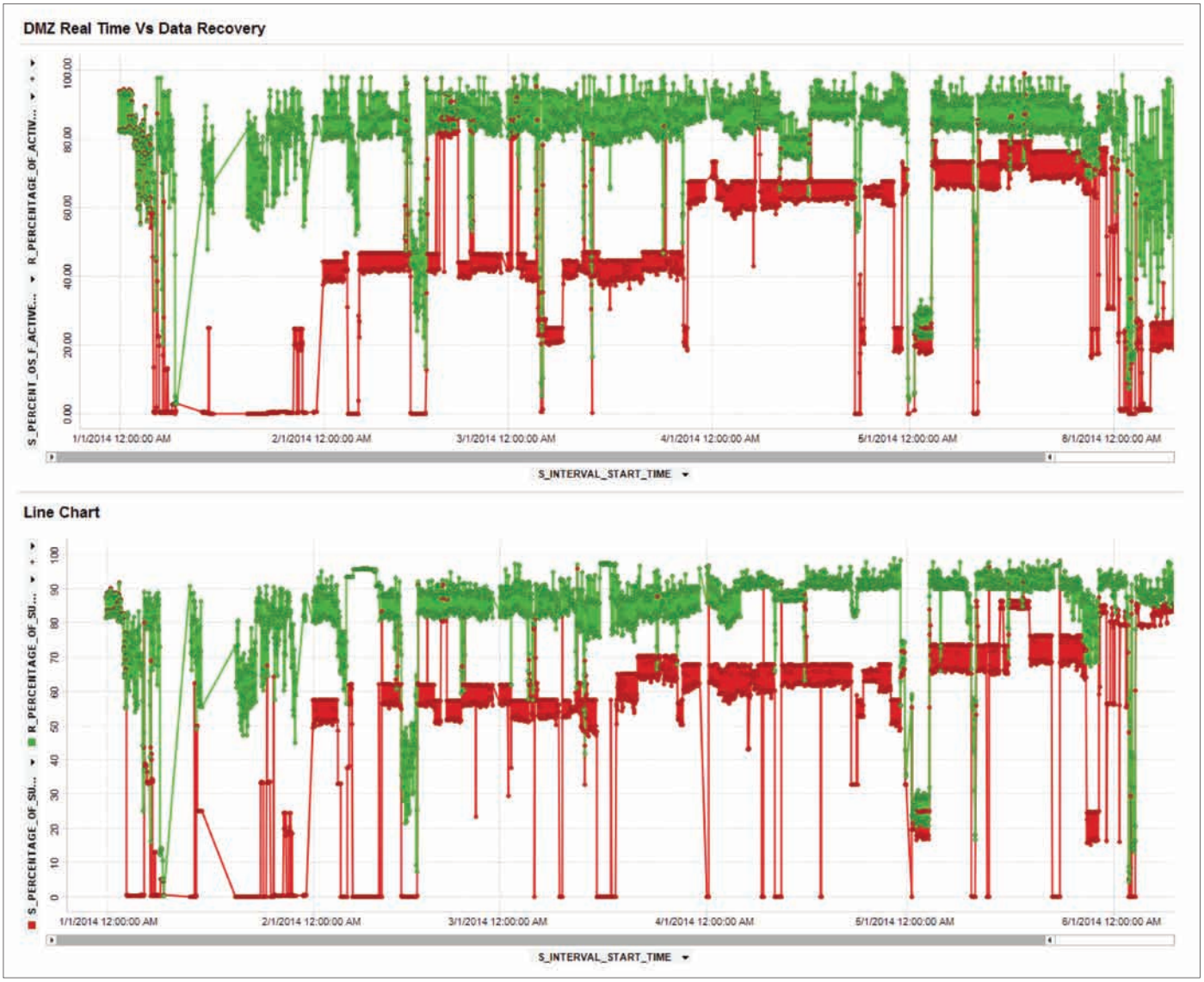

Fig. 6. Data transmission recovery status report.

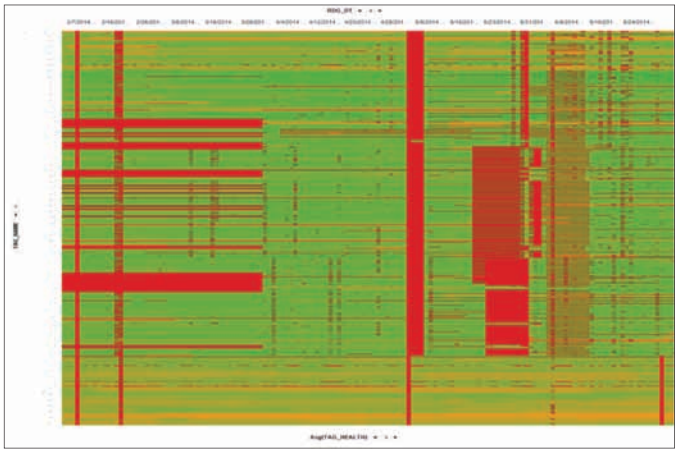

Fig. 7. Historical data reliability heat map.

ACKNOWLEDGMENTS

The authors would like to thank the management of Saudi Aramco for their support and permission to publish this article.

This article was presented at the International Petroleum Technology Conference, Kuala Lumpur, Malaysia, December 10-12, 2014.

REFERENCES

1. Al-Amer, A.A., Al-Gosayir, M., Al-Naser, N. and Al-Towaileb, H.: "Real Time Data: Interactive Monitoring of Data Flow for Continuous and Reliable Data Transmission," SPE paper 167418, presented at the SPE Middle East Intelligent Energy Conference and Exhibition, Dubai, UAE, October 28-30, 2013.
2. Naser, N.A. and Awaji, M.A.: "Intelligent Field Data Management: Case Study," SPE paper 149040, presented at the SPE/DGS Saudi Arabia Section Technical Symposium and Exhibition, al-Khobar, Saudi Arabia, May 15-18, 2011.
3. Al-Dhubaib, T.A., Issaka, M.B., Barghouty, M.F., Al-

Mubarak, S.M., Dowais, A.H., Shenqiti, M.S., et al.: "Saudi Aramco Intelligent Field Development Approach: Building the Surveillance Layer," SPE paper 112106, presented at the Intelligent Energy Conference and Exhibition, Amsterdam, The Netherlands, February 25-27, 2008.

4. Al-Dhubaib, T.A., Shenqiti, M.S., Al-Madi, S.M. and Al-Mansour, A.M.: "Intelligent Field Data Acquisition and Delivery Infrastructure: Case Study," SPE paper 112201, presented at the Intelligent Energy Conference and Exhibition, Amsterdam, The Netherlands, February 25-27, 2008.
5. Ruvalcaba Velarde, S.A. and Al-Ghamdi, A.A.: "The Impact of an Infrastructure Reliability and Data Communication Index on Improving Intelligent Field Operation in an Oil Field in Saudi Arabia," SPE paper 164400, presented at the SPE Middle East Oil and Gas Show and Conference, Manama, Bahrain, March 10-13, 2013.

BIOGRAPHIES

Abdulrahman A. Al-Amer is a Petroleum Engineering System Analyst in the Intelligent Field and Producing Systems Division of Saudi Aramco's Petroleum Engineering Application Services Department, where he is intensively working with intelligent field visualization environments and real-time data handling. Abdulrahman's experience also includes work as a Plant Information System Administrator and as a Plant Engineer in the Safaniyah onshore plant.

He received his B.S. degree in Industrial Engineering from King Fahd University of Petroleum and Minerals (KFUPM), Dhahran, Saudi Arabia.

Naser A. Al-Naser is a Petroleum Engineering System Analyst in Saudi Aramco's Petroleum Engineering Application Services Department. He has 11 years of experience in providing and supporting software solutions for E&P upstream operating systems, mainly in the real-time domain.

In 2002, Naser received his B.S. degree in Computer Science from King Fahd University of Petroleum and Minerals (KFUPM), Dhahran, Saudi Arabia, and in 2008, he received his M.S. degree in Petroleum Engineering from Robert Gordon University, Aberdeen, Scotland.

Muhammad M. Al-Gosayir is a Petroleum Engineering Systems Analyst with the Intelligent Fields and Production Systems Division in Saudi Aramco's Petroleum Engineering Application Services Department. He has been with Saudi Aramco since 2007.

Muhammad received his B.S. degree in Software Engineering from King Fahd University of Petroleum and Minerals (KFUPM), Dhahran, Saudi Arabia, in 2007. In 2012, he received his M.S. degree in Petroleum Engineering from the University of Alberta, Edmonton, Canada.

Waleed Y. Al-Awadh is a Petroleum Engineering Systems Consultant with Saudi Aramco's Intelligent Fields Systems Division. He joined Saudi Aramco in 1987, working at the Exploration and Petroleum Engineering Center (EXPEC) in the Computing Technology Division as a Database Designer and Administrator. During Waleed's 27 years of working in the IT field, he has contributed to EXPEC in both technical and managerial disciplines.

Waleed is a member of the Society of Petroleum Engineers (SPE) and a member of the Dhahran Toastmasters Club, where he serves as a mentor to young Saudis, developing their talents and directing them effectively to improve their communication and presentation skills.

Waleed received his B.S. degree in Computer Science from Western Michigan University, Kalamazoo, Michigan, in 1987.

Use of the Rietveld Method for Describing Structure and Texture in XRD Data of Scale Deposits Formed in Oil and Gas Pipelines: An Important Industrial Challenge

Authors: Dr. Husin Sitepu, Dr. Syed R. Zaidi and Dr. Shouwen Shen

ABSTRACT

Texture, or crystallographic preferred orientation, in crystalline materials is a common feature of experimental X-ray powder diffraction (XRD) data. Preferred orientation can cause serious systematic errors in both quantitative phase analysis and crystal structure determination. Studies show that the generalized spherical harmonic (GSH) description provides a better Rietveld fit than the March model for the uniaxially pressed molybdite and calcite powders[1-3]. Therefore, it was recommended to use the GSH description for correction of the preferred orientation in XRD and neutron diffraction analyses, for both crystal structure refinement and quantitative phase analysis. In the present study, the GSH description was extended to describe crystal structure and texture in the XRD data of scale deposits formed in an amine trim cooler. The results revealed that the structural refinement parameter obtained from the Rietveld refinement with the GSH description agreed well with the corresponding single crystal structure. Additionally, the GSH description provided better results for the materials investigated in the present study than the March model. Therefore, the GSH approach should be used for preferred orientation correction in XRD Rietveld analysis, for both crystal structure refinement and phase composition analyses.

INTRODUCTION

Corrosion deposits formed in oil and gas pipelines can cause major operational problems and can frequently shut down plants. X-ray powder diffraction (XRD) allows the direct measurement of the phase content[4] in corrosion deposits. When analysts perform a quantitative phase analysis of the identified compounds using the Rietveld method, they frequently assume that the corrosion deposits in oil and gas pipelines are randomly oriented. The powder samples, however, often have a preferred orientation, meaning that one or more of the XRD peaks may be missing. This crystallographic preferred orientation is a common feature of XRD patterns for experimental powders, and can cause serious systematic errors in subsequent quantitative phase analysis and crystal structure determination[1-3, 5-10]. Therefore, achieving a comprehensive quantification of the various phases of corrosion deposits using XRD with a Rietveld method is an important industrial challenge.

The Rietveld refinement method adjusts the refinable parameters until the best fit of the entire calculated pattern to the entire measured pattern is achieved. Additionally, the refined atomic parameters should agree well with the structure derived from the single-crystal XRD data. In the General Structure Analysis System (GSAS) Rietveld refinement program[11], a mathematical method has been developed that calculates an intensity, Y_c, at every point in the pattern, i.e.,

$$Y_c = \sum_h SKF_h^2 P(\Delta T_h) + Y_b \qquad (1)$$

where the first term is the Bragg scattering containing a scale factor, S, a correction factor, K, a structure factor, F_h, and a profile function, $P(\Delta T_h)$, as determined by the displacement, ΔT_h, of the profile point from the reflection position; the second term, Y_b, is the background intensity. The sum is the total of overall profile points in all the scans included in the refinements. Within K in Eqn. 1 is a term that describes the change in intensity for a Bragg reflection due to texture[2, 3]. The March (1932)[12] model and generalized spherical harmonic (GSH) description are described as follows.

The March-Dollase Preferred Orientation Factor for Powder Diffraction

The March model proposed by Dollase (1986)[5] is based on the function:

$$P_j = \left[r^{-1}\sin^2\theta_j + r^2\cos^2\theta_j\right]^{-3/2} \qquad (2)$$

where θ_j is the angle between the direction of crystallographic preferred orientation and the reciprocal-lattice vector for the Bragg peak that is corrected. The single March r-parameter controls the distribution shape. In addition, the r-parameter is an index of the extent of preferred direction, being unity for ideal random orientation powder diffraction data. The March model does not require the use of data acquired with a multi-axis diffractometer for the correction of intensities due to the preferred orientation direction effects. The March model is symmetric and smooth across $\theta_j = 0^\circ$ and $\theta_j = 90^\circ$. It also yields

a preferred orientation correction factor, which has either a maximum or minimum at $\theta_j = 0^o$, and can be normalized over the full $2\theta_j$ angular range. The normalization is important in that changes in the preferred orientation correction factor shape conserve the total intensity within the powder diffraction pattern[3].

The GSH Texture Correction Factor

To apply the GSH description[2, 13-15], which is generated using selection rules depending on the crystal symmetry of the phase under investigation, the general axis distribution $A(\varphi, \beta, \psi, \gamma)$ is used:

$$A(\varphi,\beta,\psi,\gamma) = 1 + \sum_{l=2}^{L}\left(\frac{4\pi}{2l+1}\right)\cdot\sum_{m=-l}^{+l}\sum_{n=-l}^{+l} C_l^{mn}\cdot K_l^m(\varphi,\beta)\cdot K_l^n(\psi,\gamma) \quad (3)$$

The $K_l^m(\varphi,\beta)$ and $K_l^n(\psi,\gamma)$ harmonic terms take on values according to the crystal and sample symmetries, respectively. These symmetry modified terms correspond to the angular portions of the atomic orbitals familiar to chemists. Terms with $l = 0$ correspond to *s*-orbitals, and so are not useful for describing preferred orientation. Since diffraction patterns — ignoring the effects of resonant scattering — are centrosymmetric, terms with l = odd numbered values, which yield non-centrosymmetric orbitals, are not useful for describing preferred orientation. Terms with $l = 2$ correspond to *d*-orbitals, $l = 4$ correspond to *g*-orbitals, etc.[3]. In the diffraction experiment, the crystal coordinates, (φ, β), and sample coordinates, (ψ,γ), are determined by the choice of reflection index, *hkl*, and sample orientation on the diffractometer, respectively. The texture is then completely described by the set of C_l^{mn} as determined from Rietveld refinement with a GSH description. In the case of XRD and neutron diffraction data having an ideal random orientation, all the harmonic coefficients are zero; therefore, the general axis distribution is unity. The magnitude of the texture can be evaluated from the texture index, *J*[13], as follows:

$$J = 1 + \sum_{l=2}^{L}\left[\frac{1}{2l+1}\right]\cdot\sum_{m=-l}^{l}\sum_{n=-l}^{l}\left|C_l^{mn}\right|^2 \quad (4)$$

Least squares of optimization of Rietveld parameters, i.e., minimization of residual over *n* observation, are calculated from the following equation:

$$R = \sum_{i=1}^{n} w_i\left(Y_i - Y_{ci}\right)^2 \quad (5)$$

where w_i is the weighting factor for phase *i*, Y_i is the measured intensity, and Y_{ci} is the calculated intensity, Eqn. 1. The sum is the total of overall profile points in all the scans included in the refinement. The usual residuals used in the Rietveld refinement, R_p and R_{wp}, are given by:

$$R_p = \sum\left|Y_o - Y_c\right| / \sum Y_o \quad (6)$$

$$R_{wp} = \left(M / \sum wY_o^2\right) \quad (7)$$

The objectives of the present study were to characterize the preferred orientation and perform crystal structure refinement using XRD data collected from uniaxially pressed scale deposits from an amine trim cooler. The data were analyzed, initially assuming a random orientation of the crystallites, and subsequently the preferred orientation correction was applied using the March model. The GSH description was independently used as a complementary method to correct the intensities due to the preferred orientation effects.

EXPERIMENTAL

The starting material was considered to be excellent for this study because high quality crystal structures of calcite[16] had been reported in it. The starting powders were manually ground in an agate mortar and a pestle for several minutes to achieve a fine particle size[2]. Then the fine powder was mounted into the XRD sample holder by back pressing. Additionally, a substantial level of preferred orientation was introduced during the specimen preparation to replicate scale deposits. Approximately 4 g of the fine powders was uniaxially pressed in a cylindrical steel die that was 3.1 cm in diameter at a pressure of 68±5 MPa, 135±5 MPa, 203±5 MPa and 270±5 MPa. The height of the resulting disk for each pressure was approximately 0.6 cm. Sitepu et al. (2005)[2] have indicated that as the uniaxial pressure increases, the level of preferred orientation increases. Because the specimen preparation procedures were reproducible[2], we used the same technique to assess the general applicability of the GSH description to the present study.

Step-scanned patterns were measured with an X-ray diffractometer (Rigaku Ultima IV) with a copper X-ray tube (λ=1.5406 Å). A monochromator and a proportional detector were used in conjunction with a 0.67° divergence slit, a 0.67° scattering slit and a 0.3 mm receiving slit at instrument settings of 40 kV and 40 mA. The XRD data were measured from 10° to 140° in 2θ Bragg-angle, using a step size of 0.04° and a counting time of 1° per minute. Then the software package (High Score Plus, PANalytical B.V.), combined with the International Center for Diffraction Data (ICDD) and Powder Diffraction File (PDF) databases as the standard reference materials, was used for the phase identification, i.e., qualitative analysis. Note that the phase identification results showed that the scale deposit was calcite. Table 1 shows the XRD pattern measurement condition.

The Rietveld refinements were performed with the GSAS software package[11]. The refinement strategy was similar to that described by Sitepu et al. (2005)[2]. The structural model used for the calcite single crystal XRD data was described[16] as the ICDD and PDF entry 01-086-2339. The refined parameters were similar to that described by Sitepu et al. (2005)[2], which are phase scale factors and the background component of the patterns with an eight-parameter Chebyshev polynomial, lattice parameters, the instrument zero-point $2\theta_o$ (offset in the

2θ scale of goniometer), the Lorentzian and the Gaussian terms of a pseudo-Voigt profile function and anisotropic strain parameters[17], structural parameters, i.e., x,y,z and frac, and isotropic thermal parameters (Uiso). After the preliminary refinement without preferred orientation correction had converged, the GSH coefficients[1-3, 9, 10, 15, 18] were then included. The default sample texture symmetry was chosen to be cylindrical — or fiber texture. Sixth-order harmonics were selected following preliminary calculations using eight orders that yielded the same figure of merit and goodness-of-fit index (GFI).

RESULTS AND DISCUSSION

Table 2 depicts the unit-cell parameters of the uniaxially pressed calcite at a pressure of 0 MPa, 68±5 MPa, 135±5 MPa, 203±5 MPa and 270±5 MPa, obtained from the Rietveld refinement with the March model and the GSH description. The numbers in parentheses give the estimated standard uncertainty for the least significant figure of the parameter. The refined unit-cell agreed well with the corresponding single crystal XRD results for calcite[16].

Table 3 shows the structural parameters of the uniaxially

Name	Description
Instrument	Rigaku Ultima IV multipurpose X-ray diffractometer
Radiation	Copper-anode tube operated at 40 kV and 40 mA Wavelength: Cu $K\alpha_1$ = 1.54060 Å
Optics	Bragg–Brentano, measuring circle diameter = 480 mm Divergence slit: 0.67°, scattering slit: 0.67° and receiving slit = 0.3 mm
Specimen	Holder: rectangular format, dimension 22 mm x 22 mm Rotation "on" for all measurements
Detector	Position sensitive detector
Acquisition	Angular range in 2θ: 10°–140°, and step size: 0.04° Scan rate: 1° per minute

Table 1. XRD pattern measurement conditions

Parameters	This Study					Maslen et al. (1995)[16]
	0 MPa	68 MPa	135 MPa	203 MPa	270 MPa	
Random orientation						
a (Å)	4.97612(5)	4.9770(6)	4.9780(5)	4.9784(6)	4.9779(8)	4.988(2)
b (Å)	4.97612(5)	4.9770(6)	4.9780(5)	4.9784(6)	4.9779(8)	4.988(2)
c (Å)	17.0893(10)	17.0947(21)	17.0980(20)	17.0988(21)	17.0926(30)	17.068(2)
V (Å)^3	366.468(33)	366.71(11)	366.93(10)	367.01(11)	366.80(16)	367.8(3)
The March model						
a (Å)	4.97630(15)	4.9771(5)	4.9781(5)	4.9785(5)	4.9782(7)	4.988(2)
b (Å)	4.97630(15)	4.9771(5)	4.9781(5)	4.9785(5)	4.9782(7)	4.988(2)
c (Å)	17.0904(9)	17.0959(9)	17.0991(19)	17.0997(19)	17.0944(24)	17.068(2)
V (Å)^3	366.520(31)	366.76(9)	366.97(9)	367.05(10)	366.88(13)	367.8(3)
The generalized spherical harmonics (GSH) description						
a (Å)	4.97645(14)	4.9770(4)	4.9779(5)	4.9783(5)	4.9791(6)	4.988(2)
b (Å)	4.97645(14)	4.9770(4)	4.9779(5)	4.9783(5)	4.9791(6)	4.988(2)
c (Å)	17.0915(9)	17.0978(16)	17.1005(18)	17.1012(17)	17.1002(20)	17.068(2)
V (Å)^3	366.564(30)	366.79(9)	366.98(9)	367.04(9)	367.15(11)	367.8(3)

Table 2. Summary of the refined cell parameters of the uniaxially pressed scale deposit from an amine cooler (calcite-$CaCO_3$) obtained from Rietveld refinement with random orientation, the March model and the GSH description

Atomic Positions	This Study					Maslen et al. (1995)[16]
	0 MPa	68 MPa	135 MPa	203 MPa	270 MPa	
Random orientation (r = 1.00)						
Ca(0,0,0)						
U_{iso}	0.0186(5)	0.0198(6)	0.0133(5)	0.0199(6)	0.0213(7)	0.00988(3)
C(0,0,1/4)						
U_{iso}	0.0109(16)	0.0059(17)	0.0047(16)	0.0068(18)	0.0022(20)	00834(9)
O(x,0,1/4)						
x	0.2530(4)	0.2536(5)	0.2549(5)	0.2519(5)	0.2514(6)	0.25700(6)
U_{iso}	0.0264(10)	0.0258(10)	0.0231(11)	0.0242(11)	0.0260(13)	01129(7)
R_P	10.23	10.94	10.78	12.03	12.68	
R_{WP}	13.99	14.54	14.14	15.97	13.61	
$R(F^2)$	11.19	13.50	11.08	14.55	14.55	
χ^2	1.94	1.85	1.81	2.68	2.80	
The March model						
Ca(0,0,0)						
U_{iso}	0.0162(5)	0.0145(5)	0.0100(5)	0.0151(6)	0.0142(6)	0.00988(3)
C(0,0,1/4)						
U_{iso}	0.0110(16)	0.0063(15)	0.0052(16)	0.0066(17)	0.0029(17)	00834(9)
O(x,0,1/4)						
x	0.2544(4)	0.2561(5)	0.2565(5)	0.2542(5)	0.2547(6)	0.25700(6)
U_{iso}	0.0247(9)	0.0218(10)	0.0204(10)	0.0203(11)	0.0208(11)	01129(7)
R_P	9.75	9.55	10.05	10.53	8.56	
R_{WP}	13.30	12.92	13.35	14.49	12.01	
$R(F^2)$	10.15	10.97	10.12	12.16	13.76	
χ^2	1.32	1.77	1.61	2.21	2.25	
r	0.854(7)	0.839(7)	0.807(6)	0.801(5)	0.758(5)	
The generalized spherical harmonics description						
Ca(0,0,0)						
U_{iso}	0.0175(5)	0.0154(5)	0.0110(5)	0.0159(5)	0.0174(5)	0.00988(3)
C(0,0,1/4)						
U_{iso}	0.0161(16)	0.0127(15)	0.0096(16)	0.0134(17)	0.0104(15)	00834(9)
O(x,0,1/4)						
x	0.2539(7)	0.2540(7)	0.2568(7)	0.2538(7)	0.2501(8)	0.25700(6)
U_{iso}	0.0286(10)	0.0271(11)	0.0233(11)	0.0246(11)	0.0299(12)	01129(7)
R_P	8.82	7.67	8.80	8.56	8.24	
R_{WP}	12.50	11.03	12.24	12.68	11.65	
$R(F^2)$	8.24	5.94	7.11	7.31	6.45	
χ^2	1.55	1.29	1.36	1.69	1.39	
J	1.017	1.026	1.048	1.065	1.093	

Table 3. Summary of the Rietveld refinement results for the uniaxially pressed scale deposit from an amine trim cooler (calcite). The space group used was R-3c (No. 167). Wyckoff coordinates: 6(c) are 0,0,0 and 0,0,1/2; 6(a) are 0,0,3/4; and 18(e) are x,0,1/4; -x,-x,1/4;-x,0,3/4;0,-x,3/4 and x,x,3/4. Cell formula unit Z=6 and formula weight = 100.09

pressed calcite at pressures of 0 MPa, 68±5 MPa, 135±5 MPa, 203±5 MPa and 270±5 MPa obtained from the Rietveld refinement with a GSH description. The numbers in parentheses give the estimated standard uncertainty for the least significant figure of the parameter. The refined structural parameters agreed quite satisfactorily with the corresponding single crystal

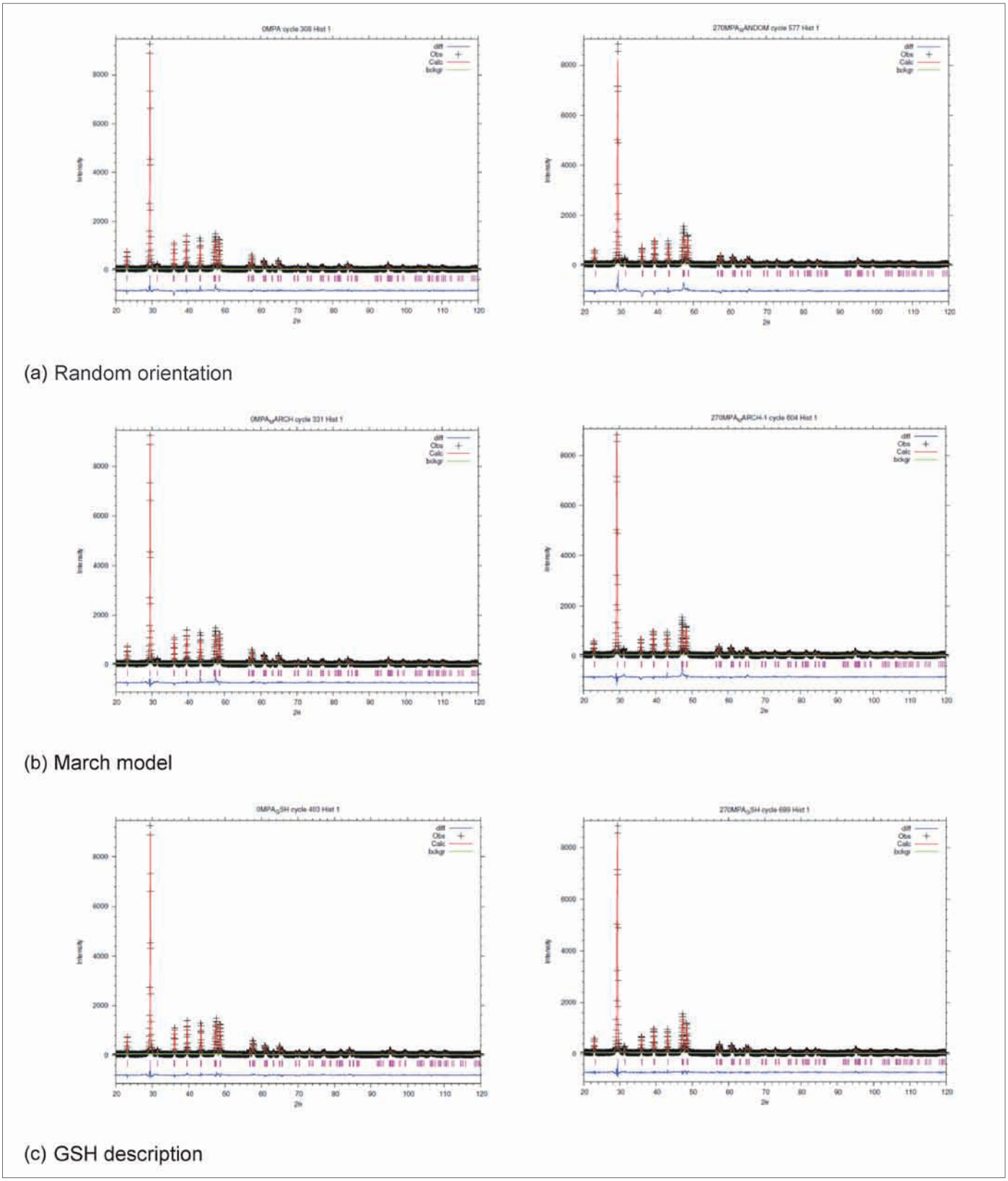

Fig. 1. The agreement between the calculated and measured XRD patterns for the unpressed calcite powders at 0 MPa (left) and the unixially pressed powders at 270±5 MPa (right), following Rietveld refinement with (a) random orientation, (b) March model, and (c) GSH description for preferred orientation correction. The observed data are indicated by a plus sign and the calculated pattern is the continuous line in the same field. The sets of vertical lines below the profiles represent the positions of all possible Bragg reflections. The lower plot is the difference between the measured and calculated patterns on the same scale as the measured and calculated patterns.

XRD results for calcite[16].

It can also be seen from Table 3 that the crystallographic R-factors, R_P, R_{WP} and $R(F^2)$, and the GFI, (χ^2), improved when the intensities were corrected using the March model and the GSH description. The March model appears to provide adequate preferred orientation representation for a moderate level of preferred orientation only. Unlike the Rietveld refinement with the GSH description, the Rietveld refinement of the same XRD data sets with the March model increasingly gave both the crystallographic R-factors and the GFI values for the uniaxially pressed powders that had the March r-parameter of less than approximately 0.9. Therefore, the GSH description approach should be used for preferred orientation correction in the XRD Rietveld analysis, for both crystal structure refinement and phase composition analyses.

Figures 1a, 1b and 1c show the agreement between the calculated and measured XRD patterns for the unpressed powder and the uniaxially pressed powder at a pressure of 270±5 MPa, following Rietveld refinement with random orientation — the March model and GSH description for preferred orientation correction. The GSH description provides better goodness-of-fit values than the March model. Therefore, the GSH description is recommended for the preferred orientation correction in XRD analysis, for both crystal structure refinement and phase composition analysis.

Figures 2a and 2b depict the variation with pressure of the preferred orientation r-parameter derived from the Rietveld refinement using the March model, and of the texture index derived from Rietveld refinements using the GSH description. In the case of an ideal random orientation powder, the texture index is unity. The March r-parameter and the texture index increase linearly as the pressure increases. While the texture index of the unpressed calcite powder is 1.017, the corresponding value for the uniaxially pressed calcite at 270±5 MPa is 1.093. As the uniaxial pressure — and therefore the level of preferred orientation — increases, the Rietveld refinements with the March model and with the GSH description for the calcite data sets all provide higher March r-parameters and

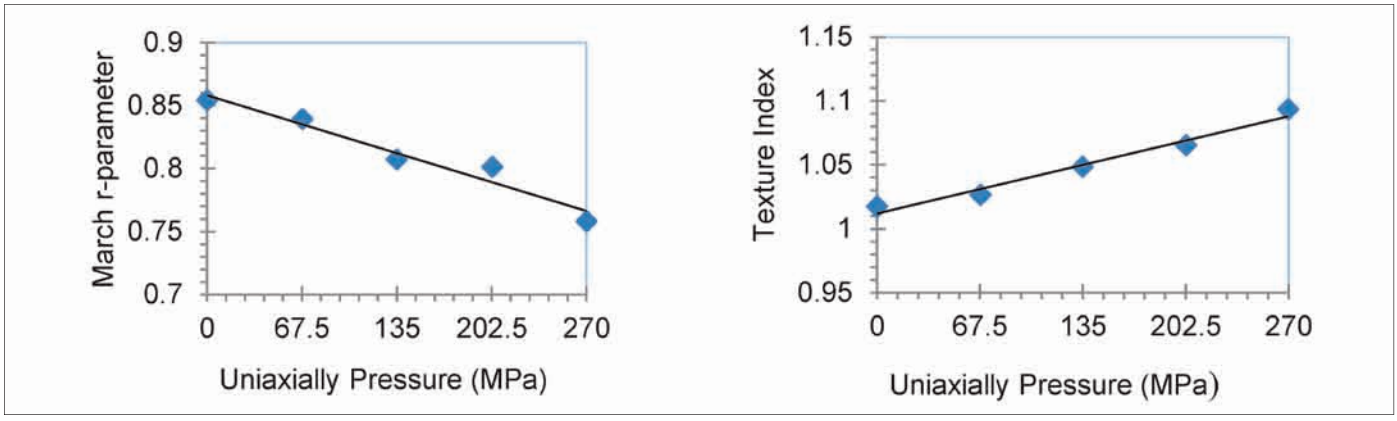

Fig. 2. Variation in the March r-parameter with uniaxial pressure (left) and texture index with uniaxial pressure (right). Linear regressions are shown for all XRD data sets. Error bars are smaller than the symbols.

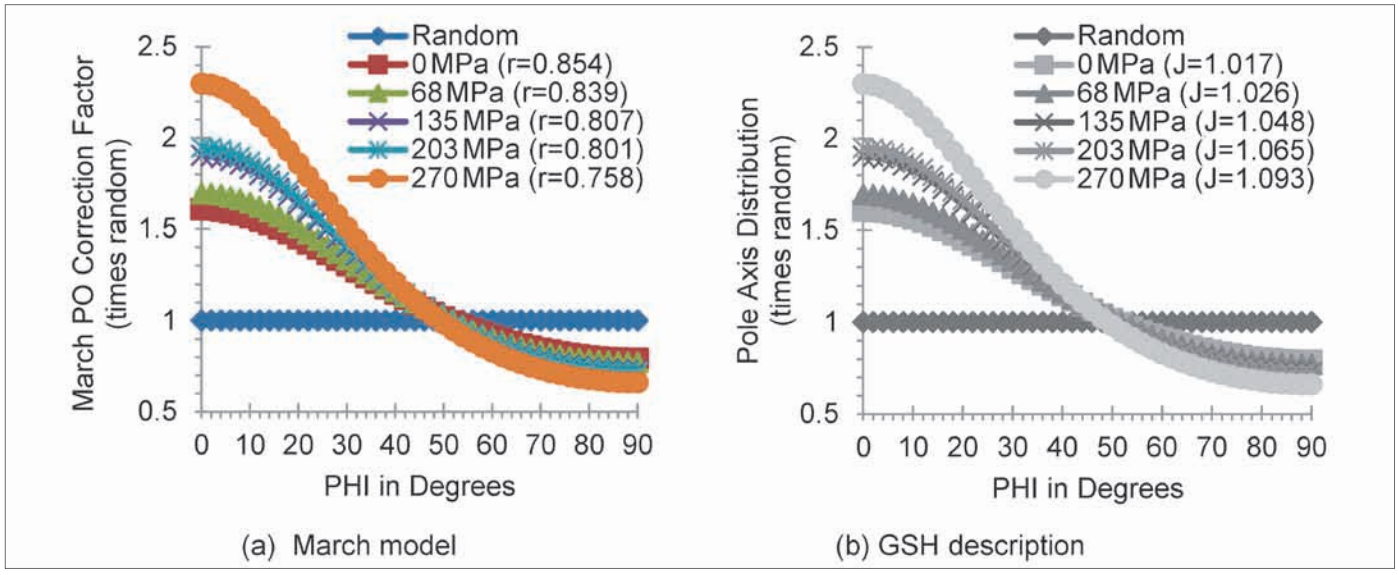

Fig. 3a. The variation between the March preferred orientation corrections with orientation angle derived from Rietveld refinement with the March model.
Fig. 3b. Pole axis distribution plot for {104} calcite XRD data derived from Rietveld refinement with the GSH description.

texture indices compared with those of unpressed samples.

Figures 3a and 3b show the plots of the March preferred orientation corrections with an orientation angle derived from the Rietveld refinement with the March model, and the pole-axis distribution for {104} calcite XRD data derived from the Rietveld refinement with the GSH description as a function of the orientation angle, φ, where φ is the angle between the pressing axis and the normal {104} calcite plane. In the case of an ideal random orientation powder, all the harmonic coefficients are zero, and therefore the general axis distribution is unity. As expected for the XRD data, the pole-axis distribution factor for {104} calcite is maximum at $\varphi = 0°$ and minimum at $\varphi = 90°$. The pole-axis distribution factor for the unpressed powders is lower than that for the uniaxially pressed powders, which indicates that the uniaxially pressed powders have substantial texture.

CONCLUSIONS

The refined structural parameters obtained from the Rietveld refinement agreed well with the single crystal XRD data results. Additionally, as the uniaxial pressure increases — and therefore the level of preferred orientation increases — the refinements for the uniaxially pressed calcite powders all provide a higher March r-parameter and texture index compared with those of the unpressed powders. Finally, the GSH description provides better goodness-of-fit values than the March model. Therefore, the GSH description is recommended for correction of the preferred orientation in XRD analysis, for both crystal structure refinement and phase composition analysis.

ACKNOWLEDGMENTS

The authors would like to thank the management of Saudi Aramco for their support and permission to publish this article. Also, Yazeed A. Al-Dukhayyil, Abdullah M. Al-Ghamdi, Mansour A. Shafei and Ali Abadi are acknowledged for their help in the study.

REFERENCES

1. Sitepu, H.: "Assessment of Preferred Orientation with Neutron Powder Diffraction Data," *Journal of Applied Crystallography*, Vol. 35, No. 2, April 2002, pp. 274-277.
2. Sitepu, H., O'Connor, B.H. and Li, D.: "Comparative Evaluation of the March and Generalized Spherical Harmonic Preferred Orientation Models Using X-ray Diffraction Data for Molybdite and Calcite Powders," *Journal of Applied Crystallography*, Vol. 38, No. 1, February 2005, pp. 158-167.
3. Sitepu, H.: "Texture and Structural Refinement Using Neutron Diffraction Data from Molybdite (MoO_3) and Calcite ($CaCO_3$) Powders and a Ni-rich $Ni_{50.7}Ti_{49.30}$ Alloy," *Powder Diffraction*, Vol. 24, No. 4, December 2009, pp. 315-326.
4. Klug, H.P. and Alexander, L.E.: *X-ray Diffraction Procedures for Polycrystalline and Amorphous Materials*, John Wiley & Sons, New York, 1974, 992 p.
5. Dollase, W.A.: "Correction of Intensities for Preferred Orientation in Powder Diffractometry: Application of the March Model," *Journal of Applied Crystallography*, Vol. 19, No. 4, August 1986, pp. 267-272.
6. O'Connor, B.H., Li, D.Y. and Sitepu, H.: "Strategies for Preferred Orientation Corrections in X-ray Powder Diffraction Using Line Intensity Ratios," *Advances in X-ray Analysis*, Vol. 34, 1991, pp. 409-415.
7. O'Connor, B.H., Li, D.Y. and Sitepu, H.: "Texture Characterization in X-ray Powder Diffraction Using the March Formula," *Advances in X-ray Analysis*, Vol. 35, 1992, pp. 277-283.
8. Sitepu, H., Prask, H.J. and Vaudin, M.D.: "Texture Characterization in X-ray and Neutron Powder Diffraction Data Using the Generalized Spherical Harmonic," *Advances in X-ray Analysis*, Vol. 44, 2001, pp. 241-246.
9. Sitepu, H.: "Structural Refinement of Neutron Powder Diffraction Data of Two-stage Martensitic Phase Transformations in $Ti_{50.75}Ni_{47.75}Fe_{1.50}$ Shape Memory Alloy," *Powder Diffraction*, Vol. 22, No. 3, September 2007, pp. 209-318.
10. Sitepu, H.: "In Situ Structural and Texture Analyses of Monoclinic Phase for Polycrystalline Ni-rich $Ti_{49.86}Ni_{50.14}$ Alloy from Neutron Diffraction Data," *Powder Diffraction*, Vol. 23, No. 1, March 2008, pp. 35-40.
11. Larson, A.C. and von Dreele, R.B.: *General Structure Analysis System* (GSAS), Report LAUR 86-748, Los Alamos National Laboratory, Los Alamos, New Mexico, 2000.
12. March, A.: "Mathematische Theorie der Regelung Nach der Korngestalt bei Affiner Deformation," *Z. Kristallogr.*, Vol. 81, 1932, pp. 285-297.
13. Bunge, H.J.: *Texture Analysis in Materials Science: Mathematical Methods*, Butterworths-Heinemann, London, 1982, 593 p.
14. Popa, N.C.: "Texture in Rietveld Refinement," *Journal of Applied Crystallography*, Vol. 25, 1992, pp. 611-616.
15. von Dreele, R.B.: "Quantitative Texture Analysis by Rietveld Refinement," *Journal of Applied Crystallography*. Vol. 30, No. 4, August 1997, pp. 517-525.
16. Maslen, E.N., Streltsov, V.A., Streltsova, N.R. and Ishizawa, N.: "Electron Density and Optical Anisotropy in Rhombohedral Carbonates, Part III: Synchrotron X-ray Studies of $CaCO_3$, $MgCO_3$ and $MnCO_3$," *Acta*

Crystallographica Section B, Vol. B51, December 1995, pp. 929-939.

17. Stephens, P.W.: "Phenomenological Model of Anisotropic Peak Broadening in Powder Diffraction," *Journal of Applied Crystallography*, Vol. 32, No. 2, April 1999, pp. 281-289.
18. Sitepu, H.: "Use of the Rietveld Method for Describing Structure and Texture in XRD Data of Dolomite [$CaMg(CO_3)_2$] and Hydromagnesite [$Mg_5(CO_3)_4(OH)_2(H_2O)_4$] Powders," *Advances in X-ray Analysis*, Vol. 56, 2013, pp. 137-145.

BIOGRAPHIES

Dr. Husin Sitepu joined Saudi Aramco's Research and Development Center (R&DC), Technical Services Division, in late December 2008. Since then, he has contributed to several research projects by providing crystallographic information file (CIF) on synthesized nano-materials and catalysts. Before joining Saudi Aramco, Husin worked at the well-established national and international laboratories at the National Institute of Standards and Technology (NIST) Center for Neutron Research in Gaithersburg, MD; at the Institut Laue-Langevin (ILL), which is an international research center based in Grenoble, France; at the Virginia Polytechnic Institute and State University (Virginia Tech) in Blacksburg, VA; at Ruhr-Universität Bochum in Bochum, Germany; at the University of British Columbia in Vancouver, Canada; and at the Curtin University in Perth, Australia.

Since 1989, he has published 38 papers in several peer-reviewed physics journals, including the International Union of Crystallography's *Journal of Applied Crystallography*, with the Herfindahl index of 9; published six lightly reveiwed papers in the *Saudi Aramco Journal of Technology* and presented 76 papers at various conferences. Husin has a very strong background in physics at a research level, and he is an expert in crystallography preferred orientation and diffraction science through his extensive experience in Rietveld refinement of polycrystalline structures using powder X-ray, synchrotron and neutron diffraction data.

He received his Postgraduate Diploma, M.S. by research and Ph.D. degrees in Physics from the Curtin University, Perth, Western Australia, in 1989, 1991 and 1998, respectively.

Husin is a member of the International Center for Diffraction Data (ICDD), the International Union of Crystallography (IUCr) and the Neutron Scattering Society of America (NSSA).

Dr. Syed R. Zaidi has been with Saudi Aramco since 1992. His specialized area of research is the mineralogical characterization of geological samples (clay and bulk rock) by using the XRD technique. Syed is also responsible for XRD method development and research work. He is familiar with other analytical techniques, such as XRF, SEM, FTIR, TGA, DSC and ICP.

Syed received his B.S. degree (with honors) and M.S. degree, both in Chemistry, from Aligarh Muslim University, Aligarh, India, in 1977 and 1980, respectively. In 1986, he received his Ph.D. degree in Inorganic Chemistry from Aligarh Muslim University, Aligarh, India.

Syed has published more than 20 papers in peer-reviewed journals. He is a member of the American Chemical Society (ACS) and the Society of Petroleum Engineers (SPE).

Dr. Shouwen Shen is a Science Specialist in the Advanced Analysis Unit of the Research & Development Center (R&DC) at Saudi Aramco. Before joining Saudi Aramco in 2006, he worked at Southwest Petroleum University in China as an Associate Professor, at the University of Miami as a Visiting Scientist and at Core Laboratories Canada Ltd. as an X-ray Specialist.

He studied the seismic facies, sedimentary facies and sequence stratigraphy of Jurassic formations in the Turpan-Hami basin of China. Shouwen used piezoelectric transducers to measure the sonic velocity of various dolomites from the Madison formation of Wyoming and Montana, and he developed an empirical formula to predict the sonic velocity of dolomite according to thin section description. He also developed new XRD methods in-house for quantitative mineral analysis of sandstone and successfully solved the problem caused by the Rietveld method limitation. Shouwen's specialties include sequence stratigraphy, clastics diagenesis, clay mineralogy and formation damage assessment, thin section description, XRF elemental analysis, XRD phase identification and quantification, crystallite size determination, texture and residual stress analyses.

Shouwen received a B.S. degree from the China University of Geosciences, Beijing, China, in 1982 and a Ph.D. degree in Petroleum Geology from Chengdu University of Technology, Sichuan, China, in 1998.

A Novel Semi-Analytical Solution for Transient Pressure Data Interpretation of a Fractured Well in an Asymmetric Reservoir

Authors: Faisal M. Al-Thawad and Dr. Mahmoud Jamiolahmady

ABSTRACT

The presence of fractures and faults plays a significant role in the recovery and performance of tight reservoirs exploited with hydraulically fractured wells. Faulting may result in asymmetric reservoirs, i.e., different quality reservoirs across the fault plane, due to the displacement of reservoir blocks along the fault plane. Typically, numerical well test packages are used to match the pressure responses of such complex geology and well geometry. The limitations of such approaches in terms of ease of use and the wide range of possible solutions plead for a more attractive approach. Therefore, a semi-analytical approach has been taken to develop a new practical and efficient flow solution for a well intersected by a finite conductivity vertical fracture in an asymmetric reservoir. The solution is characterized mainly by the bilinear flow resulting from the formation and fracture linear flows. The shape of the derivative plot suggests a bilinear flow and quarter slope, addressing the fracture characteristics, followed by a radial flow and zero slope, articulating the quality of the two reservoirs. Type curves of dimensionless time and pressure are presented along with field cases for vertical and horizontal wells intersected by natural fractures or exploited by hydraulic fractures. The results of this article will enable reservoir engineers to carry out modeling of such complex reservoir/well scenarios with increasing certainty, leading to long-term benefits and greater additional business.

INTRODUCTION

Ramey (1976)[1] and Raghavan (1977)[2] have previously presented a review of the work done on radial flow along and toward fractures. They find that intersecting fractures will strongly affect the transient flow behavior of the well. Houze et al. (1988)[3] have described a well intersecting an infinite conductivity fracture in a naturally fractured reservoir that was simulated using a double-porosity model. Cinco-Ley and Samaniego (1981)[4] have presented a semi-analytical solution to conducting a transient pressure analysis for fractured wells in symmetric reservoirs, which is most likely to occur in the case of small fractures or strike-slip faults. Yet, in the case of reverse or normal faulting with a large throw (juxtaposing), different quality reservoirs would adjoin the fault plane. That is, faulting may result in a sudden displacement of rock along the fault planes, which can lead to a large-scale slippage, resulting in different quality fault blocks on both sides of the fault. Production logs have shown the presence of two different fault blocks after a reverse fault offset the sequence of two zones. Figure 1 offers a good example of faulting that juxtaposes different geology across the fault plane. Data interpretation is

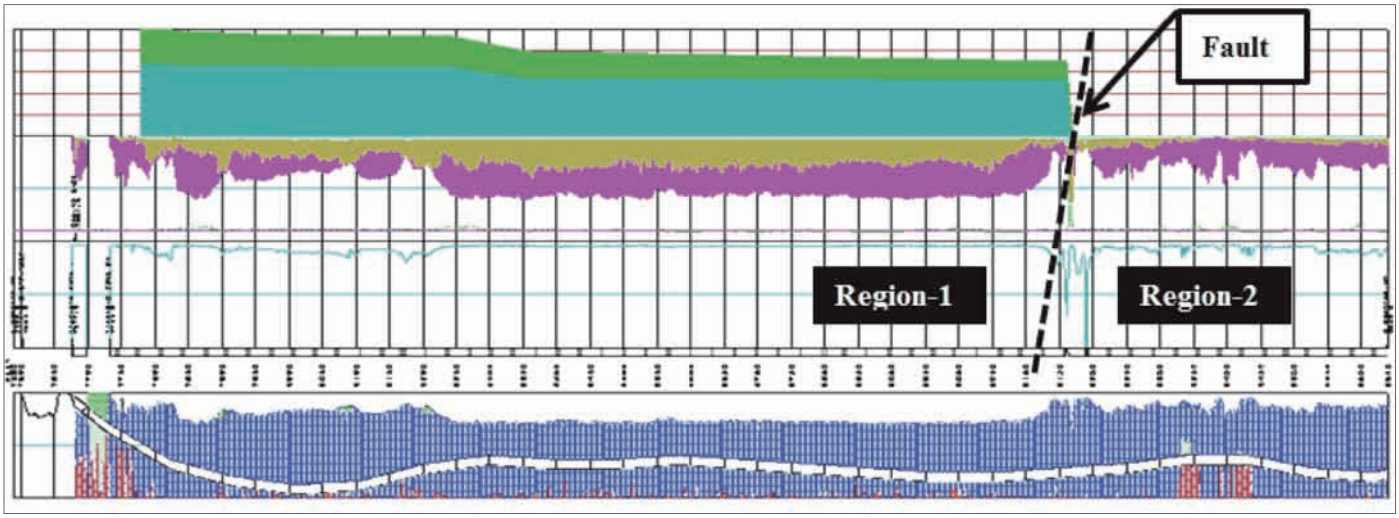

Fig. 1. A fault that has juxtaposed different geology across the fault plane.

more complex when two different quality zones are aligned through the fault plane. There is a semi-analytical solution for such a scenario.

Numerical well test packages are limited and are largely affected by grid geometries and sizes, especially when analyzing wells with complex geometry or geological settings. Analytical solutions, on the other hand, can enable the well test analyst to carry out modeling of complex reservoir/well scenarios more easily and with increasing certainty. In this study, a mathematical model was developed for a well intersecting a natural fracture (or hydraulic fracture) in a linear composite reservoir, where the fracture (and intersecting well) is located between the two different permeability regions. The solution provided can handle different fracture/reservoir complexities, including radial homogeneous reservoirs, fractured wells in a homogeneous reservoir and fractured wells between two regions with different properties.

PROBLEM STATEMENT AND SOLUTION DEVELOPMENT

As previously mentioned, this investigation provides a semi-analytical solution to a finite conductivity fracture separating two regions of different mobilities. Figure 2 shows the flow geometry that was investigated. The flow domain of the statement problem has been divided into three flow regions: (1) a reservoir region-1 (with its specific properties) that defines flow into the fracture from below; (2) a fracture (with its specific fracture properties) that allows fluids to flow along the fracture toward the well; and (3) a reservoir region-2 (with its specific properties) that defines the fluid flow into the fracture from the top. The flow per unit area was defined as positive from above and negative from below. It should be noted that our goal was to develop a solution that provides the pressure vs. time and space in general and wellbore pressure vs. time in particular.

Laplace and Fourier transforms were performed to the three equations governing the 2D flow in these three regions with respect to dimensionless time, in terms of the transformed parameter, s, and space variable, and in terms of the transformed parameter, p, respectively. The equations — with the associated boundary conditions — are presented in the Laplace space and inverted numerically using the Gaver-Stehfest numerical

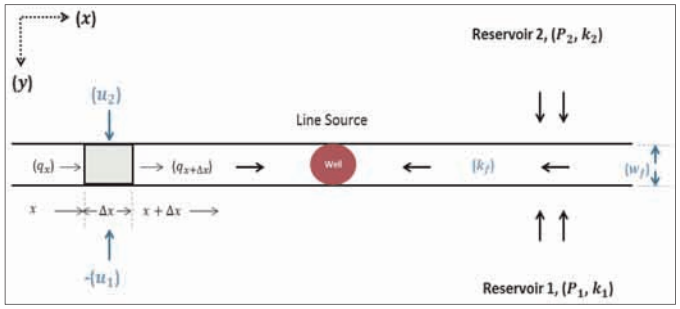

Fig. 2. A schematic of the flow geometry under study.

inversion[5]. For more details, please contact the authors.

The resultant expression for the wellbore pressure in the Laplace domain is:

(1)

where

(2)

and η_{Df}, η_{D1} and η_{D2} are the dimensionless hydraulic diffusivities of the fracture, region-1 and region-2, respectively:

(3)

(4)

(5)

F_{CDf} is the dimensionless fracture conductivity:

(6)

The fracture's reference permeability is the arithmetic average of the two adjoining regions — the well is located in the center between the two regions:

(7)

The region's reference permeability is:

(8)

and k_{d1} and k_{d2} are the dimensionless permeabilities for region-1 and region-2, respectively:

(9)

(10)

The reservoir parameters that can be determined from the type curve matching of the forwarded solution are reservoir permeabilities, k_1 and k_2, fracture permeability, k_f, fracture width, w_f, dimensional fracture conductivity, $k_f \cdot w_f$, and dimensionless fracture conductivity, F_{CDf}. The fracture half-length, x_f, can also be estimated by estimating the flux distribution. The finite conductivity fracture dictates a non-uniform inflow flux distribution along the fracture plane.

SOLUTION BEHAVIOR

The type curve solution of dimensionless pressure and its log derivative vs. dimensionless time for different dimensionless

fracture conductivities has been plotted in Fig. 3. It shows some distinctive features, including a homogeneous infinite acting reservoir when the fracture conductivity is zero, and fractured well pressure behavior in early-time data, where the curve signifies a one-quarter slope, which generates a bilinear flow reflecting two linear flow regimes along and into the fracture. The solution code is enabled with dimensionless skin and wellbore storage (WBS) using dimensionless equations and those limited to positive skin[6] only, Fig. 4.

Flux Distribution

The nature of finite conductivity fractures dictates a nonuniform inflow flux distribution. The flux distribution alongside the fracture plane is nonuniform because the fracture pressure, P_f, is considerably smaller closer to the well and gets larger at the tip of the fracture due to the larger volume around the tip area, thereby yielding a nonuniformly distributed flux. It is also worth mentioning that the larger fluid volume around the tip will also cause larger inflow flux there. It has been observed[7] that producing fractured wells at high flow rates will cause non-Darcy effects in the fracture, resulting in a pessimistic estimate of fracture conductivity, and will also cause different flux distribution. The same assumption is valid for cases featuring highly propped fractures and a damaged fracture face. As a result of estimating the flux distribution, the fracture half-length can also be estimated.

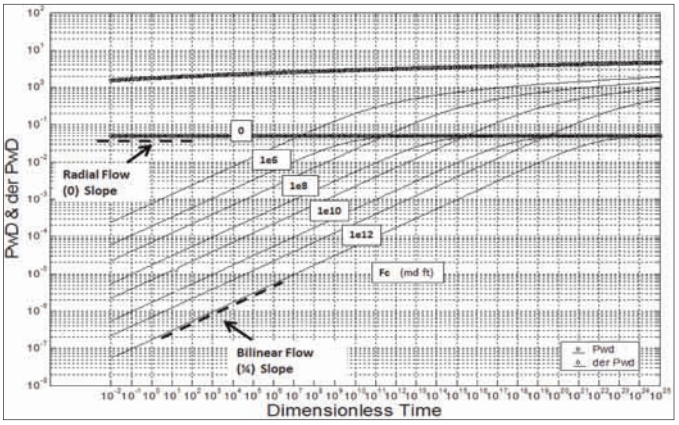

Fig. 3. Dimensionless time vs. dimensionless pressure and pressure derivative using numerical inversion from the Laplace transform.

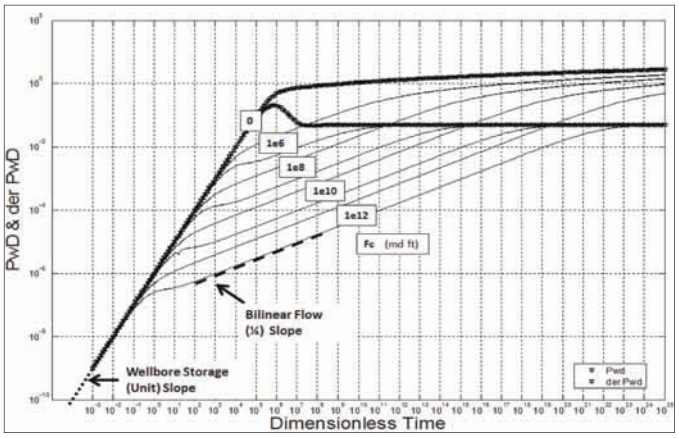

Fig. 4. Dimensionless time vs. dimensionless pressure and pressure derivative with WBS using dimensionless equations[6].

VALIDATION OF SOLUTION

Synthetic Case 1: Fractured Well Bounded by Two Different Regions

Analysis of a synthetic case of a fractured well in an asymmetric reservoir was carried out for this study, where region-1 and region-2 permeabilities were 20 md and 80 md, respectively, and the average permeability calculated from this solution was the arithmetic average, or 50 md. This case was compared to another case — that of a well located in a homogeneous reservoir with an average reservoir permeability of 50 md. By superimposing the two pressure derivatives of these cases, a perfect overlay was achieved through the late-time data of the radial flow, confirming the reliability of the average permeability calculation method proposed by this solution, Fig. 5. This was anticipated as the well described in the proposed solution is located in the center between the two regions.

Synthetic Case 2: Analytical Data from a Commercial Software Package

A synthetic, analytically built symmetric reservoir model of a well intersecting a finite conductivity fracture was constructed to validate the proposed semi-analytical solution using a commercial well test package. Table 1 shows the input data to the analytical model and the results obtained by superimposing the pressure data of this solution on the proposed type curve, Fig. 6. A good agreement between the two was noted. There is a slight deviation in the match between dimensionless time, t_D, of 1.0e5 to 1.0e8, which is attributed to the infinite fracture half-length concept of this study.

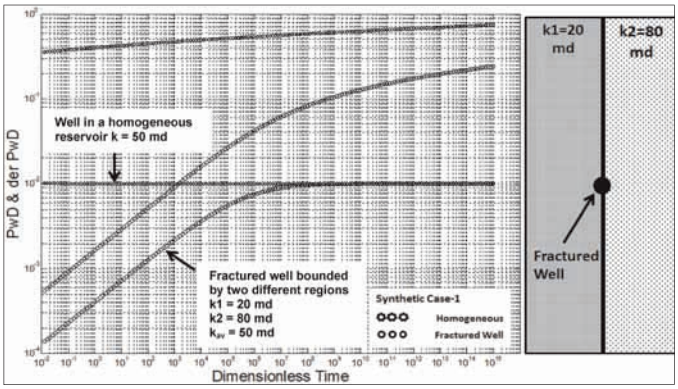

Fig. 5. Derivative overlay of a vertical well in a homogeneous reservoir and a fractured well in an asymmetric reservoir where both reservoirs have the same average permeability of 50 md.

Analytical Model			This Solution				Remarks
x_f (ft)	F_{cf} (md-ft)	k_n (md)	x_f (ft)	F_{cf} (md-ft)	k_1 (md)	k_2 (md)	
2,000	8e4	33	Not Estimated	8e4	33	33	The match to the synthetic model is fair.

Table 1. Comparison between an analytical model and the proposed solution

Numerical Model			This Solution				Remarks
x_f (ft)	F_{cf} (md-ft)	k_n (md)	x_f (ft)	F_{cf} (md-ft)	k_1 (md)	k_2 (md)	
2,000	1.32e6	33	Not Estimated	1.32e6	13	53	Numerical data is affected by the grids.
					k_{av} = 33 md		

Table 2. Comparison between a numerical model and the proposed solution

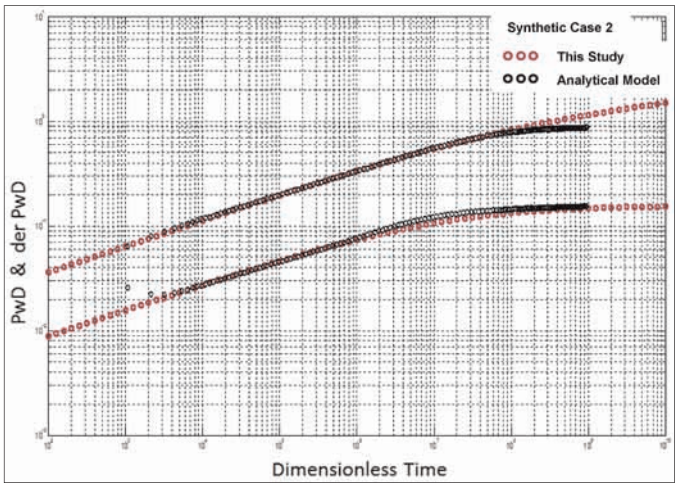

Fig. 6. Pressure and derivative match between the proposed solution and synthetic analytical model.

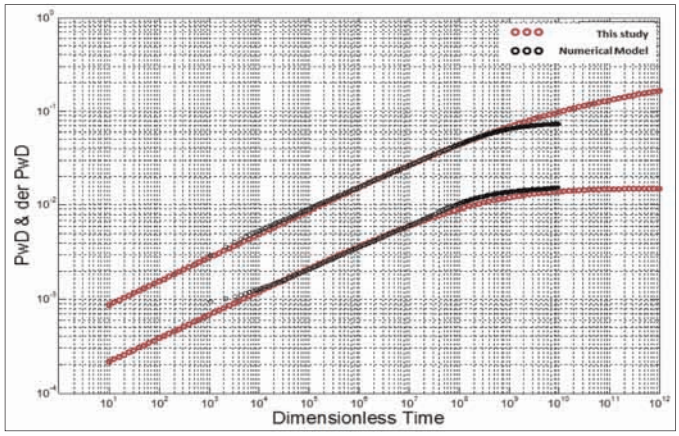

Fig. 7. Pressure and derivative match between the proposed solution and synthetic numerical model.

Synthetic Case 3: Numerical Data from a Commercial Software Package

A synthetic, numerically built asymmetric reservoir model of a well intersecting a finite conductivity fracture was constructed to validate the proposed semi-analytical solution using a commercial well test package. The two region's permeabilities were 13 md and 53 md, respectively, where the arithmetic average of both regions was 33 md. Table 2 shows the input data to the numerical model and the results obtained by superimposing the pressure data of this solution on the proposed type curve, Fig. 7. A good agreement between the two was noted. Table 2 also shows the results of the proposed solution and a total agreement between the two models. As before, the slight deviation in the match, between the t_D of 1.0e7 to 1.0e10, is attributed to the infinite fracture half-length concept of this study.

FIELD CASES

Field data for an asymmetric reservoir case was not available, yet considering that the model matches the numerically built asymmetric case, it is expected that the proposed solution's applicability can be extended to field cases of asymmetric reservoirs.

Field Case 1: A Fractured Vertical Well in a Sandstone Reservoir

The first field case considered was a vertical well intersecting a finite conductivity fracture in a sandstone reservoir, selected to evaluate the reliability of our solution for a practical field example where the flow is partially dominated by the fracture bilinear flow regime and followed by a radial flow regime. A fracture skin and WBS flow regimes were also evident from the early-time data. Table 3 summarizes well and reservoir properties.

The data was matched to the curve provided by the new

Property	Value
Wellbore Radius (ft)	0.23
Pay Zone (ft)	100.0
Porosity (%)	19.0%
Formation Volume Factor (bbl/STB)	1.39
Viscosity (cp)	0.35
Total Compressibility (psi^{-1})	$7.17e^{-6}$

Table 3. Field Case 1 well and reservoir properties

solution, Fig. 8, and validated[4], Fig. 9, using a commercial software package. The flow capacity to oil was found to be nearly the same, 2,400 md-ft from the proposed solution and 2,500 md-ft from the validation solution[4], and fracture conductivities were identical, Table 4.

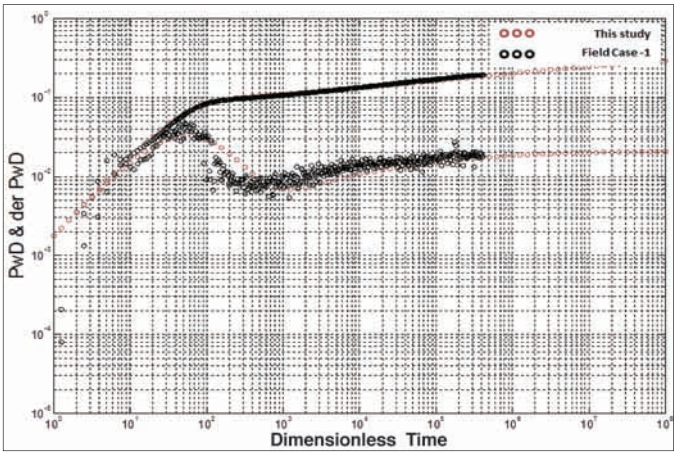

Fig. 8. Pressure and derivative match between the proposed solution and Field Case 1.

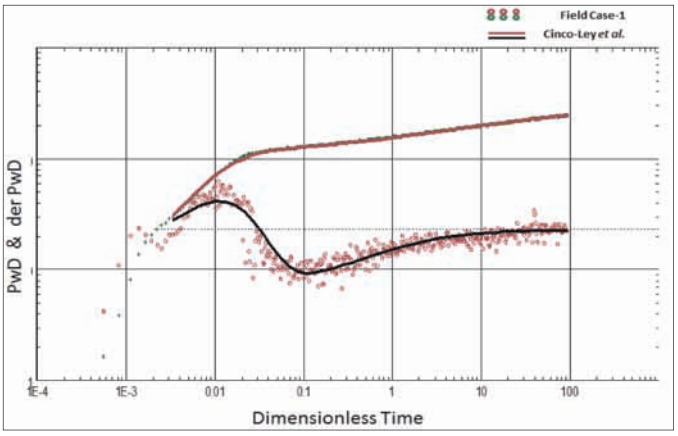

Fig. 9. Validation of pressure and derivative match with Field Case 1 using Cinco-Ley and Samaniego's solution[4].

Field Case 2: A Fractured Horizontal Well in a Carbonate Reservoir

A field case of a horizontal well intersecting a finite conductivity fracture in a carbonate reservoir was considered to evaluate the reliability of our solution for a practical field example where the flow is completely dominated by the fracture. The early-time data was acquired from the productivity index test and a horizontal section drilled in the top, which has been slightly distorted due to WBS and phase segregation. Table 5 summarizes the well and reservoir properties.

The flow capacity to oil was found to be 26,600 md-ft. The proposed solution was used to match the pressure data, and the results were compared to the solution[4] for a well intersecting a finite conductivity fracture in a symmetrical reservoir. This shows that the solution, which was developed for more complex geological systems (two regions), can handle a simple system as well. As clearly shown in Table 6, the consistency of the proposed solution was confirmed over the estimated reservoir parameters, which were in excellent agreement. The parameters were found to be identical in both solutions for a symmetric reservoir case. The data was matched to the curve provided by the new solution, Fig. 10, and validated by the solution[4], Fig. 11, using a commercial software package.

Property	Value
Wellbore Radius (ft)	0.26
Pay Zone (ft)	140.0
Porosity (%)	15.0
Formation Volume Factor (bbl/STB)	1.39
Viscosity (cp)	0.73
Total Compressibility (psi^{-1})	$7.8e^{-6}$

Table 5. Field Case 2 well and reservoir properties

Cinco-Ley and Samaniego's Solution[4]				This Solution					Remarks
x_f (ft)	F_{cf} (md-ft)	F_{CDf}	k (md)	x_f (ft)	F_{cf} (md-ft)	F_{CDf}	k_1 (md)	k_2 (md)	
240	12.6e3	2.0	25	Not Estimated	12.6e3	2.0	28	20	Numerical data is affected by the grids.
							k_{av} = 24 md		

Table 4. Comparison between the proposed solution and commercial software results for Field Case 1

Cinco-Ley and Samaniego's Solution[4]				This Solution					Remarks
x_f (ft)	F_{Cf}(md-ft)	F_{CDf}	k (md)	x_f (ft)	F_{cf} (md-ft)	F_{CDf}	k_1 (md)	k_2 (md)	
240	58.4e3	1.0	190	Not Estimated	58.4e3	1.0	190	190	Numerical data is affected by the grids.
							k_{av} = 190 md		

Table 6. Comparison between the proposed solution and commercial software results for Field Case 2

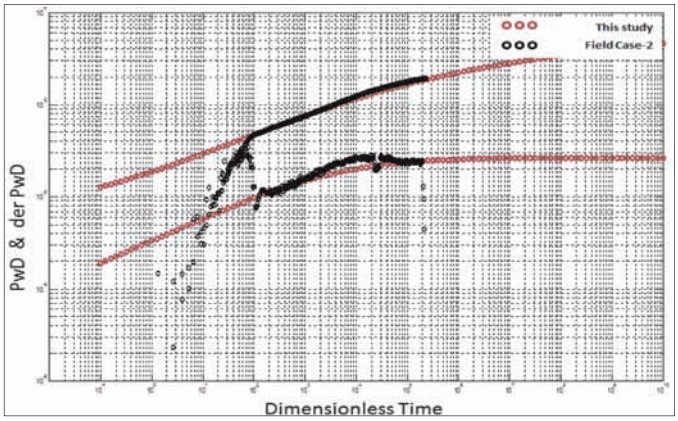

Fig. 10. Pressure and derivative match between the proposed solution and Field Case 2.

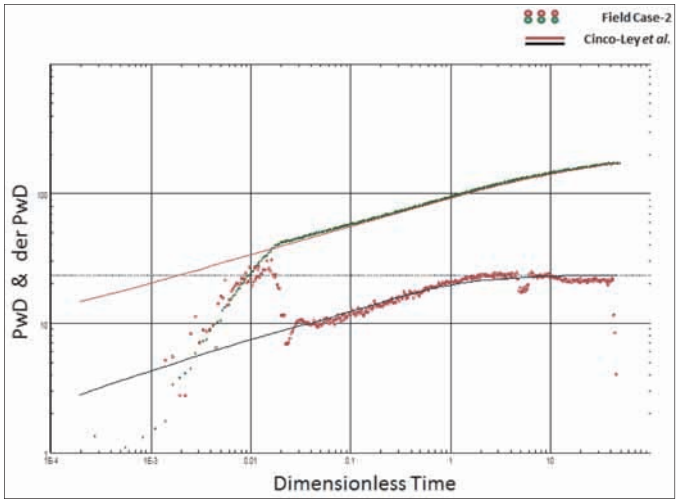

Fig. 11. Variation of pressure and derivative match with Field Case 2 using Cinco-Ley and Samaniego's solution[4].

CONCLUSIONS

The reliability of the proposed solution was demonstrated by matches with data from three synthetic cases and two field cases. First, after a perfect comparison of the proposed solution for a synthetic case in an asymmetric reservoir with data from a well in a homogeneous reservoir with the same average reservoir permeability, analytically and numerically built models were constructed of the simulated flow geometry, and the models' pressure data behavior displayed an excellent agreement with the type curves of the proposed solution. The estimated reservoir parameters from the type curves were also confirmed to be in good agreement with input data. Second, confirmation was achieved through comparisons with two field cases of vertical and horizontal wells that intersected natural fractures in a sandstone and carbonate reservoir, respectively. In conclusion, we note the following:

- A new semi-analytical solution has been developed to handle a finite conductivity fracture in symmetric and asymmetric reservoirs — two different regions bounding the fracture plane.
- The solution was validated by analytical and numerical models and led to identical results.
- The solution estimates the fracture's conductivity and width, and the flow capacity of both regions bounding the fracture.
- The solution calculates the arithmetic average permeabilities of the two regions bounding the fracture plane.

ACKNOWLEDGMENTS

The authors would like to thank the management of Saudi Aramco and Heriot-Watt University for their support and permission to publish this article. Also, the authors would like to express their appreciation for the support and fruitful discussions they had with Dr. N.M. Anisur Rahman and Hassan Nooruddin.

This article was presented at the SPE International Petroleum Technology Conference, Kuala Lumpur, Malaysia, December 10-12, 2014.

NOMENCLATURE

a	distance from origin, ft
B	formation volume factor, RB/STB
C	wellbore storage, bbl/psi
c_f	formation compressibility, psi–1
c_t	total compressibility, psi–1
d_F	distance to fault, ft
d_f	distance to fracture, ft
F_{CDf}	dimensionless fracture conductivity
F_{Cf}	dimensional fracture conductivity, md-ft
h	formation thickness, ft
k	matrix permeability, md
k_1	fracture permeability, md
k_2	fracture permeability, md
k_f	fracture permeability, md
k_{d1}	fracture permeability, md
k_{d2}	fracture permeability, md
k_{df}	fracture permeability, md
$k_f.w_f$	fracture conductivity, md-ft
k_r	reference permeability, md
k_n	(n) reservoir permeability, md
P_i	initial formation pressure, psi
P_1	region-1 pressure, psi
P_2	region-2 pressure, psi
P_f	fracture pressure, psi
P_{wf}	flowing BHP, psi
P_d	dimensionless pressure
P_{d1}	dimensionless region-1 pressure
P_{d2}	dimensionless region-2 pressure
P_{df}	dimensionless fracture pressure

P_{dwf} dimensionless fracture pressure
$\bar{p}$ pressure in Laplace domain
$\bar{\bar{p}}$ pressure in Fourier domain
q flow rate at surface, STB/D
r_w wellbore radius, ft
r distance from the center of wellbore, ft
S skin factor, dimensionless
s Laplace parameter
t_D dimensionless time
t_{Df} fracture dimensionless time
w_f fracture width, ft
x_f fracture half-length, ft
x_d dimensionless x-coordinates
y_d dimensionless y-coordinates
Δp pressure change since start of transient test, psi
Δt time elapsed since start of test, hours
η 0.0002637 $k/\phi ct$, hydraulic diffusivity, ft^2/hr
η_{Df} fracture hydraulic diffusivity, dimensionless
η_{D1} region-1 hydraulic diffusivity, dimensionless
η_{D2} region-2 hydraulic diffusivity, dimensionless
μ viscosity, cp
ϕ porosity, fraction
ρ Fourier parameter

SUBSCRIPT

C = conductivity
D = dimensionless
F = fault
f = fracture
w = wellbore

REFERENCES

1. Ramey Jr., H.J.: "Practical Use of Modern Well Test Analysis," SPE paper 5878, presented at the SPE California Regional Meeting, Long Beach, California, April 8-9, 1976.
2. Raghavan, R.: "Pressure Behavior of Wells Intercepting Fractures," Proceedings of the Invitational Well Testing Symposium, Berkeley, California, October 19-21, 1977.
3. Houze, O.P., Horne, R.N. and Ramey Jr., H.J.: "Pressure Transient Response of an Infinite Conductivity Vertical Fracture in a Reservoir with Double Porosity Behavior," *SPE Formation Evaluation*, Vol. 3, No. 3, September 1988, pp. 510-518.
4. Cinco-Ley, H. and Samaniego, F.: "Transient Pressure Analysis for Fractured Wells," *Journal of Petroleum Technology*, Vol. 33, No. 9, September 1981, pp. 1749-1766.
5. Villinger, H.: "Solving Cylindrical Geothermal Problems Using Gaver-Stehfest Inverse Laplace Transform," *Geophysics*, Vol. 50, No. 10, October 1985, pp. 1581-1587.
6. Kucuk, F. and Ayestaran, L.: "Analysis of Simultaneously Measured Pressure and Sandface Flow Rate in Transient Well Testing," *Journal of Petroleum Technology*, Vol. 37, No. 2, February 1985, pp. 323-334.
7. Guppy, K.H., Cinco-Ley, H., Ramey Jr., H.J. and Samaniego, F.: "Non-Darcy Flow in Wells with Finite Conductivity Vertical Fractures," *Society of Petroleum Engineers Journal*, Vol. 22, No. 5, October 1982, pp. 681-698.

BIOGRAPHIES

Faisal M. Al-Thawad is a General Supervisor of the Well Testing Division and a senior consultant in pressure transient analysis with Saudi Aramco's Reservoir Description and Simulation Department. He has extensive experience in exploratory testing operations and supervision and is specialized in complex well tests, including modeling faults and fractures, and multilateral wells. Faisal has nearly 25 years of total experience in various petroleum disciplines, including drilling, reservoir management and simulation. His experience includes the completion of a 6-year Specialist Development Program on "Reservoir Testing/New Technologies" with a focus on fractures identification, characterizing and modeling.

Faisal is a member of the Society of Petroleum Engineers (SPE) and has participated in a number of international conferences. He has authored several technical papers in the field of well testing and pressure transient analysis. Faisal was an SPE Distinguished Lecturer during the 2013/2014 cycle with a lecture entitled "Fractures Network; Reservoir's Friend or Foe?"

Faisal received his B.S. degree in Petroleum Engineering from King Fahd University of Petroleum and Minerals (KFUPM), Dhahran, Saudi Arabia, and his M.S. degree in Petroleum Engineering from Heriot-Watt University, Edinburgh, U.K.

Dr. Mahmoud Jamiolahmady is a Professor of Petroleum Engineering at Heriot-Watt University, a fellow member of the U.K. Higher Education Academy and Technical Director of Petroc Technologies Ltd. He has over 25 years of experience in studying fluid flow in porous media at the pore, core and field scale levels. Mahmoud leads the Heriot-Watt University gas and gas condensate research team. He also delivers a number of industry-based continuing professional development courses, including "Gas Condensate Reservoir Engineering," and is involved in a number of other enhanced oil recovery projects.

Mahmoud has supervised over 100 M.S. and Ph.D. research projects. He has coauthored over 100 papers relevant to the petroleum industry.

Use of Nano-Emulsion Surfactants during Hydraulic Fracturing Treatments

Authors: Mashhoor S. Al-Anazi, Dr. Mohammed H. Al-Khaldi, Alhasan B. Fuseni and Khalid M. Al-Marshad

ABSTRACT

Hydraulic fracturing has been extensively used as an efficient method to enhance hydrocarbon production, especially in tight formations; however, this technique has been associated with long-lasting formation damage and is a challenge due to fracturing fluid filtrate leakoff. According to the Laplace equation, this fluid leakoff results in a phenomenon called water blockage due to capillary forces. Recent studies have shown that surfactants can be used as an additive to fracturing fluids and that they will reduce the pressure required to displace the injected fracturing fluids. This study investigated the performance of two new nano-emulsion surfactants (NESs).

NES mixtures were prepared at different concentrations ranging from 0.5 gallons per 1,000 gallons (gpt) to 5 gpt using field mixing water. Mixing water and representative field condensate samples were tested for both surface tension and contact angle at a temperature range of 77 °F to 325 °F. The Laplace equation was used to calculate capillary pressure (P_c) values based on those surface tension and contact angle values.

The results based on this study have demonstrated the effectiveness of NESs to recover the fracturing fluid filtrate during flow back. The performance of these surfactants was investigated as a function of several parameters, such as surfactant concentration, soaking time and temperature. In addition, this article explores the adsorption behavior of these surfactants on formation rock and the effect of NESs on the rock wettability. Optimal design parameters for using these NESs to achieve significant enhancement in injected fracturing fluid recovery are also discussed.

INTRODUCTION

Among other important sources of damage, water trapping (water blockage) around the critical near wellbore area has been one of the main causes of the formation damage that occurs during different field activities, such as drilling, completion and stimulation. This phenomenon has an especially significant impact during fracturing treatments of water-wet tight gas wells: it is considered one of the main long-lasting challenges, given that more than 70% of injected water-based fracturing fluid is lost, remaining in the near vicinity of the created fracture[1-8]. This fracturing fluid filtrate loss accumulates as a ring of high water saturation around the fracture where it acts as a barrier to gas flow. As a result, the effective gas permeability is significantly reduced, and subsequently, the well productivity decreases. The effect of water blockage on gas well productivity is even more pronounced in gas wells with a reservoir pressure below the dew point pressure. This is mainly because the presence of condensate, in addition to the trapped water, results in further reduction of effective gas permeability, and therefore, has a dramatic negative impact on well productivity. Over the last few decades, many techniques and methods have been used to enhance the cleanup process to remove entrapped fluid in gas wells[9-13].

Approaches to water blockage and its cleanup are mainly governed by the interaction of both capillary pressure (P_c) and relative permeability. P_c is a function of pore geometry, the interfacial tension of entrapped and produced fluids, and rock wettability[14] as follows:

$$\frac{\sigma \cos\theta}{R} \qquad (1)$$

where σ is the interfacial tension of entrapped and produced fluids in dyne/centimeters (cm), θ is the contact angle in degrees, and R is pore radius in cm.

The reservoir drawdown pressure must first overcome the P_c for produced gas to displace entrapped water. Subsequently, effective gas permeability will increase with further gas production due to the evaporation of the entrapped fluid. According to Mcleod and Coulter (1966)[12], application of alcohol treatments, such as methanol and isopropyl alcohol, improves the entrapped fluid displacement by lowering the interfacial tension and enhancing the water evaporation rate. It has been reported[11], however, that the evaporation process of entrapped water can last for thousands of pore volumes of produced gas. This unhurried evaporation process is even slower in tight and strong water-wet formations. The report suggested that the cleanup of entrapped water can be improved by increasing pressure drawdown, increasing temperature, changing the wettability of the rock to a more gas-wet condition, and decreasing the interfacial tension of entrapped and produced fluids. When used to facilitate the last action, surface active chemicals (surfactants) have improved post-fracturing fluid recovery, especially in tight formations.

Surfactants have been extensively used in different field activities. Their applications have a wide range: they have been added as acid retarders, emulsifiers, demulsifiers, anti-sludge agents and acid diverters[15-18]. In addition to these applications, surfactants have also been used as an additive to reduce the interfacial tension of fluid filtrate and reservoir produced fluids. The use of surfactants in tight formations is essential because the effect of capillary forces is more pronounced in small pore throat formations[14]. Generally, a typical surfactant is an amphiphilic molecule composed of a hydrophilic head and a hydrophobic tail. Typically, the head group is composed of ethylene oxide, acting as a hydrophile agent. When dissolved in water near their critical micelle concentration (CMC), surfactant molecules aggregate into self-assembly orientations, creating cylindrical or spherical micelles, thereby reducing the surface tension of any injected fluid. These surfactants are classified according to either the charge they acquire when dissolved in water or the charge of the head group. There are mainly four types of surfactants: cationic, anionic, nonionic and amphoteric (zwitterionic).

Besides its concentration, other factors affect surfactant performance. One of these factors is temperature[19-22]. At high temperatures, the hydration bonds between water molecules and the polyethylene oxide group start to break. As a result, the surfactant solubility limit, or its cloud point, decreases and the surfactant starts to precipitate. This precipitation forms two immiscible phases: a surfactant-rich phase and a surfactant-lean phase. Additionally, it has been reported that different salts have a negative effect on surfactant solubility[21]. The calcium chloride and magnesium chloride salts depress the cloud point of a surfactant and cause a phase separation. Although these surfactants have been extensively used to prevent water blockage, the surfactant adsorption problems in both carbonate and sandstone formations have been detrimental to their performance[19, 20, 23, 24].

In this article, nano-emulsion surfactants (NESs) are explored as an alternative to conventional surfactants to overcome the challenges posed by the adsorption problems. These surfactants are a blend of anionic surfactant, nonionic surfactant, short chain alcohol and water. The presence of both surfactant and alcohol has a dual effect: it both lowers interfacial tension and also increases water evaporation. This combination outperforms water blockage treatments using surfactants or alcohol alone. NESs are thermodynamically stable and homogeneous dispersions of two immiscible fluids, stabilized by a surfactant and a co-surfactant of short chain alcohol. The diameter size of these stabilized emulsions is approximately 10 nm to 20 nm. Generally, these emulsions can be classified as one of four types: WINSOR I, WINSOR II, WINSOR III and WINSOR IV. WINSOR I, WINSOR II and WINSOR III are systems consisting of a nano-emulsion phase in equilibrium with oil, water and oil/water phases, respectively. WINSOR IV is a system consisting of the nano-emulsion phase only[25].

This study assessed the performance of two NESs, NES-1 and NES-2. The effectiveness of these two surfactants in lowering the interfacial tension was investigated under various conditions expected in both gas and gas condensate reservoirs. Additionally, the effect of the use of these surfactants on formation rock wettability was studied along with their adsorption behavior.

EXPERIMENTAL WORK

Materials

Two NESs, NES-1 and NES-2, were received from local service companies; they were used as received. Both NES-1 and NES-2 are blends of anionic surfactant, nonionic surfactant, short chain alcohol and water. NES-1 is a light amber liquid that consists of oil and isopropanol with a pH of 6.7. NES-2 is clear colorless liquid that consists mainly of citrus and isopropanol with a pH of 8.7. These two surfactants were dispersed in two different formation waters at a concentration range of 0.5 gallons per 1,000 gallons (gpt) to 5 gpt. Tables 1 and 2 show the geochemical analysis of the two formation waters. Formation rock substrates were used to take contact angle measurements at different nano-emulsion concentrations. Table 3 illustrates the mineral composition of the formation rocks used.

Contact Angle and Interfacial Tension (Drop Shape Analysis)

The contact angle and interfacial tension measurements were made at temperature ranges of 77 °F to 325 °F, under pressure of 1,500 psi. These measurements were made using a pendant drop instrument, model PD-E700LL-H, manufactured by Eurotechnica Ingenieurbüro GmbH, Germany. The image analysis module of the instrument is a Krüss model DSA100HP. The wetted surfaces of the instrument (the cell and needle) are constructed from Hastelloy-C. Surface tension measurements were

Ion	Content (Unit)
HCO_3^-	209 mg/L
Cl^-	< 10 mg/L
Conductivity	2,909 Microhms
pH at 25 °C	8.0
TDS	1,445 mg/L
Specific Gravity at 60 °F	1.0010
SO_4^{2-}	670 mg/L
Ca^{2+}	160 mg/L
Sr^{2+}	16 mg/L
K^+	18 mg/L
Mg^{2+}	82 mg/L
Na^+	314 mg/L

Table 1. Chemical composition of formation water used as mixing water for NES-1

Ion	Content (Unit)
HCO_3^-	147 mg/L
Cl^-	302 mg/L
Conductivity	1,564 Microhms
pH at 25 °C	7.9
TDS	1,042 mg/L
Specific Gravity at 60 °F	1.0004
SO_4^{2-}	276 mg/L
Ca^{2+}	115 mg/L
Sr^{2+}	8 mg/L
K^+	< 10 mg/L
Mg^{2+}	49 mg/L
Na^+	153 mg/L

Table 2. Chemical composition of formation water used as mixing water for NES-2

Mineral	Weight Percentage (wt%)
Calcite-$CaCO_3$	86
Dolomite-$CaMg(CO_3)_2$	7
Quartz-SiO_2	3
Pyrite-FeS_2	1
Kaolinite-$Al_2Si_2O_5(OH)_4$	2
Illite-$KAl_2(Si_3Al)O_{10}(OH)_2$	1

Table 3. Mineral composition of the formation rocks used for contact angle measurements

carried out by generating a pendant drop at the end of a capillary tube — outside diameter = 1.575 mm — in compressed nitrogen gas. The DSA100HP was used to determine the contact angle from the shape of the sessile drops. The instrument provides precise measurements of contact angle and interfacial tension with a measuring resolution of 0.1° and 0.01 mN/m for the contact angle and the interfacial tension, respectively. The maximum operating pressure and temperature are 10,000 psi and 200 °C, respectively.

Both contact angle and interfacial tension measurements were made at different surfactant concentrations of 0.5 gpt to 5 gpt in the presence and absence of condensate liquid to simulate the conditions of both gas and gas condensate wells. Prior to making the contact angle measurements in the presence of condensate, the formation rock substrate was soaked in a condensate sample for nearly 24 hours.

Adsorption Tests

Adsorption tests of each NES were performed at room temperature. These tests were conducted using crushed samples of representative reservoir rock, which were immersed overnight in formation water samples containing nano-emulsion fluid at CMC under vacuum influence at a solid-liquid ratio of 1:1. Then the slurry of NES solutions and crushed core samples was filtered using 0.5 µm paper. To assess the degree of adsorption for each NES, interfacial tension values of the NES fluids at CMC were compared before and after the adsorption experiments.

RESULTS AND DISCUSSIONS

Interfacial Tension

Fracturing fluid filtrate leakoff can cause severe formation damage due to water blockage. According to Eqn. 1, the main driving force for water blockage is P_c, which is mainly a function of both interfacial tension and contact angle. Several experiments were conducted using two NES solutions to measure surface tension and interfacial tension at different surfactant concentrations and at temperature ranges of 77 °F to 325 °F. These experiments were conducted in the presence and absence of a representative condensate field sample.

Figures 1 and 2 show the surface tension (gas-liquid interfacial

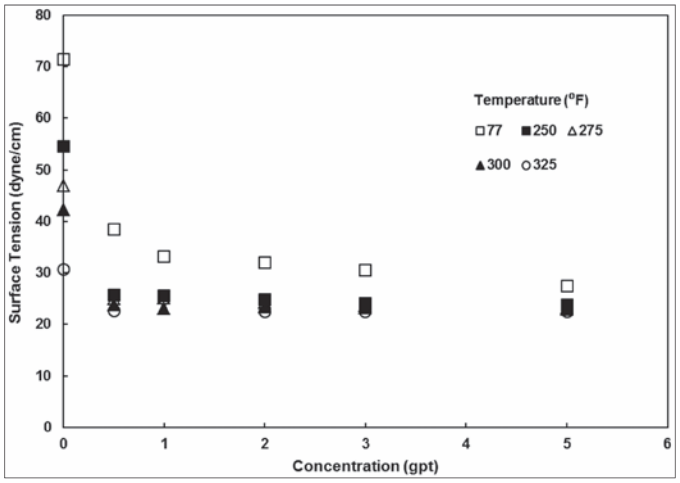

Fig. 1. Surface tension of NES-1 as a function of concentration and temperature.

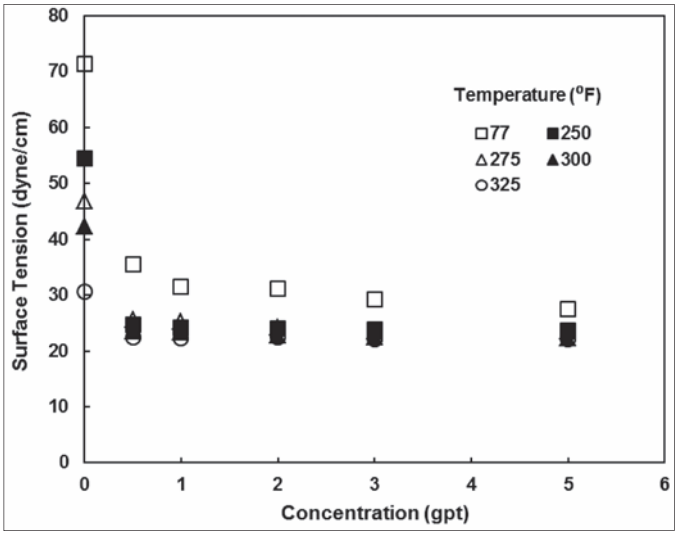

Fig. 2. Surface tension of NES-2 as a function of concentration and temperature.

tension ($\sigma_{w/air}$)) as a function of surfactant concentration and temperature for NES-1 and NES-2, respectively. As shown in these figures, the CMC of these two surfactants is nearly 0.5 gpt. The surface tension decreased as both the surfactant concentration and the temperature increased. This decrease in $\sigma_{w/air}$ continued until the surfactant concentration reached a CMC value of 0.5 gpt and the temperature value was at 250 °F. Beyond these two values of surfactant concentration and temperature, there was no significant decrease in $\sigma_{w/air}$ value.

At a concentration of 0.5 gpt and a temperature of 250 °F, the surface tension of NES-1 and NES-2 decreased from nearly 54.3 dyne/cm to nearly 24.62 dyne/cm and 23.54 dyne/cm, respectively. This reduction represents a drop of almost 54% and 56% in $\sigma_{w/air}$. At higher temperatures, the percentage of the reduction in surface tension was not as significant as that observed at 250 °F, Fig. 3. For example, at 325 °F, the surface tension of NES-1 and NES-2 at 0.5 gpt decreased by only 26.6% and 24.80%, respectively. This is attributed mainly to the fact that water at high temperatures has relatively lower $\sigma_{w/air}$, which cannot be reduced as significantly as it can be at lower temperature values.

In gas condensate reservoirs, the fracturing fluid cleanup is dependent on the interfacial tension between water and condensate rather than water and air. The interfacial tension values between representative condensate field samples and NES-1 and NES-2 solutions, Figs. 4 and 5, respectively, were determined at various surfactant concentrations and temperature values. NES-1 and NES-2 were very effective in lowering the interfacial tension of water against condensate ($\sigma_{w/c}$). The reduction in interfacial tension was a function of both surfactant concentration and temperature. Generally, $\sigma_{w/c}$ increased with increases in temperature at a constant surfactant concentration. For example, at 0.5 gpt of NES-1, the $\sigma_{w/c}$ increased from 28.02 dyne/cm to 56.45 dyne/cm when the temperature was increased from 77 °F to 325 °F; however, the $\sigma_{w/c}$ decreased when the surfactant concentration was increased at a constant temperature. For example, it decreased from 40.9 dyne/cm to 15.94 dyne/cm when the NES-2 concentration was increased from 0 gpt to 5 gpt at a constant 325 °F. Figure 6 shows the percentages of reduction in $\sigma_{w/c}$ as a function of different NES-1 concentrations at different temperatures. It is obvious that at various temperatures, the most significant decrease in $\sigma_{w/c}$ was observed at a surfactant concentration of almost 1 gpt to 2 gpt. For example, at 250 °F, $\sigma_{w/c}$ decreased by 67%, 74% and 85% when the NES-1 concentration was increased from 0 gpt

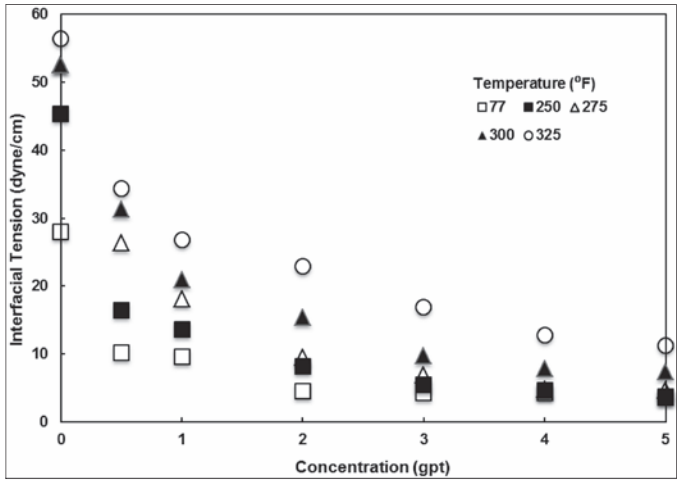

Fig. 4. Interfacial tension of NES-1 against condensate as function of concentration and temperature.

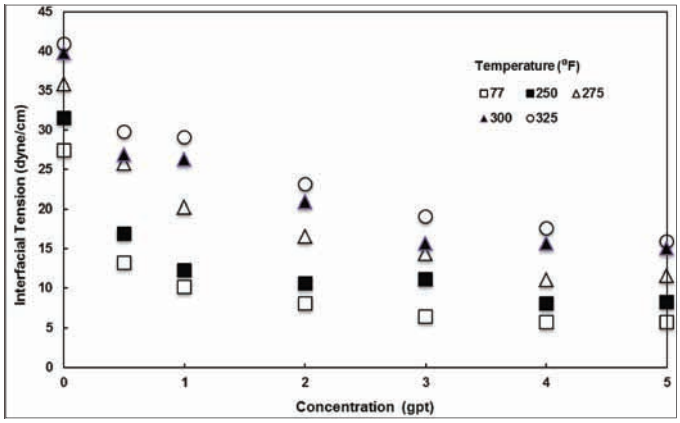

Fig. 5. Interfacial tension of NES-2 against condensate as function of concentration and temperature.

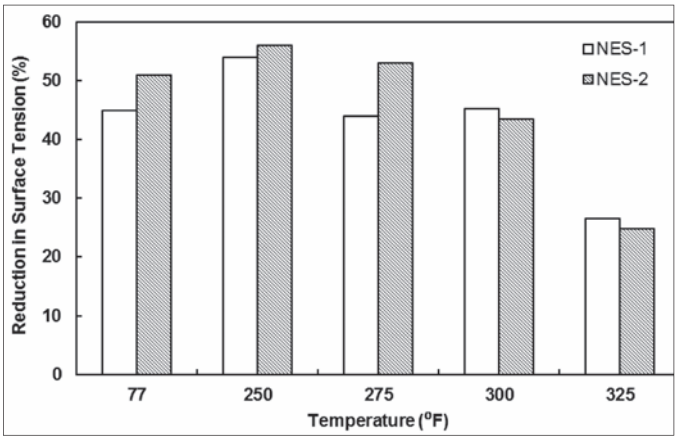

Fig. 3. The reduction percentage in surface tension of NES-1 and NES-2 at 0.5 gpt as a function of temperature at 0.5 gpt.

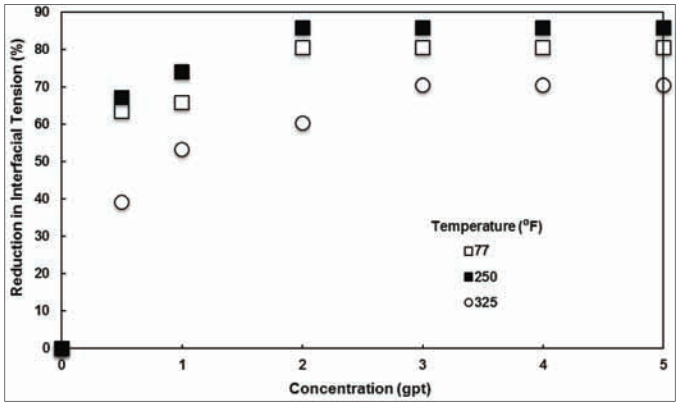

Fig. 6. The percentages of reduction in interfacial tension of NES-1 as a function of temperature and concentration.

to 0.5 gpt, 1 gpt and above 2 gpt, respectively.

To study the effect of surfactant adsorption on its effectiveness, the $\sigma_{w/air}$ values of the NES-1 and NES-2 solutions at 0.5 gpt were calculated before and after the adsorption tests. These tests were conducted using crushed samples, which were immersed overnight in formation water samples containing nano-emulsion fluid at CMC under vacuum influence at a solid-liquid ratio of 1:1 and 77 °F. It was found that the $\sigma_{w/air}$ values of the NES-1 and NES-2 solutions at 0.5 gpt before and after adsorption tests were equal, at an average of 36 dyne/cm. This clearly indicates that these two NESs have no tendency to adsorption on formation rock. Unlike conventional surfactants during fracturing treatments, these NESs will remain present in the leading edge of the penetrating fluid rather than being lost in the few inches of fracture vicinity area. Therefore, compared to conventional surfactants, fracturing fluid filtrate with NES will have lower interfacial tension and higher flow back recovery.

Contact Angle

In addition to interfacial tension, P_c is a function of contact angle, Eqn. 1. Several experiments were conducted using the two NES solutions to measure the contact angle at different surfactant concentrations and a temperature value of 77 °F. These experiments were conducted in the presence and absence of representative condensate field samples. In all the experiments, water was taken as the reference fluid phase, and the contact angle was always measured through the water phase independent of whether water was the wetting phase or not.

Contact angle measurements were made using cube samples of formation rock. Preliminary experiments investigated the change in average contact angle with time. It was observed that the contact angle of 0 gpt NES solutions reached a stable value after nearly 5 minutes at 77 °F and at atmospheric pressure, Photo 1. Therefore, all contact angle measurements were made after 5 minutes of contact time between a water droplet and the formation rock substrate. Generally, results showed that the average contact angle decreased as the NES concentration increased at 77 °F, Photo 2 and Fig. 7. For example, the average contact angle decreased from 55.44° to 9.83° when the NES-2 concentration was increased from 0 gpt to 2 gpt. It is clear that the NES interacted with the formation rock, and as a result the rock became more water-wet. This effect was not permanent, however; the contact angle at 0 gpt remained constant at 55° before and after a formation substrate was soaked in 5 gpt NES solutions for 24 hours at 77 °F.

The average contact angle was also measured through water in the presence of condensate using cube samples of formation rock. The rock substrates were first immersed in condensate, and then a drop of NES solution was placed on the top flat surface of the formation sample. It was observed that the contact angle of the NES drop increased from nearly 55° to 140° at 77 °F when condensate was present, Photo 3. It had been expected that in the presence of condensate, the rock affinity toward water decreased and became non-water wet. Subsequently, the experimental procedure was modified so that the water drop was first placed on the rock substrate, after which

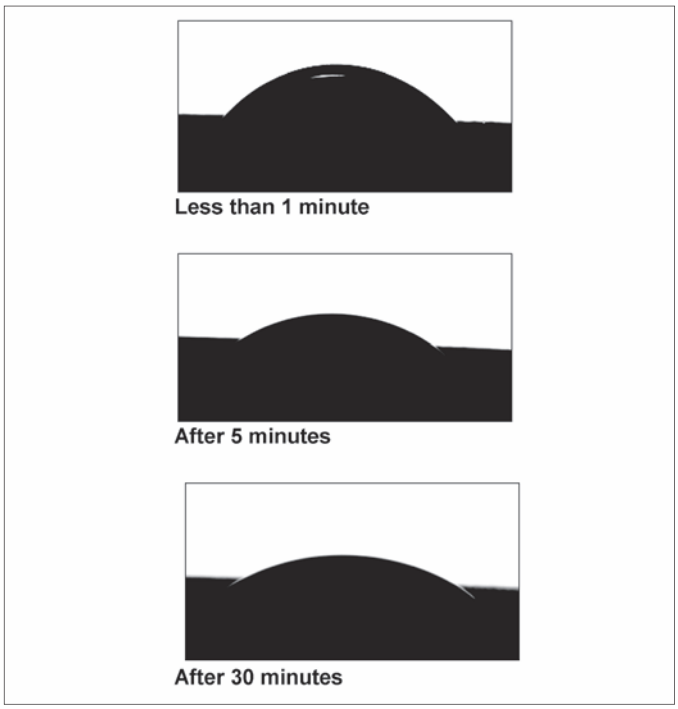

Photo 1. Effect of time on contact angle at 0 gpt and 77 °F.

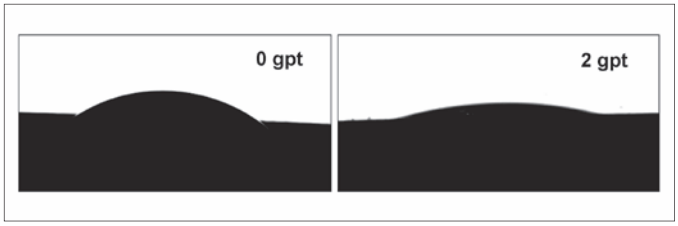

Photo 2. Effect of NES concentration on contact angle at 77 °F in NES/air system.

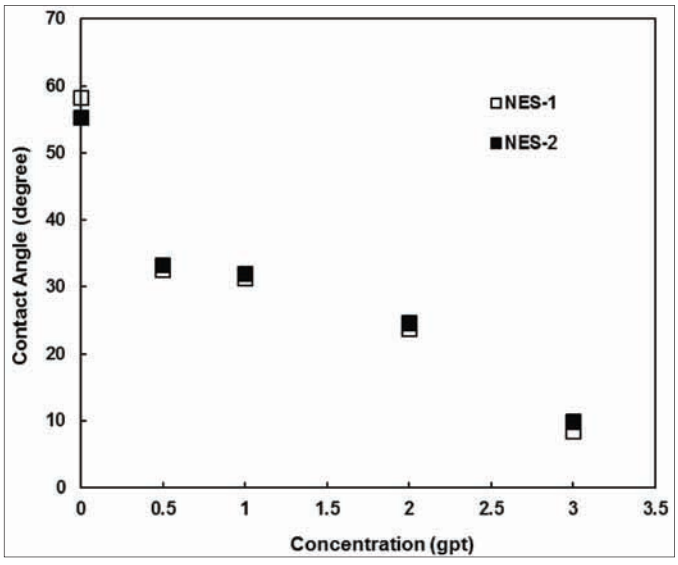

Fig. 7. The average contact angle of NES-1 and NES-2 as a function of concentration at 77 °F.

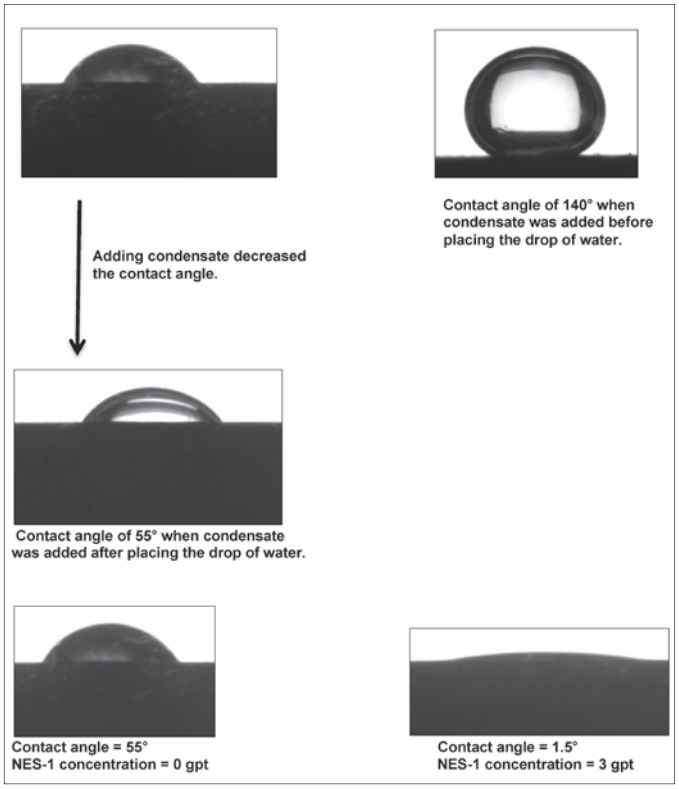

Photo 3. Effect of condensate on NES contact angle at 77 °F.

the sample was immersed in condensate; in that case, it was found that the contact angle had decreased in the presence of condensate. It is believed that in the experiment when the rock substrate was immersed in condensate before placing the water drop, a thin condensate film formed under the water drop. This thin condensate film prevented the interaction of the water drop with the rock substrate and resulted in the large contact angle observed. Therefore, in all subsequent experiments, the water drop was first placed on the rock substrate before it was immersed in condensate.

Figure 8 shows the contact angles of NES drops at different concentrations at 77 °F in the presence of condensate. As before, the average contact angle decreased when the NES concentration was increased. For example, the average contact angle decreased from nearly 55° to almost 1.5° when the NES-1 concentration was increased from 0 gpt to 3 gpt at 77 °F, Photo 3. It is obvious that in the presence of condensate, the decrease in the contact angle with the NES concentration increase was more significant, compared to those observed in the NES air system.

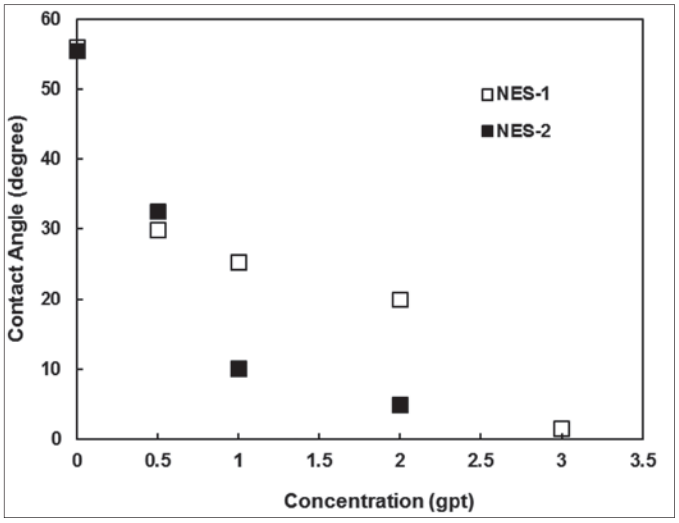

Fig. 8. The average contact angle of NES-1 and NES-2 in the presence of condensate as a function of concentration at 77 °F.

Capillary Pressure

P_c values at different NES concentrations were calculated from values presented in Figs. 1, 2 and 7, based on Eqn. 1. Figures 9 to 12 present the P_c values at a pore radius of 0.01 µm. It is clear from Figs. 9 and 10 that the optimum concentration of NES-1 and NES-2 is nearly 0.5 gpt. At various temperatures, the P_c decreased with NES concentrations up to 0.5 gpt, after which it increased with the increase in surfactant concentration. This behavior is attributed to the interplay of both the positive effect (lower surface tension) and negative effect (lower contact angle) of these surfactants. The average percent-

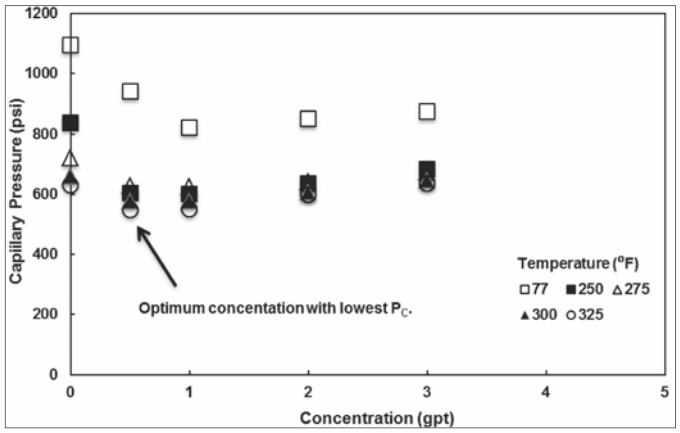

Fig. 9. Capillary pressure of NES-1/air as a function of concentration and temperature.

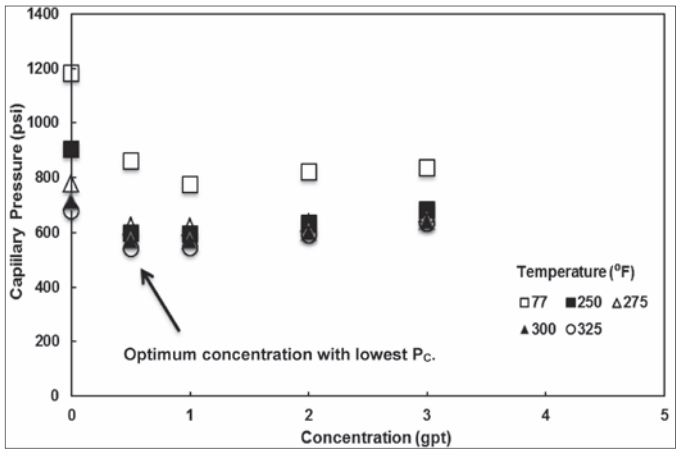

Fig. 10. Capillary pressure of NES-2/air as a function of concentration and temperature.

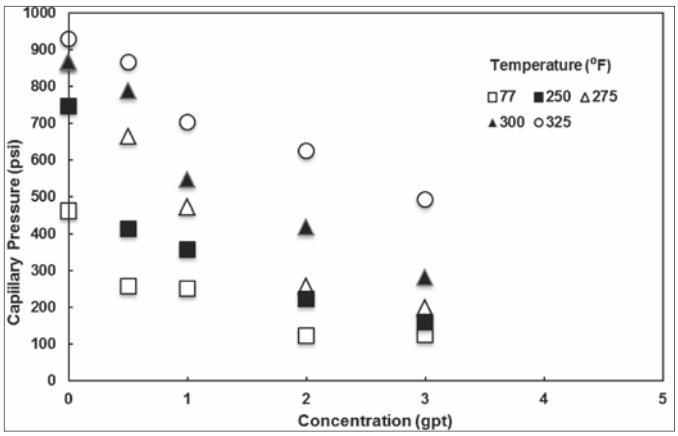

Fig. 11. Capillary pressure of NES-1/condensate as a function of concentration and temperature.

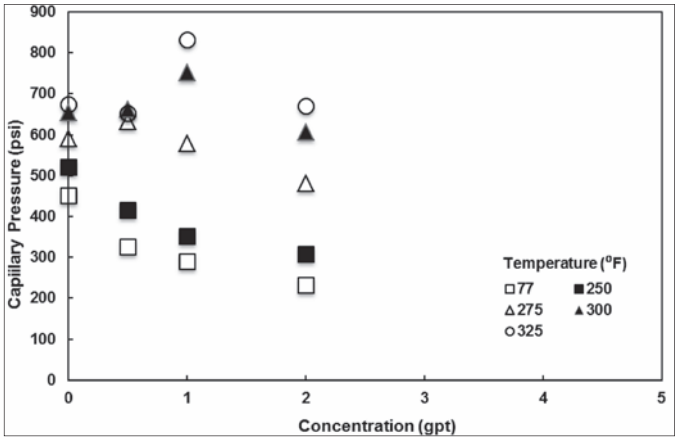

Fig. 12. Capillary pressure of NES-2/condensate as a function of concentration and temperature.

age of reduction in P_c was nearly 19% to 27%. For example, at 300 °F, the P_c decreased from 650 psi to nearly 525 psi when the NES-1 concentration was increased from 0 gpt to 0.5 gpt. The NES had a more pronounced effect on the P_c in the presence of condensate, Figs. 11 and 12. P_c decreased with the increase of the NES concentration, and the lowest value was observed at the highest NES concentration. For example, the P_c decreased from nearly 930 psi to 490 psi when the NES-1 concentration was increased from 0 gpt to 3 gpt at 325 °F. Compared to the NES air system, the percentage of reduction in P_c in the NES condensate system was higher, ranging between 47% and 80%. This is mainly due to the significant effect of these surfactants on the interfacial tension of water and condensate compared to that of the NES air system.

CONCLUSIONS

Several experiments were conducted to investigate the effect of NES on interfacial tension, contact angle and P_c in both water-air and water-condensate systems to simulate conditions in gas and gas condensate wells. These experiments were conducted at different NES concentrations and temperature values from 77 °F to 325 °F. Based on this work, the main conclusions are:

- Both surfactants, NES-1 and NES-2, were effective in lowering both the surface tension and the interfacial tension of water-air and water-condensate systems at temperatures of 77 °F to 325 °F.
- The CMC of NES-1 and NES-2 is 0.5 gpt in the water-air system. Interfacial tension decreased with a NES concentration increase in the water-condensate system at various temperatures.
- The NES did not exhibit any adsorption tendency with formation rock. The surface tension remained constant at CMC before and after the adsorption tests.
- The contact angle decreased with the NES concentration increase at room temperature. The effect of NES on the contact angle was even more pronounced in the presence of condensate. The rock substrates became more water-wet with the NES concentration increase.
- The effect of NES on rock formation affinity was not permanent. A contact angle for 0 gpt NES solution remained at 55° before and after the sample was soaked in 5 gpt NES solution at room temperature for 24 hours.
- The P_c decreased with the NES concentration increase in the water-air system. The lowest value was observed at 0.5 gpt at different temperatures.
- The P_c decreased with the NES concentration increase in the water-condensate system at different temperatures. The lowest value was obtained with the maximum NES concentration used.

ACKNOWLEDGMENTS

The authors would like to thank the management of Saudi Aramco for their support and permission to publish this article.

This article was presented at the Abu Dhabi International Petroleum Exhibition and Conference, Abu Dhabi, UAE, November 10-13, 2014.

REFERENCES

1. Kamath, J. and Laroche, C.: "Laboratory-based Evaluation of Gas Well Deliverability Loss Caused by Water Blocking," *Society of Petroleum Engineers Journal*, Vol. 8, No. 1, March 2003, pp. 71-80.
2. Mahadevan, J. and Sharma, M.M.: "Factors Affecting Cleanup of Water Blocks: A Laboratory Investigation," *Society of Petroleum Engineers Journal*, Vol. 10, No. 3, September 2005, pp. 238-246.
3. Holditch, S.A.: "Factors Affecting Water Blocking and Gas Flow from Hydraulically Fractured Gas Wells," *Journal of Petroleum Technology*, Vol. 31, No. 12, December 1979, pp. 1515-1524.

4. Ahmadi, M., Sharma, M.M., Pope, G., Torre, D.E., McCulley, C.A. and Linnemeyer, H.: "Chemical Treatment to Mitigate Condensate and Water Blocking in Gas Wells in Carbonate Reservoirs," *SPE Production and Operations*, Vol. 26, No. 1, February 2011, pp. 67-74.
5. Ali, J.K., Butler, S., Allen, L. and Wardle, P.: "The Influence of Interfacial Tension on Liquid Mobility in Gas Condensate Systems," SPE paper 26783, presented at the Offshore European Conference, Aberdeen, U.K., September 7-10, 1993.
6. Ahmed, T., Evans, J., Kwan, R. and Vivian, T.: "Wellbore Liquid Blockage in Gas-Condensate Reservoirs," SPE paper 51050, presented at the SPE Eastern Regional Meeting, Pittsburgh, Pennsylvania, November 9-11, 1998.
7. Li, K. and Firoozabadi, A.: "Experimental Study of Wettability Alteration to Preferential Gas-Wetting in Porous Media and Its Effects," *SPE Reservoir Evaluation and Engineering*, Vol. 3, No. 2, April 2000, pp. 139-149.
8. Bang, V.S.S., Yuan, C., Pope, G.A., Sharma, M.M., Baran Jr., J.R., Skildum, J., et al.: "Improving Productivity of Hydraulically Fractured Gas Condensate Wells by Chemical Treatment," SPE paper 19599, presented at the Offshore Technology Conference, Houston, Texas, May 5-8, 2008.
9. Franco, C.A., Zabala, R.D., Zapata, J., Mora, E., Botero, O., Candela, C., et al.: "Inhibited Gas Stimulation to Mitigate Condensate Banking and Maximizing Recovery in Cupiagua Field," SPE paper 151575, presented at the SPE International Symposium and Exhibition on Formation Damage Control, Lafayette, Louisiana, February 15-17, 2012.
10. Barnum, R.S., Brinkman, F.P., Richardson, T.W. and Spillette, A.G.: "Gas Condensate Reservoir Behaviour: Productivity and Recovery Reduction due to Condensation," SPE paper 30767, presented at the SPE Annual Technical Conference and Exhibition, Dallas, Texas, October 22-25, 1995.
11. Mahadevan, J. and Sharma, M.M.: "Clean-up of Water Blocks in Low Permeability Formations," SPE paper 84216, presented at the SPE Annual Technical Conference and Exhibition, Denver, Colorado, October 5-8, 2003.
12. McLeod, H.O. and Coulter, A.W.: "The Use of Alcohol in Gas Well Stimulation," SPE paper 1663, presented at the SPE Eastern Regional Meeting, Columbus, Ohio, November 10-11, 1966.
13. Tang, G-Q. and Firoozabadi, A.: "Relative Permeability Modification in Gas/Liquid Systems through Wettability to Intermediate Gas Wetting," *SPE Reservoir Evaluation and Engineering*, Vol. 5, No. 6, December 2002, pp. 427-436.
14. Bennion, D.B., Thomas, F.B. and Bietz, R.F.: "Low Permeability Gas Reservoirs: Problems, Opportunities and Solutions for Drilling, Completion, Stimulation and Production," SPE paper 35577, presented at the SPE Gas Technology Symposium, Calgary, Alberta, Canada, April 28 - May 1, 1996.
15. Zhou, H., Dismuke, K.I., Lett, N.L. and Penny, G.S.: "Development of More Environmentally Friendly Demulsifiers," SPE paper 151852, presented at the SPE International Symposium and Exhibition on Formation Damage Control, Lafayette, Louisiana, February 15-17, 2012.
16. Hirasaki, G.J., Miller, C.A. and Puerto, M.: "Recent Advances in Surfactant EOR," *Society of Petroleum Engineers Journal*, Vol. 16, No. 4, December 2011, pp. 889-907.
17. Wang, D., Liu, C., Wu, W. and Wang, G.: "Novel Surfactants that Attain Ultra-Low Interfacial Tension between Oil and High Salinity Formation Water without Adding Alkali, Salts, Co-surfactants, Alcohols and Solvents," SPE paper 127452, presented at the SPE EOR Conference at Oil and Gas West Asia, Muscat, Oman, April 11-13, 2010.
18. Toseef, A., Beaman, D.J. and Birou, P.: "Viscoelastic Surfactant Diversion: An Effective Way to Acidize Low Temperature Wells," SPE paper 136574, presented at the Abu Dhabi International Petroleum Exhibition and Conference, Abu Dhabi, UAE, November 1-4, 2010.
19. Adkins, S., Chen, X., Nquyen, Q.P., Sanders, A.W. and Johnston, K.P.: "Effect of Branching on the Interfacial Properties of Nonionic Hydrocarbon Surfactants at the Air-Water and Carbon Dioxide-Water Interfaces," *Journal of Colloid and Interface Science*, Vol. 346, No. 2, pp. 455-463.
20. Wakamatsu, T. and Fuerstenau, D.W.: "The Effect of Hydrocarbon Chain Length on the Adsorption of Sulfonates at the Solid/Water Interface," *Advances in Chemistry*, Vol. 79, 1986, pp. 161-172.
21. Nasr-El-Din, H.A., AL-Othman, A.M., Taylor, K.C. and Al-Ghamdi, A.H.: "Surface Tension of Acid Stimulating Fluids at High Temperatures," *Journal of Petroleum Science and Engineering*, Vol. 43, 2004, pp. 57-73.
22. Hinkel, J.J., Brown, J.E., Gadiyar, B.R. and Beyer, E.: "New Environmentally Friendly Surfactant Enhances Well Cleanup," SPE paper 82214, presented at the SPE European Formation Damage Conference, The Hague, The Netherlands, May 13-14, 2003.
23. Lawson, J.B.: "The Adsorption of Nonionic and Anionic Surfactants on Sandstone and Carbonate," SPE paper 7052, presented at the SPE Symposium on Improved Methods of Oil Recovery, Tulsa, Oklahoma, April 16-19, 1978.

24. Rubio, J. and Kitchener, J.A.: "The Mechanism of Adsorption of Polyethylene Oxide Flocculent on Silica," *Journal of Colloid and Interface Science*, Vol. 57, No. 1, October 1976, pp. 132-142.

25. Friberg, S. and Bothorel, P.: *Microemulsions: Structure and Dynamics*, Chapter 2, CRC Press, Boca Raton, Florida, 1987, 219 p.

BIOGRAPHIES

Mashhoor S. Al-Anazi joined Saudi Aramco in March 2001 as a Lab Scientist with the Research and Development Center, and then was moved to the Exploration and Petroleum Engineering Center – Advanced Research Center (EXPEC ARC) to work as a Petroleum Engineer. He has worked on several projects related to formation damage and stimulation, water injection and water control.

In 2001, Mashhoor received his B.S. degree in Chemical Engineering from King Fahd University of Petroleum and Minerals (KFUPM), Dhahran, Saudi Arabia.

Dr. Mohammed H. Al-Khaldi is a Petroleum Engineer in the Saudi Aramco's Exploration and Petroleum Engineering Center – Advanced Research Center (EXPEC ARC). He has more than 15 years of experience in upstream research and technology. Since joining Saudi Aramco, he has been involved in applied research projects dealing with hydraulic/acid fracturing, VES technology, formation damage mitigation, corrosion control, drilling fluids and conformance control. Currently, he is leading a group of 15 engineers and 10 technicians.

Mohammed's experience includes the investigation of microbial corrosion by evaluating sulfate-reducing bacteria, development of mechanical methods to remove iron sulfide scale, and corrosion inhibition during acidizing of deep gas wells. Additionally, he has designed and optimized water shut-off techniques using gels and viscoelastic surfactants. Mohammed developed a new acid treatment for acid-sensitive crude oils of new oil field developments. He has identified and provided field solutions to formation damage occuring during drilling and completion of tight unconventional gas reservoirs.

Mohammed has written more than 60 technical papers, contributed to journals and many technial reports, and has seven patents. He is an active member of the Society of Petroleum Engineers (SPE) and has chaired SPE workshops and conferences. In addition, Mohammed has been invited to give presentations at various universities and research organizations all over the globe. He is recognized as a lead researcher worldwide in the field of formation damage and well stimulation. Mohammed received the Vice President's Recognition Award for significant contributions toward the safe and successful completion of the first 100 fracture treatments of gas wells and the 2011 GCC SPE Award for best young professional technical paper.

He received his B.S. degree in Chemical Engineering from King Fahd University of Petroleum and Minerals (KFUPM), Dhahran, Saudi Arabia, and his M.S. and Ph.D. degrees in Petroleum Engineering from the University of Adelaide, Adelaide, Southern Australia.

Alhasan B. Fuseni joined Saudi Aramco in 2006 and is a member of the Chemical Enhanced Oil Recovery (EOR) team of the Exploration and Petroleum Engineering Center – Advanced Research Center (EXPEC ARC). Prior to joining Saudi Aramco, he worked for the King Fahd University of Petroleum and Minerals (KFUPM) Research Institute as a Research Engineer, and for Hycal Energy Research, Calgary, Canada, as an EOR technologist. Alhasan has taught an in-house course on core flooding applications in chemical EOR at EXPEC ARC, and he teaches the chemical EOR section of the course on EOR at Saudi Aramco's Upstream Professional Development Center. He has authored and coauthored several papers in petroleum engineering and is currently serving as a reviewer for Elsevier's *Journal of Petroleum Science and Engineering*.

Alhasan received both his B.S. and M.S. degrees in Petroleum Engineering from KFUPM, Dhahran, Saudi Arabia, in 1985 and 1987, respectively.

Khalid M. Al-Marshad is a Laboratory Technician working with the Formation Damage & Stimulation Unit of Saudi Aramco's Exploration and Petroleum Engineering Center – Advanced Research Center (EXPEC ARC). He joined Saudi Aramco in 2009 and began his training at the Industrial Training Center, graduating in 2011. Khalid's first assignment was in the Eastern Region Distribution Department, where he worked until May 2012. At that time, he was moved to his current assignment.

SUBSCRIPTION ORDER FORM

To begin receiving the *Saudi Aramco Journal of Technology* at no charge, please complete this form.

Please print clearly.

Name _____

Title _____

Organization _____

Address _____

City _____

State/Province _____

Postal code _____

Country _____

E-mail address _____

Number of copies _____

TO ORDER

By phone/email:

Saudi Aramco Public Relations Department
JOT Distribution
+966-013-876-0498
william.bradshaw.1@aramco.com

By mail:

Saudi Aramco Public Relations Department
JOT Distribution
Box 5000
Dhahran 31311
Saudi Arabia

Current issues, select back issues and multiple copies of some issues are available upon request.

The *Saudi Aramco Journal of Technology* is published by the Saudi Aramco Public Relations Department, Saudi Arabian Oil Company, Dhahran, Saudi Arabia.

GUIDELINES FOR SUBMITTING AN ARTICLE TO THE SAUDI ARAMCO JOURNAL OF TECHNOLOGY

These guidelines are designed to simplify and help standardize submissions. They need not be followed rigorously. If you have additional questions, please feel free to contact us at Public Relations. Our address and phone numbers are listed on page 77.

Length

Varies, but an average of 2,500-3,500 words, plus illustrations/photos and captions. Maximum length should be 5,000 words. Articles in excess will be shortened.

What to send

Send text in Microsoft Word format via email or on disc, plus one hard copy. Send illustrations/photos and captions separately but concurrently, both as email or as hard copy (more information follows under file formats).

Procedure

Notification of acceptance is usually within three weeks after the submission deadline. The article will be edited for style and clarity and returned to the author for review. All articles are subject to the company's normal review. No paper can be published without a signature at the manager level or above.

Format

No single article need include all of the following parts. The type of article and subject covered will determine which parts to include.

Working title

Abstract

Usually 100-150 words to summarize the main points.

Introduction

Different from the abstract in that it "sets the stage" for the content of the article, rather than telling the reader what it is about.

Main body

May incorporate subtitles, artwork, photos, etc.

Conclusion/summary

Assessment of results or restatement of points in introduction.

Endnotes/references/bibliography

Use only when essential. Use author/date citation method in the main body. Numbered footnotes or endnotes will be converted. Include complete publication information. Standard is *The Associated Press Stylebook*, 49th ed. and *Webster's New World College Dictionary*, 5th ed.

Acknowledgments

Use to thank those who helped make the article possible.

Illustrations/tables/photos and explanatory text

Submit these separately. **Do not place in the text.** Positioning in the text may be indicated with placeholders. Initial submission may include copies of originals; however, publication will require the originals. When possible, submit both electronic versions, printouts and/or slides. Color is preferable.

File formats

Illustration files with .EPS extensions work best. Other acceptable extensions are .TIFF, .JPEG and .PICT.

Permission(s) to reprint, if appropriate

Previously published articles are acceptable but can be published only with written permission from the copyright holder.

Author(s)/contributor(s)

Please include a brief biographical statement.

Submission/Acceptance Procedures

Papers are submitted on a competitive basis and are evaluated by an editorial review board comprised of various department managers and subject matter experts. Following initial selection, authors whose papers have been accepted for publication will be notified by email.

Papers submitted for a particular issue but not accepted for that issue will be carried forward as submissions for subsequent issues, unless the author specifically requests in writing that there be no further consideration. Papers previously published or presented may be submitted.

Submit articles to:

Editor
The *Saudi Aramco Journal of Technology*
C-86, Wing D, Building 9156
Dhahran 31311, Saudi Arabia
Tel: +966-013-876-0498
E-mail: william.bradshaw.1@aramco.com.sa

Submission deadlines

Issue	Paper submission deadline	Release date
Winter 2015	September 1, 2015	December 31, 2015
Spring 2016	December 1, 2015	March 31, 2016
Summer 2016	March 1, 2016	June 30, 2016
Fall 2016	June 1, 2016	September 30, 2016

Formation Evaluation in Gas-Bearing Reservoirs Drilled with Na/K Formate WBM, Using LWD Time-Lapse Data Acquisition

Kehinde M. Fakolujo, Ali R. Al-Belowi, Kais Gzara, Oluchukwu L. Onuigbo and Ihsan T. Pasaribu

ABSTRACT

The introduction of formate-based drilling muds has successfully addressed drilling challenges related to barite-weighted muds. The new muds, however, exhibited peculiar petrophysical properties that adversely affected log interpretation. First, the mud present inside the borehole and surrounding the tool required different environmental corrections. Second, invading mud filtrate present inside the formation was difficult to account for. Because of the higher density, lower hydrogen index and high gamma ray readings associated with Na/K formate-based drilling fluids, petrophysical analysis typically resulted in inaccurate mineralogy and pessimistic porosity and permeability estimates. Such estimates also became strongly dependent on the extent of invasion by the mud.

Creating Multiple Fractures in Cemented Horizontal Laterals: An Efficient Way to Improve Productivity of Tight Carbonate Formations in Saudi Arabia

Dr. Zillur Rahim, Dr. Hamoud A. Al-Anazi, Adnan A. Al-Kanaan and Rifat Kayumov

ABSTRACT

During the last decade, significant efforts to develop gas reserves from relatively tight carbonate formations have been made in the southern part of Saudi Arabia. An important role in this effort was played by the multistage acid fracturing technique, which enables maximized reservoir contact by creating multiple fractures along the wellbore. Lessons learned from many such treatments highlighted the following challenges related to open hole multistage fracturing (MSF) completions:

- Communication between the stages.
- Bottom-hole treating pressure (BHTP) dropping below the fracture gradient.
- Limited reservoir contact due to only one fracture propagating between the open hole packers.

Development of New Kill Fluids with Minimum Sagging Problems for High-Pressure Jilh Formation in Saudi Arabia

Ziad A. Al-Abdullatif, Dr. Abdullah S. Al-Yami, Dr. Vikrant Wagle, Abdulaziz S. Bubshait and Ali M. Al-Safran

ABSTRACT

A successful kill fluid formulation for the overpressured Jilh formation has been achieved. The Jilh formation is a dolomitic Middle Triassic tight zone that ranges from 8,000 ft to 10,000 ft true vertical depth (TVD) with abnormal saltwater pressure that requires a kill fluid with a density up to 150 lb/ft^3 (pcf) to stop reservoir flow. The addition of weighting materials, such as barite ($BaSO_4$) or hematite (Fe_2O_3), is needed for the kill fluid to achieve the desired density to produce hydrostatic pressure. Subsequently maintaining a high volume of solids content — whether for $BaSO_4$ particles or any other weighting material — in suspension is challenging, especially for an extended period of time. Failing to do so is a phenomenon described in the industry as static barite sag, and it may lead to serious well control incidents and lost circulation.

A Decade of Experience with Multiphase Flow Meters

Mohammad S. Al-Kadem, Dr. Faisal T. Al Khelaiwi, Ali S. Al-Mashhad and Mohammad S. Al Dabbous

ABSTRACT

Multiphase flow metering is considered one of the most essential technologies in well testing. Since the mid-1990s, multiphase flow meters (MPFM) have evolved from a revolutionary new technology into a consolidated solution widely adopted by the major operators worldwide. This evolution has taken place thanks to the high quality of measurements, the low operational cost and the capability of enabling remote monitoring of well performance with ease. The meters have proven to be durable for testing the oil wells of Saudi Aramco's fields.